A Molecular Analysis of Skeletal Morphogenesis in the Sea Urchin Embryo

by

Ashrifia Adomako-Ankomah

Submitted in Partial Fulfillment of the Requirements for the Degree of Doctor of Philosophy

Department of Biological Sciences
Carnegie Mellon University

February 18th, 2013

Thesis Advisor: Charles A. Ettensohn

To my Family

My parents, Joseph and Frances Gogo

My brother and sister, Ashifi and Osenkor Gogo

And most of all, my husband, Yaw Adomako-Ankomah

ACKNOWLEDGEMENT

I am thankful to my advisor, Dr. Charles Ettensohn for his guidance, encouragement and support, and for allowing me to take full ownership of my various projects, which was a remarkable and much appreciated vote of confidence. I also appreciate the advice and support of my thesis committee: Drs. Veronica Hinman, Jonathan Minden, and Mark Rebeiz.

I am thankful for the help, support, advice and encouragement of several past and present members of the Ettensohn Laboratory: Kiran Rafiq, Zhongling Sun, Tanvi Shashikant, Margarida Anjos, Dr. Tara Sharma, and Quinn Weismann, among many others. Additionally, I appreciate the help of several rotation and summer students who worked on various projects over the years. I am thankful to members of the Hinman Laboratory, Carnegie Mellon University, for their generosity in sharing equipment, reagents, animals and advice. I am thankful to Dr. Haibing Teng of the Molecular Biosensor and Imaging Center, Carnegie Mellon University, for help with confocal microscopy.

Lastly, I am thankful to my friends in the Department of Biological Sciences, Carnegie Mellon University, and my friends scattered all around the world.

Table of Contents **Page**

Abstract

Cell migration and differentiation are fundamental aspects of embryogenesis, essential to the development of any complex multicellular organism. Like most biological processes, the directional migration of different cell types and their differentiation into various specified cells with unique functions are regulated by intricate mechanisms, many details of which remain unresolved. The sea urchin embryo, which is optically clear and amenable to a wide variety of experimental manipulations, is an excellent model system to study these processes. Of specific significance is the formation of the embryonic endoskeleton, in which early cell migration and differentiation events can be observed *in vivo*. The sea urchin embryonic endoskeleton is formed by the sequential ingression, directed migration, and fusion of the primary mesenchyme cells (PMCs). The fused PMCs then secrete a calcareous matrix, forming the characteristic rigid endoskeleton of the embryo. The mechanisms governing skeletogenesis have been of interest to researchers for decades. However, several aspects of its regulation are still unclear.

The work described in this thesis details progress made in understanding cell migration and differentiation using skeletogenesis in the sea urchin embryo as a model. Skeletogenesis is regulated by a complex gene regulatory network (GRN) which is arguably the most complete developmental GRN presently available. The aim of this work was to build linkages between the components of this GRN and observable morphological events during skeletogenesis. Recent research into skeletogenesis has been mainly focused on deciphering the roles that upstream transcription factors play in the specification of PMCs. Hence, a significant gap exists in our knowledge of the functions of downstream morphoeffector genes regulated by these well-studied transcription factors. To this end, we have analyzed the roles of two novel morphoeffector genes, *p58-a* and *p58-b*, which encode similar type 1 transmembrane proteins. These two genes are expressed specifically in the PMCs throughout development. We find that the knockdown of either *p58-a* or *p58-b* results in defects in skeletogenesis, though PMC specification, migration and fusion occur unperturbed. We conclude that *p58-a* and *p58-b* most likely play a role in biomineralization.

Additionally, we describe progress made in understanding the role that ectodermal cues play during skeletogenesis, another poorly understood aspect of this process. The precise and

extremely replicable pattern of PMC migration to specific sites within the blastocoel during skeletogenesis has long been of interest to researchers. However, the molecular mechanisms controlling this process have remained mostly elusive. Recent studies have identified the fibroblast growth factor (FGF) and vascular endothelial growth factor (VEGF) signaling pathways as playing significant roles in regulating cell migration and differentiation during skeletogenesis in the sea urchin species *Paracentrotus lividus*, though these studies provided few details on the specific roles each of these pathways play. The FGF and VEGF pathways have long been shown to play complex, sometimes interacting roles in cell migration during development, and our research aimed at revealing the fine details of their functions in the sea urchin embryo. We have found that in the sea urchin species *Lytechinus variegatus*, VEGF signaling plays a more significant role in regulating skeletogenesis than the FGF pathway. Blocking VEGF signaling leads to profound defects in skeletogenesis: all aspects of PMC migration are abolished in these morphants, and the extension of filopodia from the PMCs is compromised. We have also identified a separate role for VEGF signaling in the synthesis of the endoskeleton and in regulating the expression of several morphoeffector genes in the PMC gene regulatory network. Conversely, we observed that inhibiting FGF signaling does not lead to severe defects in skeletogenesis, as FGF morphant embryos form extensive skeletal elements. Lastly, we document the presence of reciprocal signals from the PMCs regulating gene expression in the ectoderm, a phenomenon not previously described. These findings significantly expand our understanding of the regulation of directional cell migration and differentiation during embryonic development.

List of Figures **Page**

List of Tables **Page**

Chapter 1
Introduction

1.1 Embryogenesis in the Sea Urchin

The sea urchin embryo has been a popular model organism for over a century. A marine invertebrate deuterostome of the Phylum Echinodermata, the sea urchin holds an important position evolutionarily as it is among the closest extant invertebrates to the chordate clade. Results obtained from research in sea urchin embryos are therefore transferrable to numerous different species. The sea urchin embryo is amenable to a wide variety of experimental manipulations, and its transparency makes the results of such manipulations easily assessable. More recently, the entire genome of the species *Strongylocentrotus purpuratus* has been sequenced, and efforts are ongoing to sequence the genomes of other species as well. This has further sped up advances in this field of research. Sea urchins continue to be a leading experimental model in the study of developmental biology.

Embryonic development in the sea urchin is a well-documented process. As reviewed most recently by Lyons *et al*. (2012), the first two cleavage divisions after fertilization occur in a plane parallel to the animal-vegetal axis, with the third division occurring perpendicular to the first two. All three divisions give rise to cells of roughly equal size. The fourth cleavage division however is unequal, giving rise to eight cells of equal size at the animal pole called mesomeres, while the vegetal hemisphere is composed of four larger cells called macromeres, and four smaller cells called micromeres. During the fifth cleavage division, the mesomeres and macromeres divide equally. The micromeres at the vegetal pole of the embryo again divide unequally, leading to the formation of four large micromeres and four small micromeres. The mesomeres give rise to most of the oral and aboral ectoderm, while the macromeres give rise to the endoderm, non-skeletogenic mesoderm (NSM) and some ectoderm. The large micromeres give rise to the primary mesenchyme cells (PMCs), which form the embryonic endoskeleton, and the progeny of the small micromeres form the germ cells. The characteristic synchrony of cell divisions in the cleaving embryo is lost after the fourth division, with the micromeres and their descendants being subsequently delayed in relation to other cells of the embryo. These early rapid cleavage events lead to the formation of the morula, which hollows out to form the blastula. As the embryo begins to gastrulate, the PMCs undergo an epithelial-to-mesenchymal transition (EMT) and ingress into the blastocoel, after which they undergo a complex series of morphogenetic behaviors that culminates in the formation of the endoskeleton. The ectoderm at

the vegetal pole of the blastula flattens, and the archenteron invaginates into the embryo. The archenteron elongates and fuses with the oral ectoderm; it subsequently segments to form the tripartite gut of the pluteus larva. The pluteus larva begins to feed and later undergoes metamorphosis to develop into the adult sea urchin.

As with other model systems, several complex interactions are involved in patterning the sea urchin embryo (reviewed in Ettensohn and Sweet, 2000). The animal-vegetal axis of the sea urchin embryo is established by maternal determinants in the cytoplasm of fertilized eggs, though there is also evidence of induction in specifying this axis during development (reviewed in Angerer and Angerer, 2000). The nuclearization of β-catenin at the vegetal pole, regulated by Disheveled, is essential to animal-vegetal axis specification in the developing embryo (Emily-Fenouil *et al*., 1998; Logan *et al.,* 1999; Angerer and Angerer, 2000; Weitzel *et al*., 2004). BMP2/4 signaling, together with its antagonist *noggin*, plays a role in establishing the ectoderm-endoderm boundary on the animal-vegetal axis (Angerer *et al*, 2000). Also, the gene *goosecoid* regulates animal-vegetal patterning downstream of the *wnt* signaling pathway (Angerer *et al.*, 2001). Unlike animal-vegetal polarity, the mechanisms leading to the initial establishment of the oral-aboral axis are not very well understood. This axis is thought to be specified first by increases in mitochondrial density or activity, leading to an increased redox potential at the presumptive oral side (Coffman *et al.*, 2004). Oral-aboral polarity becomes evident at the end of gastrulation, when the mouth is formed from the opening created by the fusion of the archenteron to the ectoderm. At this stage, the aboral ectoderm makes up most of the epithelial layer of cells surrounding the embryo, while the oral ectoderm surrounds the mouth. These two regions of epithelium are separated by the ciliary band. Nodal, a TGF-β signaling molecule expressed specifically in the oral ectoderm, has been shown to act upstream of BMP signaling and downstream of TCF/Lef signaling in the specification of the oral ectoderm (Flowers *et al.*, 2004, Duboc *et al*., 2004) . *Nodal* expression is blocked by ectopic expression of *antivin* and *univin* (Range *et al*., 2007), and spatially restricted by *lefty* (Duboc *et al*., 2008). The expression of *goosecoid*, known to play a role in animal-vegetal patterning, also specifies the oral ectoderm (Angerer *et al.*, 2001). Additionally, the *not* homeodomain gene has recently been identified as an intermediary mediator of oral ectoderm specification downstream of nodal signaling (Li *et al*., 2012). Upstream of *nodal* and *goosecoid* expression, P38 MAP kinase regulates oral-aboral patterning, and represses the expression of genes which specify the aboral ectoderm (Bradham

and McClay, 2005). Nodal signaling also regulates the establishment of the left-right axis (Duboc *et al.*, 2005). Together, the complex interactions between these numerous genes specify the body axes of the embryo.

1.2 Skeletogenesis in the Sea Urchin Embryo

The formation of the embryonic endoskeleton by the PMCs is one of the most studied features of sea urchin embryogenesis (Fig. 1.1). In the pre-hatching blastula, the progeny of the large micromeres are integrated into the developing embryo at the vegetal pole, having undergone three or four more rounds of cleavage (Lyons *et al.*, 2012). The PMCs soon undergo an epithelial-to-mesenchymal transition (EMT), delaminating from other cells in the ectoderm and ingressing into the blastocoel (Wu *et al*., 2007). The EMT is regulated by the transcription factors *alx1* (Ettensohn *et al.*, 2003), *ets1* (Kurokawa *et al.*, 1999), *twist* (Wu *et al.*, 2008), *snail* (Wu and McClay, 2007) and *foxN2/3* (Rho and McClay, 2011), and facilitated by changes in cell adhesion properties of the PMCs and the epithelial layer of cells forming the blastula, in which PMCs downregulate the expression of integrins and cadherins on their surface relative to the rest of the developing embryo (Miller and McClay, 1997; Ettensohn, 1999; Lyons *et al*., 2012). The PMCs divide one last time after ingression, giving rise to about 32-64 PMCs, depending on the species of sea urchin (Ettensohn *et al*., 1997).

PMC ingression is followed by cell migration. As described by Okazaki (1965, 1975) and Gustafson and Wolpert (1999), the ingressed PMCs position themselves in two dense clusters of cells at specific locations along the blastocoel wall. These ventro-lateral clusters (VLCs) are linked by two chains of PMCs, one located orally and the other aborally. This entire network of PMCs, known as the sub-equatorial ring, is formed by the mid-gastrula stage. Later in development, a chain of PMCs migrates longitudinally from each VLC towards the animal pole of the embryo. PMC migration is facilitated by interactions between the PMCs and specific molecules in the extracellular matrix, including EMC3 (Hodor *et al.*, 2000) and fibronectin (Katow *et al.*, 1990), and by specific signals from the ectoderm (Duloquin *et al.*, 2007; Rottinger *et al.*, 2008; Cavalieri *et al.*, 2011).

PMCs migrate by the extension and retraction of numerous filopodia. These filopodia make contact with the ectoderm as the cells move, and persist even after the sub-equatorial ring is formed (Malinda *et al*., 1995; Miller *et al*., 1995). The filopodia extended by the PMCs are about 0.2- 0.4µm in diameter, mostly made of actin, and are thought to sense environmental cues (Karp and Solursh, 1985; Miller *et al*., 1995). Filopodia are most dynamic during the first two hours after ingression, after which they stabilize as PMCs begin to fuse (Karp and Solursh, 1985). Detailed studies of filopodial dynamics by Malinda *et al.* (1995) have shown that approximately 120 filopodia, both branched and unbranched, are extended per hour by migrating PMCs, and each PMC usually has 5-7 filopodia at any given moment, with an average length of 5-10 µM (Ettensohn *et al.,* 1997). The direction of filopodial extension is initially random and unbiased, but later, as the cells approach the site of ring formation, more filopodia extend towards the sites of ring formation (Malinda *et al.*, 1995). Positional cues from the ectoderm also regulate the length of filopodia extended (Miller *et al.*, 1995).

PMCs fuse as they migrate, leading to the formation of a single continuous syncytium within which the endoskeleton is secreted (Okazaki, 1965). PMC fusion begins approximately two hr after the cells ingress and continues as the sub-equatorial ring forms (Hodor and Ettensohn, 1998). PMC fusion is a dynamic process involving the formation of transient connections between the tips of the filopodia, and these connections later stabilize as the cells fuse (Okazaki, 1965). The ability of PMCs to fuse has been observed in cultured PMCs, thereby demonstrating that it is an inherent ability of the cells independent of extrinsic factors (Hodor and Ettensohn, 1998).

Biomineralization begins with the secretion of a triradiate spicule rudiment at each VLC (reviewed in Killian and Wilt, 2008). The spicule matrix, which is composed of 95% calcium carbonate, approximately 5% magnesium carbonate, and 0.1% occluded proteins, is secreted within a privileged space created by the syncytial filopodia of the PMCs (Wilt, 1999). The spicules are initially deposited as amorphous calcium carbonate, which is then converted into calcite between the prism and pluteus stages. The proteins occluded within the spicule matrix are thought to play a role in maintaining the stability of amorphous calcium carbonate and converting it into calcite (Killian and Wilt, 2008; Gong *et al*. 2012). The spicule rudiments, soon after deposition, orient to align two of their three branches to the oral and aboral chains of PMCs,

with the third branch aligning to the chains of PMCs migrating towards the animal pole (Ettensohn *et al*., 1997). The spicule rudiments then undergo an elaborate series of elongation and branching events (described in detail in Ettensohn *et al*., 1997) to give rise to the complex endoskeleton of the embryo. The structure of the endoskeleton, which is extremely consistent within individuals of a species but varied among different species of sea urchin, determines the shape of the larva and plays a role in its orientation and swimming (Ettensohn *et al*., 1997; Ettensohn, 2013).

Obviously, the morphological events occurring during sea urchin development have been documented in detail, and the focus of recent research has shifted to elucidating the genetic basis of these morphological events. The construction of complex gene regulatory networks (GRNs) greatly facilitates the study of the genetic regulation of anatomy. GRNs are basically wiring diagrams depicting interactions among the various genes regulating a specific event, and the representation of gene interactions in GRNs aids in visualizing the connections between upstream transcription factors and the downstream morphoeffector genes they regulate (reviewed in detail in Ettensohn, 2013). A lot of work has been done separately observing the morphological events occurring during sea urchin development and constructing the complex GRN of the sea urchin embryo, and the research presented here documents progress made towards linking the genes in this complex PMC GRN to various morphological processes during skeletogenesis.

1.3 The PMC Gene Regulatory Network

The study of skeletogenesis in the sea urchin embryo gives great insight into how morphology is encoded within a genome, as gene expression in the PMCs controlled by a complex network of interacting transcription factors, signaling molecules and morphoeffector genes (Fig. 1.2). The PMC GRN is regulated upstream by the nuclearization of maternal β-catenin at the vegetal pole of the embryo, which activates the paired class homeodomain protein *pmar1* in the progeny of the micromeres (Oliveri *et al.*, 2002; Oliveri *et al.*, 2003; Oliveri *et al.*, 2008). Active Pmar1 then functions to repress *hesc* in the descendants of the large micromeres (Revilla-i-Domingo *et al.*, 2007), an event pivotal to the expression of genes involved in skeletogenesis (reviewed in

Ettensohn, 2009). The repression of *hesc* in the PMC precursor cells regulates the expression of transcription factors such as *t-brain* (Croche *et al.*, 2001; Fuchikami *et al.*, 2002), *ets1* (Kurokawa *et al.*, 1999) and *dri* (Oliveri *et al.*, 2002; Amore *et al.*, 2003**),** though the activation of at least *alx1*, which encodes a homeodomain protein necessary for the development of the embryonic skeleton (Ettensohn *et al.*, 2003), is independent of this *pmar-hesc* double repression gate (Sharma and Ettensohn, 2010). Rottinger *et al.* (2004) showed that the activation of Ets1 by MAPK signaling regulates the expression of several of these early transcription factors in the network, therefore also regulating the expression of downstream morphoeffector genes. ERK activation also regulates the expression of *delta, ets1, tbr, alx1, dri* and *erg* (Fernandez-Serra *et al.*, 2004). The activation and expression of several transcription factors, most importantly *alx1* and *ets1*, and to a lesser extent *tbr, erg, hex, tgif , deadringer, foxb and foxo* leads to the cascade of complex gene interactions necessary for the regulation of the morphoeffector genes which control PMC differentiation and skeletogenesis (Oliveri *et al.*, 2008; Ettensohn, 2009; Rafiq *et al.*, 2012**).**

Genome-wide (Zhu *et al.*, 2001; Illies *et al.*, 2002; Livingston *et al.*, 2006; Rafiq *et al.*, 2012), and proteome-wide (Mann *et al.*, 2010) approaches have led to the identification of numerous downstream morphoeffector genes specifically expressed or enriched in the PMCs. The expression patterns of several of these genes have been described (Zhu *et al*, 2001; Illies *et al*, 2002; Rafiq *et al*, 2012), but unfortunately, efforts to study their functions have lagged behind research into the upstream transcription factors regulating their expression. Some morphoeffector proteins, such as SM50 (Benson *et al.*, 1987), PM27 (Harkey *et al.*, 1995) and SM30 (Killian *et al.*, 2010) are known to be occluded in the spicule matrix, likely playing a role in regulating the stability of the calcite that forms the spicules (Wilt *et al.*, 2008). Others, such as the glycoprotein MSP130 (Anstrom *et al.*, 1987; Harkey *et al.*, 1992), may play a role in calcium uptake from sea water during skeletogenesis (Killian and Wilt, 2008). Illies *et al.* (2002) conducted a comparative study of the structures, conserved domains and expression patterns of several spicule matrix proteins, and though their functions were not studied, this research led to a better understanding of the similarities and classes of biomineralization proteins. A few recent studies have shown the functions of some of these proteins: Peled-Kamar *et al.* (2002) showed that SM50 is essential for spiculogenesis, and the transmembrane protein P16 has been shown to regulate PMC differentiation, but not PMC specification, migration or fusion (Cheers and Ettensohn, 2005).

Obviously, the functions of the vast majority of these genes are unknown, and more detailed analyses of morphoeffector genes in the PMC GRN is essential to the identification of key effectors in controlling morphogenetic processes and elucidating their regulatory control.

1.4 Alternative Deployment of the Skeletogenic Gene Regulatory Network

As evident from several studies analyzing axis specification in the sea urchin embryo (cited above), polarity, patterning and cell fate specification are established early in sea urchin development. It is therefore surprising that the sea urchin embryo retains a remarkable ability to respecify several territories under experimental conditions (reviewed in Ettensohn, 2009). Most relevant to this body of work is the phenomenon of non-skeletogenic mesoderm (NSM) transfating, where the blastocoelar cells adopt skeletogenic fates when PMCs are surgically removed from the embryo (Fig. 1.3) (Ettensohn and McClay, 1988; Ettensohn *et al.*, 2007; Sharma and Ettensohn, 2011). Research has shown that several aspects of the PMC GRN are recapitulated by transfating cells- the transcription factor *alx1*, which is necessary PMC specification (Ettensohn *et al.*, 2003), is also essential for NSM transfating (Ettensohn *et al.*, 2007). Additionally, transfating cells have been shown to express the transcription factors *ets1* and *tbr* as well as several morphoeffector genes in the PMC GRN in a temporal pattern apparently similar to their expression in PMCs under normal conditions (Ettensohn and McClay, 1988; Ettensohn *et al.*, 2007; Sharma and Ettensohn, 2011). There is, however , a significant difference in the mechanisms activating the PMC GRN in transfating NSM cells: the GRN which runs in transfating cells is activated by MAPK signaling (Ettensohn *et al.*, 2007; Sharma and Ettensohn, 2011) while under normal conditions the PMC GRN is regulated upstream mostly by the *pmar1-hesc* double repression gate (Oliveri *et al.*, 2002; Revilla-i-Domingo *et al.*, 2007; Oliveri *et al.*, 2008), and maintained by MAPK signaling (Sharma and Ettensohn, 2010). The detailed mechanisms of activating the PMC GRN in NSM cells during transfating remain unclear.

1.5 Regulation of Skeletogenesis by Ectodermal Cues

It has long been recognized that ectodermal cues play an important role in PMC migration and differentiation. Gustafson and Wolpert (1961), and Galileo and Morrill (1985) observed that even before PMC migration, there was characteristic thickening of ectodermal cells at the sites where the future PMC ring would form. Ettensohn and McClay (1986) noted that the migratory response to seemingly predefined regions was specific to PMCs only. Also, this research showed that PMCs migrated to pre-specified regions in the blastocoel, suggesting that directional migration by the PMCs was in response to specific ectodermal cues. Additionally, it was shown by transplantation experiments among embryos of different stages that the PMCs behave in a manner characteristic of the embryo in which they were implanted (Ettensohn and McClay, 1986). Ettensohn (1990) discovered that the size of the embryonic endoskeleton is not determined by the number of PMCs present in the embryo. He hypothesized that cues from the ectoderm may rather be responsible for determining the final size of the skeleton, an argument reiterated by Ettensohn and Malinda (1993). Moreover, the perturbation of oral-aboral patterning by treatment with nickel chloride leads to the disruption of skeletogenesis, providing additional evidence for the involvement of the ectoderm in skeletogenesis (Hardin *et al.,* 1992). Armstrong *et al*. (1993) also noted this relationship, and showed that the eventual size of the endoskeleton is based on the surface area of ectoderm with which the PMCs interact. Guss and Ettensohn (1997) suggested that signals from the ectoderm may be responsible for the cessation of growth of specific skeletal rods. Additional proof of an involvement of the ectoderm in skeletogenesis was found in the fact that many PMC-specific mRNAs are enriched in the VLCs, and expressed in lower levels in the oral and aboral chains. This pattern of expression was maintained even when the number of PMCs was experimentally reduced, eliminating the hypothesis that gene expression in the VLCs was due to the increased density of PMCs in these regions (Guss and Ettensohn, 1997).

Though the ectoderm is known to regulate skeletogenesis, relatively few genes have been identified as specifically playing a role in this process. The first ectodermal gene identified to be expressed in a pattern suggestive of a role in regulating skeletogenesis in the sea urchin was a homolog of the mammalian and *Drosophila* homeobox gene *orthopedia (otp)*. In the sea urchin species *Paracentrotus lividus*, *otp* is expressed in the regions of ectoderm overlying areas of

rapid skeletal element elongation during embryogenesis (Di Bernardo *et al.*, 1999). This research also showed that the overexpression of *otp* caused spiculogenesis to occur in a radialized pattern. Complementary experiments by Cavalieri *et al.* (2003) showed that inhibiting the expression of *Pl-otp* by morpholino antisense oligonucleotide (MO) technology abolished the directed migration of PMCs and skeletogenesis. Cavalieri *et al*. (2011) also identified a novel gene, *strim1*, which is expressed in the ectoderm overlying the VLCs. The misexpression of *strim1* gene led to the formation of supernumerary skeletal rods, while its knockdown abolished PMC migration and differentiation (Cavalieri *et al*., 2011). The most detailed information on the nature of the ectodermal signals regulating skeletogenesis came from two studies, Duloquin *et al.* (2007) and Rottinger *et al.* (2008), which described the roles the vascular endothelial growth factor (VEGF) and fibroblast growth factor (FGF) pathways play in sea urchin development.

1.6 VEGF and FGF Pathways as Regulators of Development

Growth factors collectively have long been linked to various essential processes in development. Many growth factors function through the Receptor Tyrosine Kinase (RTK) signaling pathway. RTKs are a group of transmembrane glycoproteins which function in transmitting extracellular signals into the cell by binding to their respective ligands (reviewed in Hubbard and Till, 2000). An RTK typically consists of an extracellular ligand-binding domain, a transmembrane domain and a cytoplasmic domain with catalytic tyrosine kinase activity. Various RTKs differ mostly in the architecture of their extracellular domains, and in the absence of a ligand, exist as monomers. The binding of a ligand to a specific RTK triggers the dimerization and autophosphorylation of the receptor, leading to the sequential phosphorylation and activation of downstream effectors of RTK signaling. This cascade usually ends in the activation of specific transcription factors which in turn regulate gene expression. In a screen for RTK signaling molecules expressed in the sea urchin embryo, Lapraz *et al*. (2006) identified multiple FGF and VEGF receptors, and efforts have been made to characterize the expression patterns and functions of specific FGF and VEGF receptors and their respective ligands in this system. The FGF and VEGF pathways have long been shown to play complex, sometimes interacting roles in cell migration during development. During the migration of mesoderm cells in the chick embryo, for example, the migrating cells respond to both FGF and VEGF signals, with FGF signals playing roles as both attractants and

repellants for these migrating cells, effectively directing their path of movement (reviewed in Chuai and Weijer, 2009).

VEGFs are a family of glycoproteins involved primarily in angiogenesis, and thus are known for their important role in tumor formation (Matsumoto and Claesson-Welsh, 2001; Lamalice *et al*., 2007; Tammela *et al.,* 2008). VEGF signaling plays other essential roles in embryonic development, regulating processes such as neurogenesis (Mackenzie and Ruhrberg, 2012) and cell migration during gastrulation (Chuai and Weijer, 2009; McLennan *et al.,* 2010). Lapraz *et al.* (2006) identified two VEGF receptors in the *S. purpuratus* genome, *vegfr-7 a*nd *vegfr-10*, named for the number of immunoglobulin repeats in each receptor. Additionally, three VEGF ligands were identified: *vegf1*, *vegf2* and *vegf3*. A VEGF receptor homologous to *Sp-vegfr-10* was identified to be expressed selectively in the PMCs of the sea urchin species *P. lividus* (Duloquin *et al*., 2007) and the *P. lividus* homolog of *vegf3* was expressed in the ectoderm overlying the VLCs of PMCs. This interesting expression pattern suggested that VEGF signaling might play a role in regulating skeletogenesis, and perturbation of VEGF signaling in fact led to defects in this process. Expression patterns of the *vegf3* ligand and *vegfr-10* receptor have also been described in embryos and larvae of sea stars (*Asterina pectinifera*) and brittle stars (*Amphipholis kochii*), and though functional studies have not been conducted in these species, the expression patterns of these genes correlate strongly with the presence and location of skeletal elements (Morino *et al.,* 2012).

FGFs are a conserved family of polypeptide growth factors ubiquitous among vertebrates and invertebrates (reviewed in Ornitz and Itoh, 2001). FGFs are known to signal across epithelial-mesenchymal boundaries, and function in cell migration, chemotaxis, cell adhesion, and cell differentiation (Böttcher and Niehrs, 2004). During embryonic development, FGFs regulate several processes, including axis specification, germ layer formation, morphogenetic movements and cell fate specification (Dorey and Amaya, 2010). Two FGF receptors, *fgfr1* and *fgfr2*, were identified in the *S. purpuratus* genome by Lapraz *et al.* (2006). A single FGF ligand, *Sp-fgf 9/16/20*, was also identified from this screen. Rottinger *et al*., (2008) showed that the *P. lividus* homolog of the *fgf 9/16/20* ligand, *Pl-fgfa*, was expressed in a pattern similar to the *vegf3* ligand. Unlike the *vegf3* ligand, *Pl-fgfa* is also expressed in the PMCs, together with an FGF receptor

homologous to *Sp-fgfr2*. This group showed that disrupting the FGF pathway also led to defects in skeletogenesis.

Though recent findings describing the role of FGF and VEGF signaling have improved our knowledge on the nature of ectodermal influences on skeletogenesis, the details of the functions of these signals from the ectoderm are still unknown. For example, these previous studies have presented the FGF and VEGF pathways as playing equivalent roles during skeletogenesis. However, as skeletogenesis involves several phases of complex interactions between the PMCs and the ectoderm of the embryo, it is highly plausible that each of these two signaling pathways has specific functions during this process, and elucidating the fine details of their functions is essential to a better understanding of not only the formation of the embryonic endoskeleton in the sea urchin, but of the regulation of cell migration and differentiation during development.

The work described in the following chapters expands our knowledge on arguably the least understood aspects of skeletogenesis in the sea urchin embryo: the functions of novel morphoeffector genes, and the regulation of skeletogenesis by ectodermal cues. Chapter Two describes two newly-identified genes, *p58-a* and *p58-b*, which encode similar transmembrane proteins and lie in tandem on the chromosome, suggesting the occurrence of a gene duplication event. We show by whole mount in situ hybridization analysis that *p58-a* and *p58-b* are expressed specifically in the PMCs in both *S. purpuratus* and *Lytechinus variegatus*. Knockdown of *p58-a* and *p58-b* individually by MOs leads to profound defects in skeletogenesis (although skeletal elements are not completely eliminated), demonstrating that these genes function in a non-redundant manner. Further analysis has shown that *p58-a* and *p58-b* do not play a role in the specification, directed migration or fusion of the PMCs, but are most likely directly involved in biomineralization. These results give us significant insight into the specific roles these morphoeffector genes play during skeletogenesis and the functions of duplicated genes in the sea urchin genome.

Chapter Three describes further insights we have made into detailing the role growth factors play in skeletogenesis. We undertake a comparative and comprehensive study of FGF and VEGF signaling during skeletogenesis in the sea urchin species *Lytechinus variegatus*. We show that in embryos of this species of sea urchin, the *fgfa* and *vegf3* ligands, together with their respective

receptors, are expressed in patterns comparable to results shown in other species. The *fgfa* and *vegf3* ligands are expressed in transiently overlapping, but mostly independent domains in the ectoderm, while both the FGF and VEGF receptors together with *fgfa* are expressed in the PMCs. Using morpholino antisense oligonucleotide technology (MOs), we observe that a knockdown of the *vegf3* ligand dramatically disrupts the migration pattern of PMCs and blocks skeletogenesis altogether. We observed, however, that, at least in *L. variegatus*, PMC migration is not affected in *fgfa* morphants. In these embryos, truncated but well-patterned skeletal elements are formed, leading to the conclusion that in this species, FGF signaling plays a less prominent role than VEGF signaling does in PMC migration and differentiation. Detailed observations of *Lv-vegf3* morphants show that VEGF signaling regulates the number and length of filopodia extended by the PMCs, though this effect is not sufficient to block cell fusion, which is mediated by filopodia. In addition to providing cues for PMC migration, VEGF signaling also regulates PMC differentiation and the expression of several genes in the PMC GRN. Lastly, the appendix shows preliminary results obtained from an analysis of the role of VEGF signaling in regulating NSM transfating. We have observed that perturbing VEGF signaling completely blocks the transfating process, and during transfating, VEGF signaling may regulate the expression of *alx1, ets1* and *tbr*, transcription factors which function upstream of VEGF signaling under normal conditions.

Chapter Four characterizes a previously undescribed phenomenon: the presence of a reciprocal signal from the PMCs which regulates gene expression in the ectoderm. Previous work has shown the presence of a signal from the ectoderm regulating PMC migration and differentiation, and our work on VEGF signaling has elaborated on the nature of this signal. In this chapter, we describe in detail the expression domains of four genes expressed in the ectoderm which have been shown to play a role in regulating skeletogenesis: *fgfa, vegf3, pax2/5/8* and *otp*. We show that the patterns of expression of these genes are strikingly altered if PMCs are eliminated by microsurgical or molecular methods. These results show that PMC-derived signals, which remain to be identified, regulate the expression of skeletogenic genes in the ectoderm, and that ectoderm-PMC signaling is not unidirectional, as previously assumed.

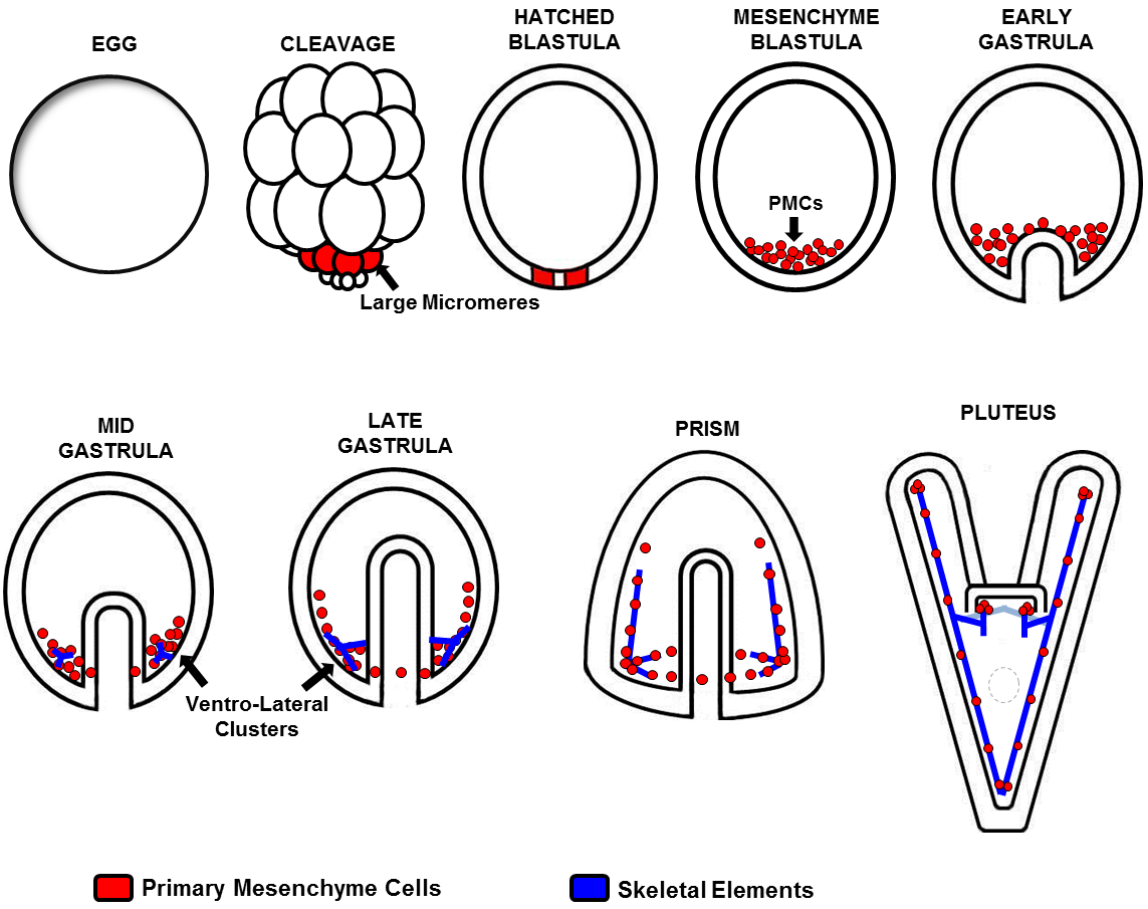

Fig.1.1. Schematic diagram of sea urchin embryonic development and skeletogenesis.

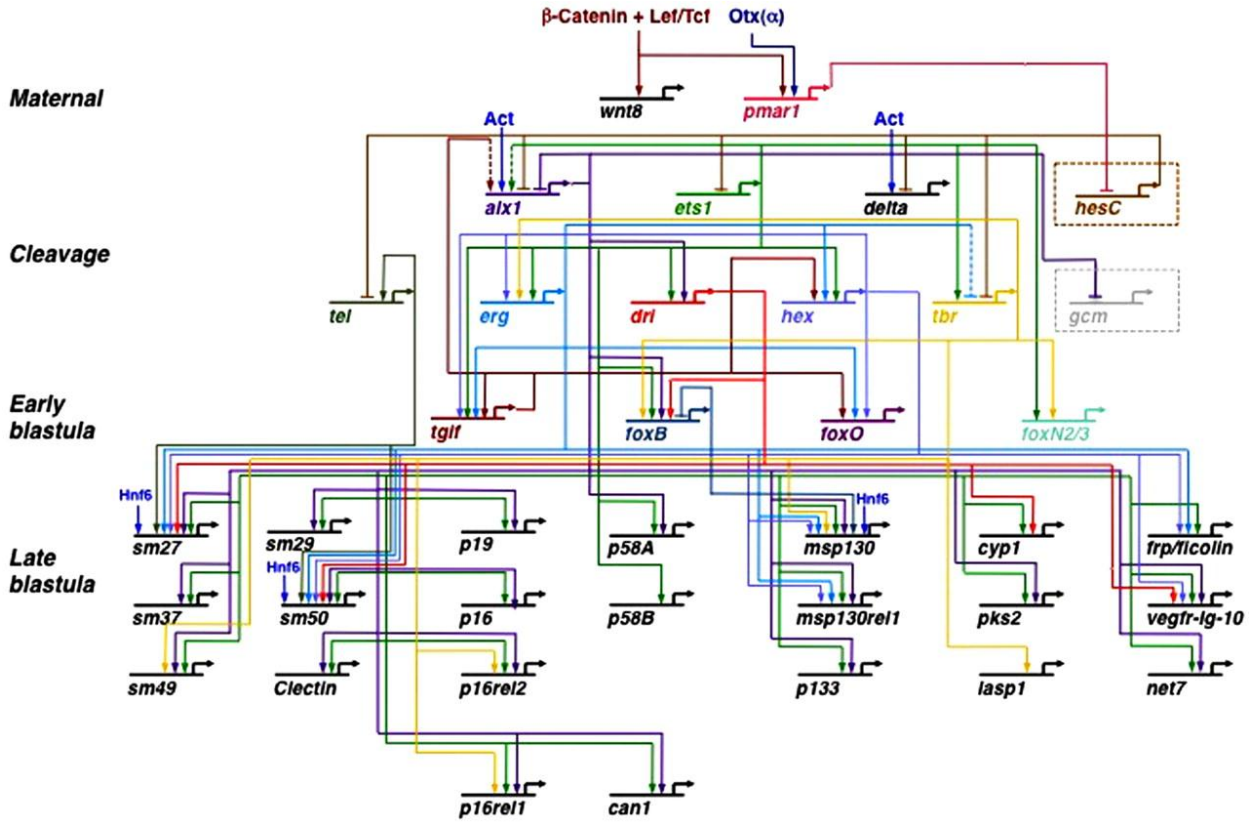

Fig.1.2. The PMC GRN (Rafiq *et al*., 2012).

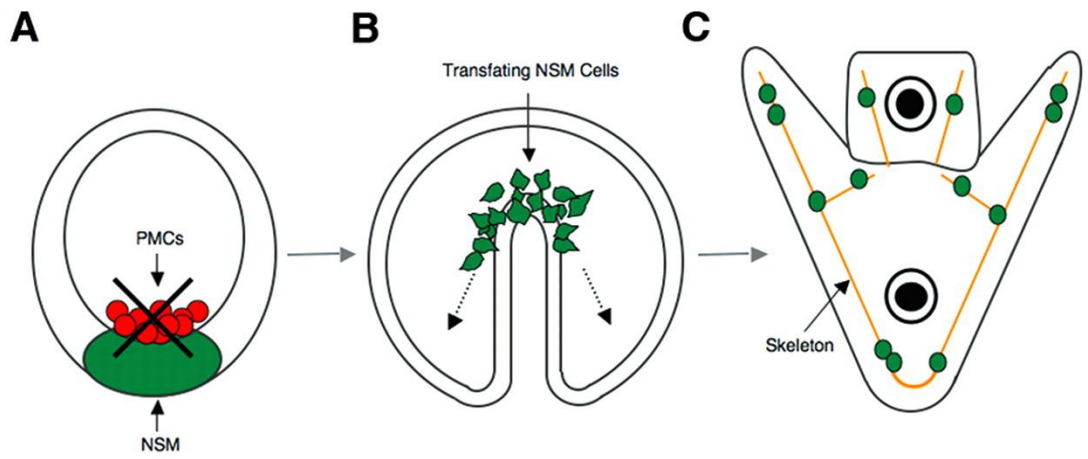

Fig.1.3. Schematic diagram of the transfating process. Upon surgical removal of the PMCs (A), the NSM cells migrate off the tip of the archenteron (B), adopt a skeletogenic fate, and synthesize the embryonic endoskeleton (C) (Sharma and Ettensohn, 2011).

Chapter 2

P58-A and P58-B: Novel Proteins That Mediate Skeletogenesis in the Sea Urchin Embryo

(Published in *Developmental Biology* (2011) **353**, 81-93)

2.1 Abstract

During sea urchin embryogenesis, the skeleton is produced by primary mesenchyme cells (PMCs). PMCs undergo a sequence of morphogenetic behaviors that includes ingression, directed migration, and cell-cell fusion. Ultimately, PMCs deposit the calcite-containing biomineral that forms the endoskeleton of the late embryo and early larva. The endoskeleton has a stereotypical structure and is the major determinant of the distinctive, angular shape of the larva. Although many candidate biomineralization proteins have been identified, functional data concerning these proteins are scant. Here, we identify and characterize two new biomineralization genes, *p58-a* and *p58-b*. We show that these two genes are highly conserved in *Strongylocentrotus purpuratus* and *Lytechinus variegatus*, two sea urchin species whose ancestors diverged approximately 100 million years ago. The *p58-a* and *p58-b* genes lie in tandem on the chromosome, suggesting that one of the two genes arose via a gene duplication event. The two genes encode closely related Type I transmembrane proteins. We have established by whole mount *in situ* hybridization that *p58-a* and *p58-b* are expressed specifically in the PMCs in both species. Knockdown of either gene by morpholino antisense oligonucleotides leads to profound defects in skeletogenesis, although skeletal elements are not completely eliminated. The P58-A and P58-B proteins do not appear to play a role in the specification, directed migration or differentiation of the PMCs, but most likely are directly involved in biomineralization during sea urchin embryonic development.

2.2 Introduction

A central objective of developmental biology is to understand how morphology is encoded in the genome. The development of the endoskeleton of the sea urchin embryo provides a valuable experimental model for the genomic encoding of a complex anatomical structure (reviewed by Okazaki, 1975; Wilt and Ettensohn, 2007). The embryonic skeleton is secreted by primary mesenchyme cells (PMCs). PMCs are the progeny of the large micromeres, four cells that arise from unequal cleavage divisions at the vegetal pole of the embryo. At the late blastula stage, PMCs undergo an epithelial-to-mesenchymal transition (EMT) and ingress into the blastocoel (Wu *et al*., 2007). After ingression, PMCs migrate directionally along the blastocoel wall and adopt a characteristic ring-like pattern (the subequatorial PMC ring). Within the subequatorial ring, clusters of PMCs (the ventro-lateral clusters, or VLCs) form at two positions. PMCs begin to fuse with one another soon after EMT, and by the end of gastrulation these cells are joined in a single, common syncytium (Hodor and Ettensohn, 1998). PMC migration and fusion are mediated by numerous, dynamic filopodial protrusions (Gustafson and Wolpert, 1961; Malinda *et al.*, 1995; Miller *et al*., 1995). Skeletogenesis begins with the deposition of one triradiate spicule rudiment in each VLC. The two spicule rudiments subsequently elongate and branch in a highly stereotypical pattern, thereby producing the complex endoskeleton of the embryo (Gustafson and Wolpert, 1961; Ettensohn and Malinda, 1993). The final structure of the larval endoskeleton is both species-specific and highly reproducible within a species.

Recent studies have begun to elucidate an elaborate gene regulatory network (GRN) that is deployed in the large micromere-PMC lineage (Oliveri *et al*, 2008; Ettensohn, 2009; Rafiq *et al*., 2012). The current model of the skeletogenic GRN contains approximately 80 genes. The network is activated by various maternal inputs, including β-catenin, which collectively trigger the expression of several early zygotic regulatory genes, such as *pmar1* (Oliveri et al., 2002); *alx1* (Ettensohn *et al.*, 2003), *ets1* (Kurokawa *et al.*, 1999), and *t-brain (*Croce *et al*., 2001; Fuchikami *et al.*, 2002), selectively in the micromere-PMC lineage. The transcription factors encoded by these genes provide inputs into other regulatory genes, and a variety of feedback and feedforward interactions among these genes stabilize the transcriptional network and drive it forward (Oliveri *et al*., 2008).

To understand the genomic wiring of skeletal anatomy, it will be essential to identify linkages between regulatory genes and downstream target genes that directly affect skeletal morphology. Recent studies have begun to identify some of the proteins that control skeletal morphogenesis. Two receptor tyrosine kinases, VEGFR-Ig-10 and FGFR-2, have been identified that mediate PMC migration and differentiation (Duloquin *et al.*, 2007; Rottinger *et al*., 2008). Many candidate biomineralization-related proteins have been identified by a wide variety of methods, including cDNA library screens (Benson *et al.*, 1987; George *et al.*, 1991; Harkey *et al.*, 1995; Lee *et al*., 1999), genome-wide bioinformatics approaches (Zhu *et al.*, 2001; Illies *et al*., 2002; Livingston *et al*., 2006), and proteomics (Mann *et al*., 2008; Mann *et al*., 2010a,b). Functional studies on these candidate biomineralization proteins, however, are surprisingly scant. Knockdown of *S. purpuratus sm50* (or its *Lytechinus pictus* homolog *lsm34*) by means of antisense oligonucleotides has shown that this protein is required for biomineralization (Peled-Kamar *et al*., 2002; Wilt *et al*., 2008b). Morpholino antisense oligonucleotides have been used to interfere with the expression of P16, a novel, PMC-specific transmembrane protein, and these studies have shown that P16 is essential for skeletal rod elongation, but not for PMC specification, migration, or fusion (Cheers and Ettensohn, 2005).

In this study, we have identified two novel proteins, P58-A and P58-B, that are essential for skeletogenesis. The genes that encode these proteins lie adjacent to one another on the same chromosome and are likely to be the product of a relatively recent gene duplication event. They are expressed specifically in the PMCs of *S. purpuratus* and *Lytechinus variegatus* embryos, and knockdown of either P58-A or P58-B using translation- or splice-blocking morpholinos results in a suppression of skeletogenesis. We have discovered that P58-A and P58-B do not play a role in PMC specification, migration, or fusion, but instead are most likely directly involved in depositing the calcite-based biomineral that composes the sea urchin endoskeleton. The discovery of these genes broadens our knowledge of the genes that interact to form the complex endoskeleton of the sea urchin embryo.

2.3 Materials and Methods

Embryo Culture

Adult *S. purpuratus* were obtained from Pat Leahy (California Institute of Technology, Pasadena, CA). Adult *L. variegatus* were obtained from Elizabeth Leaser (Wilmington, NC) or from Reeftopia, Inc. (Key West, FL). Spawning was induced by intracoelomic injection of 0.5 M KCl and embryos were cultured in artificial seawater (ASW) at 15°C (*S. purpuratus*) or at 23°C (*L. variegatus*).

Gene Sequence Analysis

The sequences of *S. purpuratus p58-a* and *p58-b* (designated *Sp-p58-a* and *Sp-p58-b*, respectively) were assembled from expressed sequence tags (ESTs) that were obtained as part of a PMC transcriptome project (Zhu *et al.,* 2001; Illies *et al*., 2002; Livingston *et al.,* 2006). Part of the sequence of *L. variegatus p58-a* (*Lv-p58-a*) was obtained by screening a *L. variegatus* mid-gastrula cDNA library (the gift of Dr. David McClay, Duke University). Clone 38-G5 contained all but the 5'-most coding sequence of the mRNA. The remainder of the sequence was obtained by 5' RACE using the GeneRacer® Kit with SuperScript® III RT and the TOPO TA Cloning® Kit for Sequencing (Invitrogen). The sequence of *L. variegatus p58-b (Lv-p58-b*) was assembled from several *L. variegatus* ESTs kindly provided by Dr. Cynthia Bradham (Boston University) and Dr. Albert Poustka (Max-Planck Institut). Comparisons of the sequences of *p58-a* and *p58-b* from *S. purpuratus* and *L. variegatus* were carried out using ClustalW (Thompson *et al.,* 1994). Predicted signal peptide and transmembrane sequences were identified using the SignalP3.0 (Emanuelsson *et al*., 2007) and DAS transmembrane prediction (Cserzö *et al.*, 1997) programs, respectively.

Whole Mount *In Situ* Hybridization (WMISH)

Embryos were fixed for one hour at room temperature in 4% paraformaldehyde in ASW and stored at 4°C in 100% methanol. WMISH was carried out as described elsewhere (Lepage *et al*., 1992, Duloquin *et al.,* 2007). *Sp-p58-a* and *Sp-p58-b* probes were synthesized using clones 146-J23 and 151-N12, respectively, from the *S. purpuratus* PMC library as templates. *Lv-p58-a* probe was synthesized using clone 38-G5 from the *L. variegatus* midgastrula library as a template. *Lv-*

p58-b probe was synthesized using a 3' fragment of sequence obtained from initial attempts to clone the gene using the GeneRacer® Kit with SuperScript® III RT and the TOPO TA Cloning® Kit for Sequencing (Invitrogen) as a template. Gene sequence obtained was cloned into the pCR4Blunt TOPO vector. *Lv-p58-b* WMISH was also conducted by cross-hybridization with the *Sp-p58-b* probe. The probe for *Sp-p19* (GLEAN3_04136) was synthesized using clone 13-P18 from the *S. purpuratus* PMC library as a template.

Microinjection of Morpholino Antisense Oligonucleotides (MOs)

Microinjections were carried out following the protocol of Cheers and Ettensohn (2004). Injection solutions contained 20% (vol/vol) glycerol and 0.16% (wt/vol) Texas Red dextran. *Sp-p58-a* splice-blocking MO was complementary to the exon 3/intron 3 boundary (sequence: 5'-ATTCATCATGTTTCGAACTTACGCG-3'). *Sp-p58-b* splice-blocking MO was complementary to the exon 2/intron 2 boundary (sequence: 5'-ACGGCTTCCATCACTAACCTGATTG -3'). *L. variegatus p58-a* translation blocking morpholino was designed to overlap the start codon of the mRNA (sequence: 5'-CGTGAGATAAAATACACCTTCCATC-3') and the *L. variegatus p58-b* translation blocking morpholino was designed complementary to sequence in the 5' UTR of the mRNA (sequence: 5'- CTCCTCTTTCCACGATAACAACTGA-3'). MOs were injected at the following working concentrations: *Sp-p58-a*: 4 mM, *Sp-p58-b*: 2 mM, *Lv-p58-a*: 0.5 mM, *Lv-p58-b*: 0.1 mM.

RT-PCR Analysis

For each experiment, RNA was extracted from 200 control and 200 MO-injected *S. purpuratus* embryos using the Nucleospin RNA II kit (Clonetech). cDNA was synthesized using the Ambion Retroscript kit, and PCR was carried out using Platinum Taq High Fidelity DNA Polymerase (Invitrogen). Forward and reverse primers for *Sp-p58-a* were 5'-CACGATCGATCGACCGGTAAGGAGTT-3' and 5'-GAACTCTAGACGCTGGGTAACCAAAG-3', respectively. Forward and reverse primers for *Sp-p58-b* were 5'-CATGCTGGAGAGTTCATTGGGTTCGC-3' and 5'-GCACTCTAGACTGTCATTGGGTCCGT-3', respectively. PCR products were analyzed on 1% agarose gels that contained 0.5% ethidium bromide. Bands were gel- purified using the

QIAquick® gel extraction kit (Qiagen), and cloned into the pCS2+ vector for sequencing, using the Cla1 and Xba1 restriction sites.

Immunofluorescence

Immunofluorescence using the 6a9 monoclonal antibody was carried out as described previously (Ettensohn and McClay, 1988). Immunostained embryos were examined using a Zeiss LSM 510 Meta/UV DuoScan Inverted Spectral Confocal Microscope.

PMC Fusion Assay

PMC fusion was monitored by dye transfer, as described previously (Hodor and Ettensohn, 2008). Briefly, one set of *L. variegatus* fertilized eggs was injected with *Lv-p58-a* MO that contained 10% (wt/vol) fluorescein dextran, while another set of fertilized eggs was injected with *Lv-p58-a* MO that lacked the dextran. At the mesenchyme blastula stage, a few (2-6) PMCs were transferred from a dextran-labeled embryo into an unlabeled host embryo. After 24 hours, embryos were visualized with a Zeiss LSM 510 Meta/UV DuoScan Inverted Spectral Confocal Microscope to assess the distribution of the dextran within the PMC syncytium. The same procedure was used to test the role of *Lv-p58-b* in PMC fusion.

2.4 Results

2.4.1 *p58-a* and *p58-b* encode related, novel proteins and are probably duplicated genes

Sp-p58-a and *Sp-p58-b* were identified from ESTs that were obtained as part of a PMC transcriptome project (Zhu *et al.*, 2001; Livingston *et al.*, 2006). Upon mapping *Sp-p58-a* and *Sp-p58-b* to contig NW_001334655.1 which was assembled as part of the sea urchin genome project, we observed that these two genes (*GLEAN3_00439* and *GLEAN3_00438*, respectively) lie directly adjacent to one another (Fig. 2.1A), though they are transcribed in opposite directions. *Sp-p58-a* contains 7 exons and encodes a 526 amino acid protein, and *Sp-p58-b* contains 6 exons and encodes a 639 amino acid protein. We identified a predicted signal sequence at the N-terminus of each protein, and each protein contains a single predicted transmembrane domain near its C-terminus. Both proteins are basic and are relatively rich in proline, glycine, and threonine residues (Tekaia and Yeramian, 2006). We cloned orthologs of *p58-a* and *p58-b* from *L. variegatus*, a species that diverged from *S. purpuratus* approximately 100 million years ago (Smith *et al*., 2006). *Lv-p58-a* and *Lv-p58-b* are very similar to their *S. purpuratus* orthologs*;* ClustalW alignments showed that Sp-P58-A and Lv-P58-A are 81% identical (Fig. 2.1B), and Sp-P58-B and Lv-P58-B are 91% identical (Fig. 2.1C). Comparisons between P58-A and P58-B within each species showed that the two paralogs are less well conserved than the orthologous pairs; the former are approximately 34% identical and 16% similar (Fig. 2.1D and data not shown).

2.4.2 *p58-a* and *p58-b* mRNAs are restricted to PMCs

We analyzed the patterns of expression of *p58-a* and *p58-b* in *S. purpuratus* (Fig. 2.2) and *L variegatus* (Fig. 2.3) by WMISH. In both species, *p58-a* and *p58-b* were expressed only by PMCs. *Sp-p58-a* and *Sp-p58-b* transcripts were not detectable by WMISH prior to hatching (Figs. 2.2A, 2.2B, 2.2I and 2.2J). Both mRNAs were first detectable at the hatched blastula stage, when they were expressed in the presumptive PMCs (Figs. 2.2C, 2.2K), which form a ring around the small micromeres at the vegetal pole (Figs. 2.2C, 2.2K inserts). *Sp-p58-a* and *Sp-p58-b* were expressed in ingressed PMCs at the mesenchyme blastula stage (Fig. 2.2D, 2.2L) and uniformly in the PMC syncytium during gastrulation (Figs. 2.2E, 2.2F and 2.2M). The level of *Sp-p58-b* declined from the late gastrula stage to the prism stage (Figs. 2.2N, 2.2O) and the mRNA was almost undetectable in pluteus larvae (Fig. 2.2P). *Sp-p58-a* was expressed at high

levels at the prism stage (Fig. 2.2G). In the pluteus larva, this mRNA was enriched in PMCs in the scheitel (Fig. 2.2H).

The patterns of expression of *Lv-p58-a* and *Lv-p58-b* were very similar to their *S. purpuratus* orthologs. *Lv-p58-a* and *Lv-p58-b* were undetectable by WMISH prior to hatching (Fig. 2.3A, 2.3B, 2.3I and 2.3J). At the hatched blastula stage, *Lv-p58-a* was expressed in presumptive PMCs (Fig. 2.3C, insert), while *Lv-p58-b* was not detectable at this stage (Fig. 2.3K). *Lv-p58-a* and *Lv-p58-b* mRNAs were restricted to PMCs at the mesenchyme blastula stage (Fig. 2.3D, 2.3L) and were expressed uniformly within the PMC ring during gastrulation (Figs. 2.3E, 2.3F, 2.3M and 2.3N). *Lv-p58-a* was expressed at high levels at the prism stage (Fig. 2.3G), and at the pluteus larva stage, was still detectable and appeared to be expressed uniformly in the PMC syncytium (Fig. 2.3H), unlike *Sp-p58-a* which is enriched in the scheitel at the pluteus stage (Fig. 2.2 H). *Lv-p58-b* mRNA, on the other hand, was not detectable by WMISH at the prism stage or in the pluteus larva (Figs. 2.3O, 2.3P). We noted that at all developmental stages at which the two mRNAs were expressed, *p58-b* was expressed at lower levels than *p58-a*, a difference particularly obvious in *L. variegatus* embryos.

2.4.3 Knockdown of *p58-a* or *p58-b* causes defects in skeletogenesis in *S. purpuratus*.

We blocked the expression of *p58-a* and *p58-b* in *S. purpuratus* and *L. variegatus* with MOs. Because information on exon/intron boundaries in *S. purpuratus* is available from the genome assembly, we used splice-blocking MOs in this species. Splice-blocking MOs are advantageous because it is possible to assess their efficacy by RT-PCR. We designed the *Sp-p58-a* MO to target the exon 3/intron 3 boundary (Fig. 2.4A). This MO was injected at concentrations of 1 mM, 2 mM, and 4 mM. We extracted RNA from 200 embryos that were injected with MO at each of these concentrations, and RT-PCR analysis was conducted using forward and reverse primers that were located in exon 2 and exon 4, respectively. RT-PCR analysis showed that there was a significant decrease in the normal splice form in *Sp-p58-a* MO-injected embryos (Fig. 2.4B, black arrow). In addition, a band approximately 350 nucleotides larger than the normal splice form appeared in samples extracted from MO-injected embryos (Fig. 2.4B, red arrow). This larger splice variant was cloned and sequenced, and was shown to have resulted from the inclusion of intron 3, which is 348 nucleotides in length. Inclusion of this intron alters the coding

sequence of SpP58-A and introduces a premature stop codon. Embryos injected with 4 mM *Sp-p58-a* MO showed the greatest reduction in the normal splice form of *Sp-p58-a* without any loss in viability (Fig. 2.4F), and we therefore used this concentration for further experiments. We noted, however, that at all concentrations of *Sp-p58-a* MO, low levels of the normal splice form persisted.

We designed the *Sp-p58-b* MO to be complementary to the exon 2/intron 2 boundary (Fig. 2.4C). This MO was also tested at concentrations of 1 mM, 2 mM, and 4 mM, and RNA was extracted from 200 embryos for RT-PCR analyses using forward and reverse primers that were located in exons 1 and 3, respectively. We noted that at all three concentrations tested, there was a marked decrease in the level of the normal splice form of *Sp-p58-b* (Fig. 2.4D, black arrow). We also noted the appearance of two different splice variants, both smaller in size than the control splice form (Fig. 2.4D). Both of these bands were cloned and sequenced, and this analysis showed that the smallest splice form, which was an estimated 1100 nucleotides smaller than the control splice form (Fig. 2.4D, blue arrow), was a splice variant that completely lacked exon 2, which is 1110 nucleotides in length. The larger splice variant (Fig. 2.4D, red arrow) contained approximately the first 700 nucleotides of exon 2, apparently as a consequence of the mobilization of an internal splice site. In both cases, the deletions caused changes in the reading frame of *Sp-p58-b* and introduced premature stop codons. Because injection of 4 mM *Sp-p58-b* MO sometimes resulted in non-specific, toxic effects, we used a concentration of 2 mM for all experiments.

We found that knockdown of either *Sp-p58-a* and *Sp-p58-b* caused defects in skeletogenesis. *Sp-p58-a* morphants had visibly truncated skeletal elements (Figs. 2.4F, 2.4I, 2.4L), though triradiate spicule rudiments were visible at the gastrula stage (data not shown). Morphant embryos had a well-developed gut and numerous pigment cells, and a reduction in the length of the skeletal rods was the only apparent defect (Fig. 2.4F). We noted that the length and complement of skeletal rods varied among embryos, even within a single batch, though no morphant embryo had fully elongated rods (Table 2.1). Out of 301 embryos scored, only 1% had no visible skeletal elements. Interestingly, 15.3 % of the morphant embryos had only body rods, a phenotype that has not been described following the knockdown of other biomineralization proteins. We also noted that several embryos had severe bifurcations and trifurcations at the tips

of the body rods (unpublished data). The vast majority of embryos, 78.7%, had shortened skeletal elements (Table 2.1).

Although *Sp-p58-b* is expressed at lower levels than *Sp-p58-a*, *Sp-p58-b* morphants exhibited a more severe phenotype. When control embryos had reached the pluteus stage, the skeleton of most *Sp-p58-b* morphants consisted of only two, granular deposits of birefringent material (Figs. 2.4J, 2.4M) that were located approximately where the triradiate spicule rudiments would ordinarily form. These deposits were not triradiate in shape, but rather rod-shaped (Fig. 2.4J) or rectangular (Fig. 2.4M). Though there were no elongated skeletal rods in *Sp-p58-b* morphants, cells that appeared to be PMCs were visible by differential interference contrast (DIC) microscopy and these cells were linked to each other by filopodial cables in the stereotypical pattern of the PMC syncytium. *Sp-p58-b* morphants did not exhibit any other developmental defects (Figs. 2.4G, 2.4M). Out of 304 *Sp-p58-b* morphant embryos scored, 10% formed no skeletal elements (Table 2.1). 57.9% formed unbranched skeletal rudiments, and another 21.4% formed abnormal, branched skeletal rudiments (Table 2.1). As with *Sp-p58-a* morphants, no *Sp-p58-b* morphants had a wild-type skeleton. *Sp-p58-a* and *Sp-p58-b* morphant embryos both had a more rounded shape than sibling control embryos, as a secondary consequence of defects in skeletal rod elongation (Figs. 2.4F, 2.4L, 2.4G and 2.4M).

2.4.4 Double knockdown of *Sp-p58-a* and *Sp-p58-b* almost completely blocks skeletogenesis

Because knockdowns of *Sp-p58-a* and *Sp-p58-b* individually impaired skeletal development, we concluded that these two proteins are not completely redundant despite their striking structural similarity. It is possible, however, that P58-A and P-58B have similar biochemical functions *in vivo* and that, in the absence of either protein, the other is capable of supporting skeletogenesis, albeit in a compromised fashion. This could explain our finding that skeletogenesis was partially, but not completely suppressed, in both *Sp-p58-a* and *Sp-p58-b* morphants.

To explore the possibility that the proteins have partially overlapping functions, we tested whether a double knockdown of both *Sp-p58-a* and *Sp-p58-b* would result in a more complete inhibition of skeletal development. We injected embryos with a solution that contained both the *Sp-p58-a* and *Sp-p58-b* MOs, each at a concentration of 2 mM. The skeletal defects that we

observed were more severe than for a single knockdown of either Sp-P58 protein, although most double knockdown embryos still produced small skeletal elements. In 300 double knockdown embryos scored, 35.3% had no skeletal elements, a percentage higher than for *Sp-p58-a* or *Sp-p58-b* morphant embryos, of which only 1% and 10.9% of morphants formed no skeletal elements, respectively (Table 2.1). 47.7% of double morphant embryos had unbranched skeletal rudiments (Figs. 2.5B, 2.5D, 2.5F, Table 2.1). Unlike *Sp-p58-b* morphants, which had symmetrical rudiments, *Sp-p58-a/Sp-p58-b* double knockdown embryos often had a single, tiny skeletal rudiment (data not shown). Double knockdown of *Sp-p58-a* and *Sp-p58-b* therefore resulted in a more complete suppression of skeletogenesis than either single knockdown, a finding which is consistent with the view that the proteins act in an additive fashion to mediate skeletogenesis. The fact that some skeletal material was still deposited in most double knockdown embryos might suggest that P58-A and P58-B do not play a role in the initiation of spicule deposition; more likely, however, this finding reflects the fact that our MOs were not 100% effective at blocking the expression of these proteins.

2.4.5 Knockdowns of *p58-a* and *p58-b* cause skeletal defects in *L. variegatus*.

We found that the amino acid sequences of Lv-P58-A and Lv-P58-B were very similar to those of their *S. purpuratus* homologs (Fig. 2.1). To validate the functional studies that we carried out in *S. purpuratus*, and to test whether P58-A and P58-B have similar roles in other species, *p58* knockdown experiments were also carried out in *L. variegatus*. We designed an *Lv-p58-a* translation-blocking MO and injected this into fertilized eggs at a concentration of 0.5 mM. *Lv-p58-a* morphants exhibited a phenotype that was very similar to that of *Sp-p58-a* morphants. In these embryos, most major skeletal rods were present and their arrangement appeared relatively normal, though these rods were severely truncated (Figs. 2.6B, 2.6F). *Lv-p58-b* morphants also had a phenotype that resembled *S. purpuratus* morphants. Embryos that were injected with an *Lv-p58-b* translation blocking MO at a concentration of 0.1 mM had severely perturbed skeletons; >90% of these embryos formed only two small deposits of skeletal material (Figs. 2.6C, 2.6G). *Lv-p58-a* and *Lv-p58-b* morphants showed no visible developmental defects that were unrelated to the extension of skeletal rods (Figs. 2.6B and 2.6C).

We also tested the effect of a knockdown of both *p58* genes in *L. variegatus* by injecting fertilized eggs with a solution that contained *Lv-p58-a* and *Lv-p58-b* MOs at concentrations of 0.5 mM and 0.1 mM, respectively. In this experiment also, the phenotypes of *L. variegatus* embryos closely resembled those of *S. purpuratus* embryos after a similar perturbation. *Lv-p58-a/Lv-p58-b* double morphant embryos formed only very small deposits of skeletal material that were visible under polarized light (Figs. 2.6D, 2.6H). As with double knockdown embryos in *S. purpuratus*, we observed some cases in which only one granule of skeletal material was visible in these double knockdown embryos (data not shown). These functional studies, carried out in two sea urchin species using MOs with different characteristics (e.g., splice-blocking versus translation-blocking) and different sequences, show that *p58-a* and *p58-b* both play important roles in skeletogenesis, although *p58-b* may have a more critical function.

2.4.6 P58-A and P58-B do not regulate PMC specification or migration

Because skeletal morphogenesis was clearly perturbed following knockdown of *p58-a* and/or *p58-b*, we tested whether PMCs were specified and migrated correctly under these conditions. At the late gastrula stage (Figs. 2.7A-H), we used P19, which is expressed only by PMCs, as a differentiation marker (Illies *et al*., 2002). We found that PMCs were specified correctly both in *Sp-p58-a* and *Sp-p58-b* morphants (Figs. 2.7B, 2.7F, 2.7C and 2.7G). WMISH analysis showed that Sp-P19 was expressed on schedule and in a pattern similar to that observed in control embryos. It was also evident that PMCs in morphant embryos were arranged in a stereotypical, subequatorial ring pattern. The two ventrolateral clusters of the sub-equatorial ring were clearly visible and were connected by oral and aboral chains of PMCs (Figs. 2.7F, 2.7G). There were also no observable defects in PMC specification and migration in *Sp-p58-a*/*Sp-p58-b* double knockdown embryos, and the subequatorial PMC ring appeared to be patterned normally in these morphants (Figs. 2.7D, 2.7H). We also examined the organization of PMCs late in development (i.e., at the pluteus larva stage) using the monoclonal antibody 6a9, which recognizes a family of PMC-specific surface glycoproteins (Figs. 2.7I-2.7T). In pluteus larvae, skeletal elements are highlighted with this antibody, which stains the PMC filopodial cables that surround the skeletal rods (Fig. 2.7A). *Sp-p58-a* knockdown embryos exhibited 6A9 immunostaining in the filopodial cables and PMC cell bodies associated with the skeletal rods that were present (Fig. 2.7J), in a manner similar to control embryos (Fig. 2.7I). Unlike *Sp-p58-a* morphants which have relatively

well defined skeletal elements (Figs. 2.4I, 2.7N), *Sp-p58-b* morphants deposit very small amounts of skeletal material (Figs. 2.4J, 2.7O). In *Sp-p58-b* morphants at the pluteus stage, we found that although there were no extended skeletal rods (as indicated by the black arrows in Fig. 2.7O), PMCs were localized in a pattern that was indistinguishable from that observed in control embryos and *Sp-p58-a* morphants. Thus, in *Sp-p58-b* morphants, PMCs pattern themselves correctly at later stages of development even in the absence of skeletal rods (Figs. 2.7K, 2.7O, 2.7S). This was also the case in *Sp-p58-a/Sp-p58-b* double knockdown embryos (Figs. 2.7L, 2.7P, 2.7T).

We assayed the presence and location of PMCs in *L. variegatus p58* morphants at the gastrula stage. 6a9 immunostaining showed that PMCs were present in *Lv-p58-a* and *Lv-p58-b* morphants and these cells formed a sub-equatorial ring with two ventrolateral clusters that were joined by oral and aboral chains of PMCs (Figs. 2.8B, 2.8J, 2.8C, 2.8K). We also determined that PMCs were correctly specified and patterned in *Lv-p58-a/Lv-p58-b* double knockdown embryos (Figs. 2.8D, 2.8L). At the pluteus larva stage, control embryos clearly showed 6a9 immunostaining throughout the skeleton, with PMC cell bodies positioned along the extended skeletal rods (Figs. 2.8M, 2.8U). The PMC syncytium was clearly visible in *Lv-p58-a* and *Lv-p58-b* morphants (Figs. 2.8N, 2.8O). PMC cables and cell bodies were found in locations similar to the location of PMCs in control embryos, though skeletal rods were severely shortened in *Lv-p58-a* morphants (Figs. 2.8R, 2.8V), and only small deposits of biomineral were present in *Lv-p58-b* morphants (Figs. 2.8S, 2.8W). We observed similar results for *Lv-p58-a/Lv-p58-b* double knockdown embryos, (Figs. 2.8P, 2.8T, 2.8X). Thus, we detected no defects in the specification and migration of PMCs in *p58* knockdown embryos, either in *S. purpuratus* or *L. variegatus*.

2.4.7 P58-A and P58-B do not regulate PMC fusion

PMC fusion may be required in order to produce an expansive, "privileged" extracellular space within which spicule elongation can occur (Wilt and Ettensohn, 2007). We used a dye-transfer assay to test the ability of individual PMCs to undergo fusion following knockdown of *p58-a* or *p58-b*. 2 to 6 PMCs were removed from an *Lv-p58-a* morphant embryo that had been labeled with fluorescein dextran and transplanted into a host embryo that had been injected with *Lv-p58-a* MO without dextran (see Materials and Methods). It was shown previously that in control

embryos, PMCs that contain dextran transfer the label to cells throughout the syncytium as a consequence of cell fusion (Hodor and Ettensohn, 1998; 2008). We observed in 7 out of 7 cases that dextran-labeled PMCs from *Lv-p58-a* morphants fused with PMCs of the unlabeled host embryo, as indicated by the spread of the dextran throughout the PMC syncytium (Figs. 2.9A, 2.9E). All host embryos also displayed the characteristic *Lv-p58-a* knockdown phenotype of severely shortened skeletal rods (Fig. 2.9C). This experiment was repeated for *Lv-p58-b* morphant embryos, in which case 13 out of 13 embryos showed fusion of dextran-labelled cells with the host PMC syncytium (Figs. 2.9B, 2.9F). 12 out of these 13 embryos showed the morphant phenotype of greatly reduced skeletal deposits (Fig. 2.9D). These studies strongly suggest that P58-A and P58-B are not required for PMC fusion in the sea urchin embryo. They are consistent with our observation that extensive filopodial cables form in morphant embryos, even in areas where no spicule material is deposited.

2.5 Discussion

The embryonic skeleton of the sea urchin is the primary determinant of the overall shape of the late embryo and the larva. This complex anatomical structure is secreted by specialized, biomineral-forming cells (PMCs), the activities of which are tightly regulated by cues provided by overlying epithelial cells (Wilt and Ettensohn, 2007). Based upon the recent elucidation of the PMC GRN, and a large body of work concerning the cell biological and embryological basis of skeletogenesis in the sea urchin, it should soon be possible to develop a relatively complete understanding of the genomic regulatory control of this major morphogenetic process. This, in turn, will provide a basis for understanding the genomic and embryological changes that have accompanied the evolutionary modification of skeletal development within the echinoderms, a phylum that exhibits remarkably diverse patterns of skeletogenesis. An important component of this analysis will be the identification and functional analysis of proteins that play direct roles in each of the various phases of skeletal morphogenesis, including biomineral deposition. Although numerous proteins have been implicated in biomineralization based upon patterns of expression and/or conserved sequence features, few studies have demonstrated the functional importance of specific, candidate biomineralization proteins; e.g., by gene knockdown approaches (Peled-Kamar *et al*., 2002; Cheers and Ettensohn, 2005 ; Wilt *et al*., 2008b).

We have shown that two novel PMC-specific proteins, P58-A and P58-B, play essential roles in skeletogenesis. Knockdown of the genes encoding either protein using splice-blocking or translation-blocking MOs impairs biomineral deposition but does not affect PMC specification, ingression, directional migration, or fusion. Our findings therefore indicate that P58-A and P58-B function as terminal biomineralization proteins. The critical role of these proteins in biomineralization has been conserved for at least 100 million years; i.e., the approximate divergence time between *L. variegatus* and *S. purpuratus* (Smith *et al*., 2006). An analysis of the regulatory control of biomineralization genes has identified some of the transcriptional inputs into *p58-a* and *p58-b*; for example, both genes receive a positive input from *ets1* and neither is regulated by *t-brain*, but only *p58-a* receives a positive input from *alx1* (Rafiq *et al.,* 2012). Despite the similarities between P58-A and P58-B, MO knockdown studies indicate that the two proteins are not fully redundant. In both species that we have examined, MO knockdown of

either P58-A or P58-B leads to an inhibition of skeleton deposition. Knockdown of P58-B, however, consistently results in a more severe suppression of skeleton deposition. Perhaps paradoxically, WMISH data indicate that *p58-b* is expressed at noticeably lower levels than *p58-a* throughout development. This observation is supported by recent QPCR studies which show that the number of *Sp-p58-a* transcripts/cell is approximately 10 times greater than the number of *Sp-p58-b* transcripts/cell (Rafiq *et al.*, 2012). The high level of *p58-a* transcripts may make it more difficult to completely suppress gene function using MOs, at least at MO concentrations that do not cause a loss of embryo viability. Indeed, our RT-PCR analysis indicated that a greater proportion of the targeted transcript was spliced normally in the presence of the *Sp-p58-a* splice-blocking MO than in the case of the *Sp-p58-b* splice-blocking MO (Fig. 2.4). It is also possible, however, that despite their similar sequences and their different levels of mRNA expression, *p58-B* plays a more critical role in biomineral deposition than does *p58-A*.

P58-A and P58-B are novel proteins and their sequences provide few clues concerning their biochemical function(s). Both proteins contain an N-terminal signal sequence and a single transmembrane domain. Several basic residues lie immediately C-terminal to the transmembrane domain and probably function as a stop-transfer signal. This organization suggests that P58-A and P58-B are synthesized on the rough endoplasmic reticulum and enter the secretory pathway as single-pass, Type I transmembrane proteins. Support for this view also comes from the finding that a GFP-tagged form of P58-A is localized primarily within the plasma membrane (Ettensohn, unpublished observations). With the exception of Lv-P58-A, the P58 proteins have extremely short cytoplasmic domains that consist of only the basic, stop-transfer sequence. It therefore seems very likely that the much larger ectodomain plays an important role in the function of these proteins. One possibility is that the P58 ectodomain is released from the membrane by proteolysis and incorporated directly into the biomineral. A recent mass spectrophotometric analysis of the proteome of purified spicules has identified more than 200 proteins, including P58-A, P58-B, and several other transmembrane proteins that have large ectodomains (Mann *et al*., 2010b). It has been proposed that the ectodomains of many of these proteins are cleaved by matrix metalloproteases, which are also abundant in the spicule matrix. The same study also identified a number of cytoplasmic proteins, such as ribosomal proteins and translation factors, in purified spicules, and therefore some artifactual redistribution of proteins might have occurred

during sample preparation. Nevertheless, these findings support a model which suggests that at some stage in the secretory pathway, the ectodomains of P58-A and P58-B are cleaved, and are later released into the extracellular space and incorporated into the biomineral. The mass of the spicule is overwhelmingly mineral (mostly $CaCO_3$, in the form of calcite), but the small amounts of occluded proteins are thought to play a critical role in regulating the assembly and physical properties of the material (Wilt and Ettensohn, 2007). We can only speculate concerning the possible function of the P58 ectodomain in biomineralization; for example, it might play a role in stabilizing amorphous calcium carbonate or in converting it to a crystalline state, or it might function in regulating the transport of calcium or other biomineralization proteins inside the cell (Politi *et al*., 2008; Wilt *et al*., 2008a).

The phenotypes of *p58-a* and *p58-b* morphants are reminiscent of those observed following MO knockdown of P16, another novel protein involved in biomineralization (Cheers and Ettensohn, 2005). Like P58-A and P58-B, P16 is a Type I transmembrane protein with an N-terminal signal sequence and a C-terminal transmembrane domain (Illies *et al*., 2002). Also like the P58 proteins, P16 has apparently undergone recent duplication, as this gene is clustered near several very closely related genes (Livingston *et al*., 2006). The ectodomain of P16, however, appears quite different from that of P58; it is acidic and contains a high proportion of serine and aspartate residues. As in the case of P58-A and P58-B, MO knockdown of P16 greatly suppresses, but does not completely block, the deposition of biomineral. There may be technical reasons for this, such as the incomplete knockdown of the target proteins. It seems very likely, however, that the many genes that mediate biomineralization have overlapping and therefore partially redundant functions. Further work is necessary though to distinguish between the possible modes of function of the P58 proteins and their interactions, if any, with other genes involved in biomineralization.

Although biomineralization evolved independently in echinoderms and vertebrates, the genes that encode secreted biomineralization proteins have undergone extensive duplication in both taxa. Whole genome duplication as well as local, tandem gene duplications have been important in the evolution of several families of extracellular biomineralization proteins in vertebrates (reviewed by Kawasaki *et al*., 2009). In sea urchins, members of the spicule matrix, MSP130, and P16 protein families are found in small clusters (Livingston *et al*., 2006). Higher order

clustering of these genes is probably obscured by the relatively small size of the scaffolds in the current *S. purpuratus* genome assembly. In the present study, we have found that P58-A and P58-B lie side by side in the genome. Although the exon-intron organization of these genes are not identical (Fig. 2.1A), their similar amino acid sequences and tandem arrangement indicate that either *p58-a* or *p58-b* arose as a duplication of the other gene (Hahn, 2009). This hypothesis is also supported by the observation that P58-A and P58-B have similar, yet non-redundant roles, a trademark of duplicated genes (Innan and Kondrashov, 2010). The duplication of the ancestral *p58* gene clearly predated the last common ancestor of *L. variegatus* and *S. purpuratus*. A more complete reconstruction of the evolutionary history of the *p58* genes, and of the other sea urchin biomineralization genes, will be possible once additional echinoderm genome assemblies become available.

A) Schematic of P58-A and P58-B location on Contig NW_001334655.1.

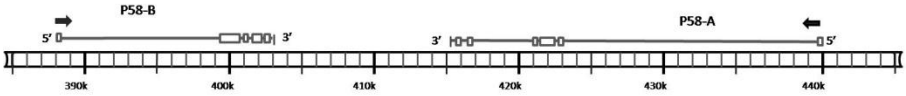

B)

```
Sp P58-A    1 MGVIFYLYTIALYAMLATLSQAQRAQ----APLDTTGKEFVFAFQSNFQNKR  47
Lv P58-A    1 MEGVFYLYTIVLCAMLYTLSQAQPARPGPAPLDTTGKEFVFAFQSNFQNKR  50
              *  .***** *.***.****** *.   **********************

Sp P58-A   48 PDKLSLLIGANEPGLTRVQIEAPNFNWQQTVQLQHKQVRNVDINPDVAAR  97
Lv P58-A   51 PDRLTLLLGANEPGLTRVQVEAPNFNWQQTVQLQHKQVRQVDLNPDIAAR 100
              **.*.**.***********.********************.**.***.***

Sp P58-A   98 GAGPVNGTLIVRATKDVSISGLNSLTMTNDAFLAIPTHGLQQEYYVASYD 147
Lv P58-A  101 GAGPVNGTLIVRATKDISVHGLNSLTMTNDAFLAIPTHGLQEAYFVASYD 150
              ****************.*. ********************. *.*.*****

Sp P58-A  148 PVPIEMSQFLITGIQPDTSVKIVLQARLQHNSQWYSKGQTLTVNVGKYQS 197
Lv P58-A  151 PVPIEMSQFLITGIQPDTTVKIVLQARLQHNSQWYSKGQTLTVNVGKYQS 200
              ******************.**********************************

Sp P58-A  198 IQFQSQEDLTGTKITSTKPLSVMSGASCTLVPTQVYRCDHLVEHLPPFNT 247
Lv P58-A  201 IQFQSQEDLTGTRITSTKPISVMSGASCTLVPTQVYRCDHLVEHLPPFNT 250
              ************.*******.**********************************

Sp P58-A  248 WGKRFTLLPFSNRSGGFIFRIIAGRPSTTVHIMGNNVQLQFEGSFREFNQ 297
Lv P58-A  251 WGKRFTLLPFSNRSGGFIFRIIAGRPSTTVHIMGNNVQLQFEGSFREFNQ 300
              **************************************************

Sp P58-A  298 PASLKTTLQSDKPIMVVQYAKGMQKDNNGDPFMTLIPPVEQYMEKEITFG 347
Lv P58-A  301 PASLKTTLQSDKPIMVVQYAKGMQKDNNGDPFMTLIPPVEQYMQKEITFG 350
              **************************************************

Sp P58-A  348 SFNQSGTDMLNMFAGVSFTSPALFTMSLNGKPAFEPSTGIPGTGISRTFT 397
Lv P58-A  351 SFNQSGTDMLNMFAGVSFTSPALFTMSLNGKSSFEPDQGIPGTGISSTFT 400
              ********************************.***  ******** ***

Sp P58-A  398 ADATVPLDDVRNILTNYEKDVREMAVIYGFASGTSFGYPAAYQLRQLTCT 447
Lv P58-A  401 ADSTIPLDNIRNILTNYEKDVHYMAIVYGFASGTSFGYPAAYQLRQITCT 450
              **.*.*** .***********..**..********************.***

Sp P58-A  448 RPGRQGPEAEYDCPETHRRPRPTAPVVPVGPGGGGDGAAMTGCTSKGVVV 497
Lv P58-A  451 RPGRQGPEAEFECPDSHRRPRPTAPVVPVGPGGGGR-LGGEGCTSKGVVV 499
              **********..**..********************.     *********

Sp P58-A  498 LAAILPALIVFIIMVIILVFVLYRMR------RKF                 526
Lv P58-A  500 LAAILPALIVFIIMVIILVFVLYRTPSTPELQKFKMFFRVNPRERTISRC 549
              ************************        .**

Sp P58-A  527          526
Lv P58-A  550 SFVRNGSL 557
```

C)

```
Sp P58-B    1 MGNLLVLAAVLLQFIGFATPQQAPYLPSNSPTFTVGSPDTRGTKFMFAMP  50
Lv P58-B    1 MGNLLVLSAVLLQYIGYATPQQAPYLPANAPTFNLGSPDTRGTKFMFAIP  50
              *******.******.**.**********.*.***..*************.*

Sp P58-B   51 SNFNVASKVTLMIGSSNPGIARVMVNIPGFKFRREITLTQRQMKTISIPG 100
Lv P58-B   51 SNFNIPSKVTLMIGSSNPGIARVMVNIPGFKFRREITLTQRQMKTISIPG 100
              ****. **********************************************

Sp P58-B  101 NVAANGGGPQNGTIVVTSNLEITVHAANIMPKTNDAFVAIPTDALGKEYV 150
Lv P58-B  101 NVAANGGGPQNGTIVVTSNLEITVHAANIMPKTNDGFVAIPTDAVGKEYV 150
              ********************************** ********.*****

Sp P58-B  151 IASYDIVTGQWSVFTITGTQQGTRIQVVPSQRTLHARQWYNPGQIINIQL 200
Lv P58-B  151 IASYDIVTGQWSVFTITGTQQGTRIQVVPSQRILHARQWYNAGQIINVQL 200
              ********************************** ******* *****.**

Sp P58-B  201 NEAQSIQIRAPMDLTGTYITADKPVAVVSGATCTRVPKDMQRCDHLVEML 250
Lv P58-B  201 SEAQSVQFRCPDDLTGTYITADKPVAVVSGATCTRVPRSMQRCDHLVEML 250
               ****.* *.* ************************. **********

Sp P58-B  251 PPISALGTRFSIVPLLNRTGYVFRMIAARPNTRVHMAGVIYTLGQRGSFR 300
Lv P58-B  251 PPISTLGTRFSVLPLLNRTGYVFRMIAARPNTKVHLAGTIYTLGQRGSFR 300
              ****.*******..*******************.**.** ***********

Sp P58-B  301 EFNQDAQLPVTITSNRPLLVMQYGKGMDIDFWGDPFMSIVPPVEQYMEGM 350
Lv P58-B  301 EFNQDAQLPVTITSNRPLLVMQYGKGMDVNFWGDPFMSIVPPVEQYMEGM 350
              ****************************. ********************

Sp P58-B  351 TTFGPLAQSGQDRFFSFLSVSVTSADLYTISLDNVLIMNTELNLPLGSET 400
Lv P58-B  351 TTFGPLAQSGQDMFFNFLSVSVTSAYLYTISLNNVLIMNTELNLPEMEET 400
              *********** ** ********* ****** ***********   **

Sp P58-B  401 IRYTADRNMRIQNIPHTLHNPSLMSRFTAICHGVSQGSGYGYPIGYNLRT 450
Lv P58-B  401 IRYTADRNMKIQNVPHTLHNPSVMSRFTAICHGVSQGSGYGYPIGYNLRT 450
              *********.***.********.**************************

Sp P58-B  451 LLCSRTDPMTGLIEEFQCPPPIPPIVPGLVPSNVPGMGGNQPIRPGLGMG 500
Lv P58-B  451 LLCSRTDPMTGLIEEFQCPPPIPPIQPGLIPSTVPGMGGNQPIRPGVGMN 500
              ************************ ***.**.************.**.

Sp P58-B  501 -GMGGYGGGYGGMYPGFTTGGQPGGYLPGNFFTGGKALNPNIPILPGLPI 549
Lv P58-B  501 PGMGGFGVGMG-MFPGFSAGGQPGAFLPGNFFTGGKALPPNIPIIPGLPI 549
               ****.* * * *.***..***** .************ *****.*****

Sp P58-B  550 DPNAGAAQTQPGFNNNPLNPVSPNNPFANPGQPFVPMLPFNPMGPGMIPP 599
Lv P58-B  550 DPNAGAAQTQPGFNNNPLNPVSPNNPFANPGQPFVPMLPFNPMGPGMIPP 599
              **************************************************

Sp P58-B  600 PENCYTLGLLILAAVAPVTVVFIVMLVILLAIVYRFKRKN 639
Lv P58-B  600 PENCYTLGLLILAAVAPVTVVFIVMLVILLAIVYRFKRKH 639
              ***************************************.
```

D)

```
Sp P58-A    1 MGVIFYLYTIALYAMLATLSQAQRAQAP----------LDTTGKEFVFAFQ  40
Sp P58-B    1 MGNLLVLAAVLLQFIGFATPQQAPYLPSNSPTFTVGSPDTRGTKFMFAMP  50
              *  .  *.  *   .  .  *    *            ** *  *.**

Sp P58-A   41 SNFQNKRPDKLSLLIGANEPGLTRVQIEAPNFNWQQTVQLQHKQVRNVDI  90
Sp P58-B   51 SNFN---VASKVTLMIGSSNPGIARVMVNIPGFKFRREITLTQRQMKTISI  98
              ***.     *..*.**.  **..** .  *.*  .. . * ..*.... *

Sp P58-A   91 NPDVAARGAGPVNGTLIVRATKDVSISGLNSLTMTNDAFLAIPTHGLGQE 140
Sp P58-B   99 PGNVAANGGGPQNGTIVVTSNLEITVHAANIMPKTNDAFVAIPTDALGKE 148
                 *** * ** ***..* .. ....   * .  *****.****  **.*

Sp P58-A  141 YYVASYDPVPIEMSQFLITGIQPDTSVKIVLQARLQHNSQWYSKGQTLTV 190
Sp P58-B  149 YVIASYDIVTGQWSVFTITGTQQGTRIQVVPSQRTLHARQWYNPGQIINI 198
              * .**** *  . * * *** *  * ...*   *  *  ***  ** ...

Sp P58-A  191 NVGKYQSIQFQSQEDLTGTKITSTKPLSVMSGASCTLVPTQVYRCDHLVE 240
Sp P58-B  199 QLNEAQSIQIRAPMDLTGTYITADKPVAVVSGATCTRVPKDMQRCDHLVE 248
              ...  **** ..  ***** **. **..*.***.** **  . *******

Sp P58-A  241 HLPPFNTWGKRFTLLPFSNRSGGFIFRIIAGRPSTTVHIMGNNVQLQFEG 290
Sp P58-B  249 MLPPISALGTRFSIVPLLNRTG--YVFRMIAARPNTRVHMAGVIYTLGQRG 297
               ***  . * **...*  **.* ..**.** ** * **. *    *   *

Sp P58-A  291 SFREFNQPASLKTTLQSDKPIMVVQYAKGMQKDNNGDPFMTLIPPVEQYM 340
Sp P58-B  298 SFREFNQDAQLPVTITSNRPLLVMQYGKGMDIDFWGDPFMSIVPPVEQYM 347
              ******* * *  *. * .*..*.** ***  *  *****...*******

Sp P58-A  341 EKEITFGSFNQSGTDMLNMFAGVSFTSPALFTMSLNGKPAFEPSTGIPGT 390
Sp P58-B  348 EGMTTFGPLAQSGQDRFFSFLSVSVTSADLYTISLDNVLIMNTELNLPLG 397
              *   ***   *** *    *  ** **  *.*.** .        ..*

Sp P58-A  391 GISRTFTADATVPLDDVRNILTNYEKDVRFMAVIYGFASGTSFGYPAAYQ 440
Sp P58-B  398 SETIRYTADRNMRIQNIPHTLHNPSLMSRFTAICHGVSQGSGYGYPIGYN 447
               .  .*** .. .  . . * *     ** *.  * . *. .*** *.

Sp P58-A  441 LRQLTCTR-------------------------------PGRQG-------- 453
Sp P58-B  448 LRTLLCSRTDPMTGLIEEFQCPPPIPPIVPGLVPSNVPGMGGNQPIRPGL 497
              ** * *.*                              **  *

Sp P58-A  454 ------------------------P---------------------------- 454
Sp P58-B  498 GMGGMGGYGGGYGGMYPGFTTGGQPGGYLPGNFFTGGKALNPNIPILPGL 547
                                      *

Sp P58-A  455 ------------EAEYDCPETHRRP---------RPTAPVVPVGPGGGGDG 484
Sp P58-B  548 PIDPNAGAAQTQPGFNNNPLNPVSPNNPFANPGQPFVPMLPFNPMGPGMI 597
                          * .  *        .*  *..* .* * *

Sp P58-A  485 AAMTGCTSKGVVVLAAILPALIVFIIMVIILVFVLYRMRRKF 526
Sp P58-B  598 PPPENCYTLGLLILAAVAPVTVVFIVMLVILLAIVYRFKRKN 639
                .* . *...***. *  .***.*..**. ..** .**
```

Figure 2.1: Analysis of *p58-a* and *p58-b* gene organization in *S. purpuratus* and comparisons of the predicted amino acid sequences of the P58-A and P58-B proteins in *S. purpuratus* and *L. variegatus*. (A) Schematic of the exon-intron structures of *Sp-p58-a* and *Sp-p58-b* and their locations on Contig NW_001334655.1. (B) ClustalW alignment of the amino acid sequences of P58-A from *S. purpuratus* and *L. variegatus*. (C) ClustalW alignment of the amino acid sequences of P58-B from *S. purpuratus* and *L. variegatus*. (D) ClustalW alignment of amino acid sequences of P58-A and P58-B from *S. purpuratus*. Signal sequences are shown in red, and transmembrane sequences are shown in blue and underlined. Asterisks indicate identical amino acids, and dashes indicate conserved amino acids.

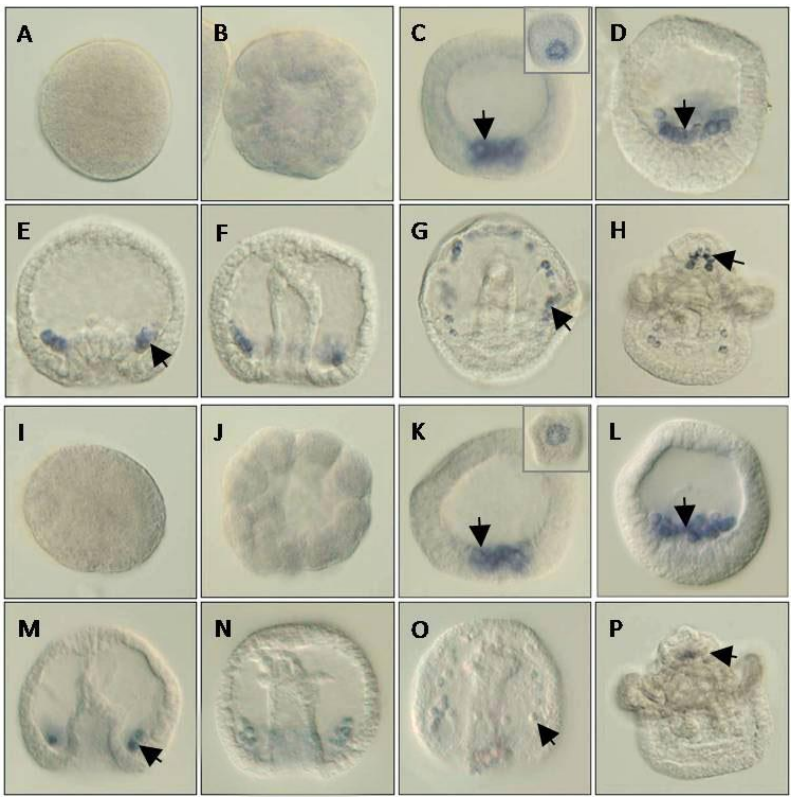

Figure 2.2: Whole mount *in situ* hybridization analysis of *p58-a* (A-H) and *p58-b* (I-P) expression in *S. purpuratus*. Expression of *p58-a* is undetectable prior to hatching (A, B). Staining is visible after hatching and is restricted to PMCs throughout later development (arrows, C-H). Expression of *p58-b* is also undetectable prior to hatching (I, J), but is apparent in PMCs from hatching until at least the late gastrula stage (arrows, K-N), after which time expression is significantly reduced (O, P). (A, I) Unfertilized egg. (B, J) Cleavage stage. (C, K) Hatched blastula. (D, L) Mesenchyme blastula. (E, M) Early gastrula. (F, N) Late gastrula. (G, O) Prism. (H, P) Pluteus larva.

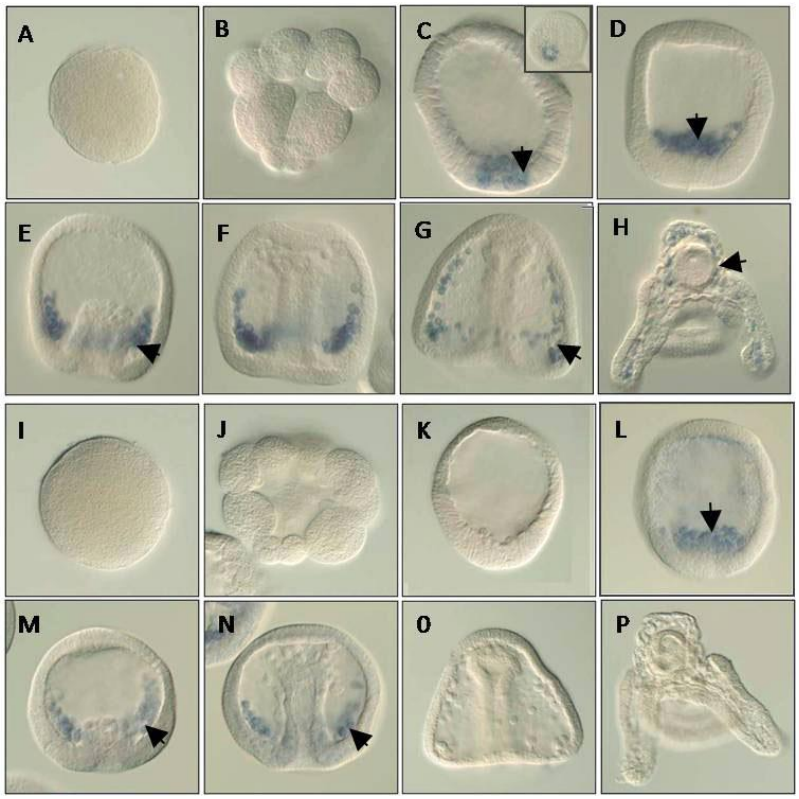

Figure 2.3: Whole mount *in situ* hybridization analysis of *p58-a* (A-H) and *p58-b* (I-P) expression in *L. variegatus*. Expression of *p58-a* is undetectable prior to hatching (A,B). Staining is visible after hatching and is restricted to PMCs throughout later development (arrows, C-H). Expression of *p58-b* is undetectable in stages prior to PMC ingression (I-K). Expression is apparent from the mesenchyme blastula stage through the late gastrula stage (arrows, L-N), after which expression decreases to undetectable levels (O-P). (A, I) Unfertilized egg. (B, J) 16-cell stage. (C, K) Hatched blastula. (D, L) Mesenchyme blastula. (E, M) Early gastrula. (F, N) Late gastrula. (G, O) Prism. (H, P) Pluteus larva.

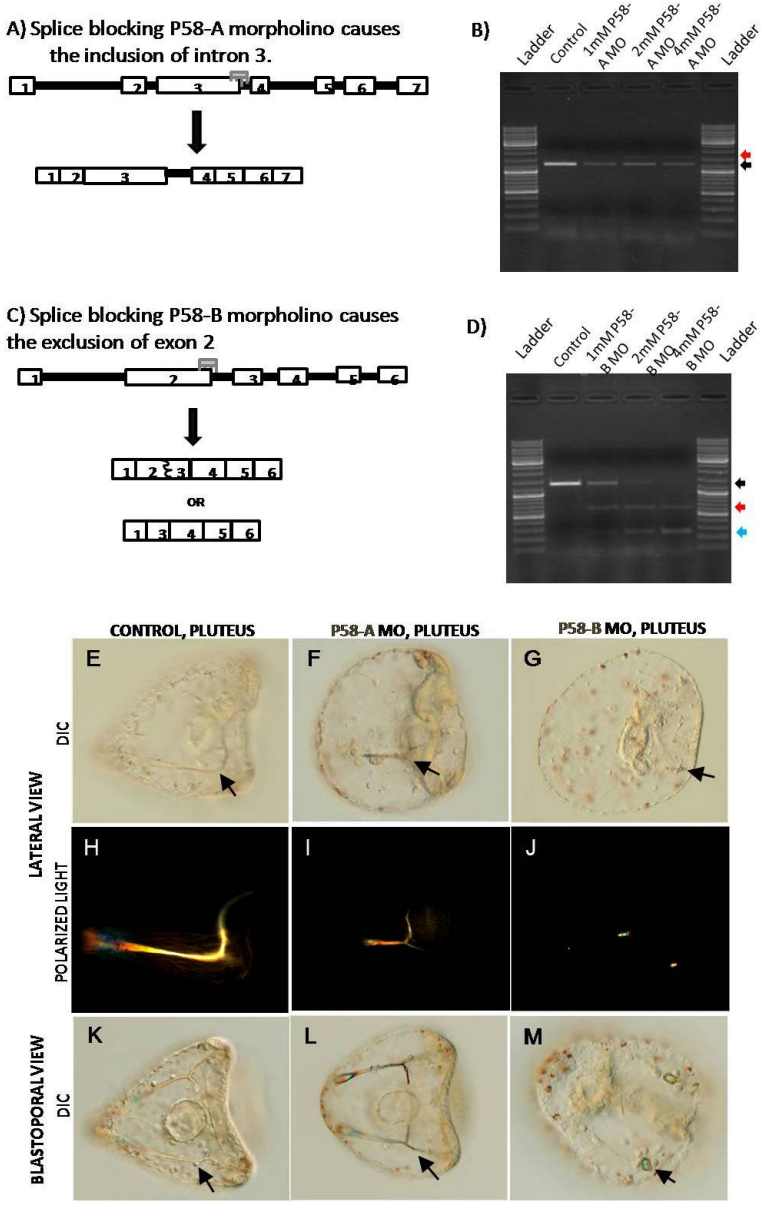

Figure 2.4: Knockdown of P58-A and P58-B in *S. purpuratus* using splice-blocking morpholinos (MOs) suppresses skeletogenesis. (A) Schematic of the design of *Sp-p58-a* splice-blocking MO. (B) Agarose gel showing the depletion of the correctly spliced form of *Sp-p58-a* (black arrow), and the accumulation of a larger, misspliced variant that contains intron 3 (red arrow). (C) Schematic of the design of *Sp-p58-b* splice-blocking MO. (D) Agarose gel showing the depletion of the correctly spliced form of *Sp-p58-b* (black arrow) and the accumulation of two misspliced variants that lack part or all of exon 2 (red and blue arrows, respectively). (E-G) DIC and (H-J) polarized light images of lateral views of control and morphant embryos at the pluteus stage. (K-

M) DIC images of blastoporal views of control and morphant embryos at the pluteus stage. (E, H, K) Control embryos. (F, I, L) *p58-a* morphants. (G, J, M) *p58-b* morphants. Skeletal elements (arrows) are reduced in P58 morphant embryos, and this effect is most pronounced in the case of P58-B morphants.

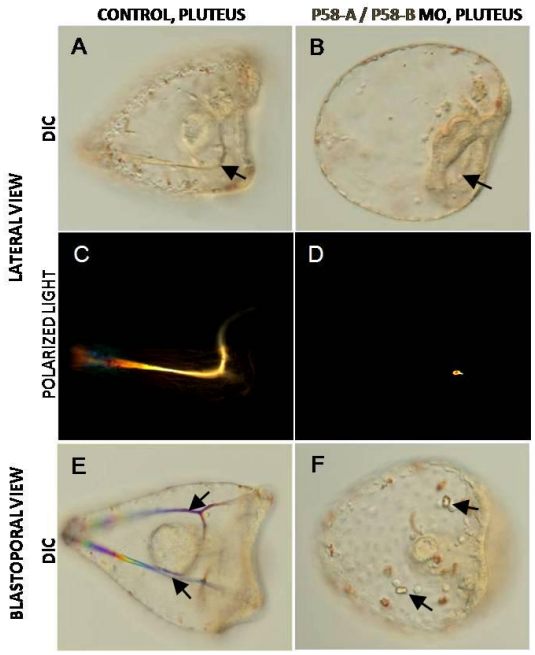

Figure 2.5: Double knockdown of *p58-a* and *p58-b* in *S. purpuratus* almost completely suppresses skeletogenesis. (A, B) DIC and (C, D) polarized light images of lateral views of control and morphant embryos. (E,F) DIC images of blastoporal views of control and morphant embryos. (A, C, E) Control embryos. (B, D, F) *p58-a/p58-b* morphants. In most double knockdown embryos at the pluteus stage, no skeletal elements, or only one or two tiny granules of birefringent material (arrows), are present.

	P58-A Morphants (301 embryos)		P58-B Morphants (304 embryos)		P58-A / P58-B Morphants (300 embryos)	
	#	%	#	%	#	%
No Skeletal Elements	3	1.0	33	10.9	106	35.3
Unbranched Skeletal Rudiments	0	0.0	**176**	**57.9**	**143**	**47.7**
Branched Skeletal Rudiments	15	5.0	65	21.4	36	12.0
Body Rods Only	46	15.3	1	0.3	9	3.0
Shortened Skeletal Rods	**237**	**78.7**	29	9.5	6	2.0
Wild Type Skeleton	0	0.0	0	0.0	0	0.0

Table 2.1: Distribution of morphant phenotypes in *S. purpuratus.* Bold type indicates prevalent phenotype.

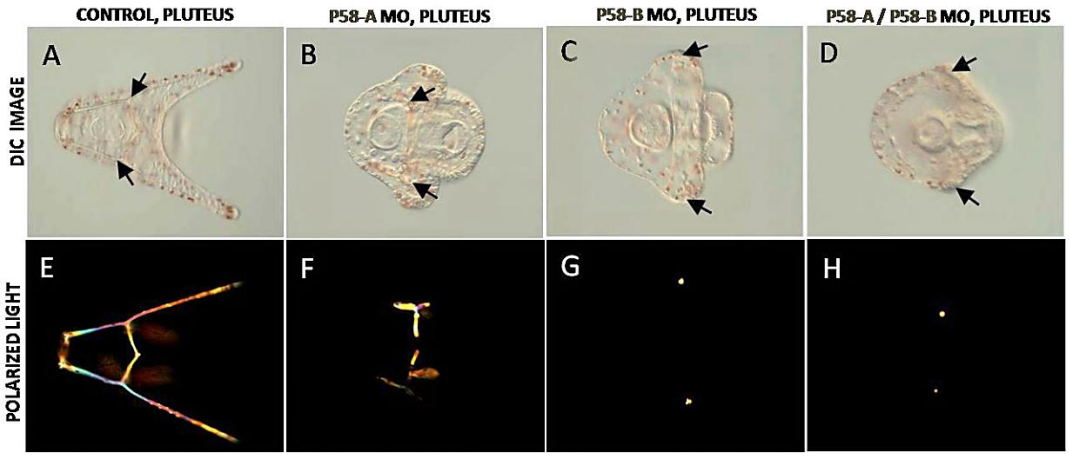

Figure 2.6: Knockdown of *p58-a* or *p58-b* inhibits skeletogenesis in *L. variegatus*. (A-D) DIC and (E-H) polarized light images of control and morphant embryos. Blastoporal views of control embryos (A, E), *p58-a* morphants (B, F), *p58-b* morphants (C, G), and *p58-a / p58-b* morphants (D, H) at the pluteus stage. Skeletal elements (arrows) are reduced in *p58* morphant embryos, this effect is more pronounced in the case of *p58-b* morphants than in *p58-a* morphants.

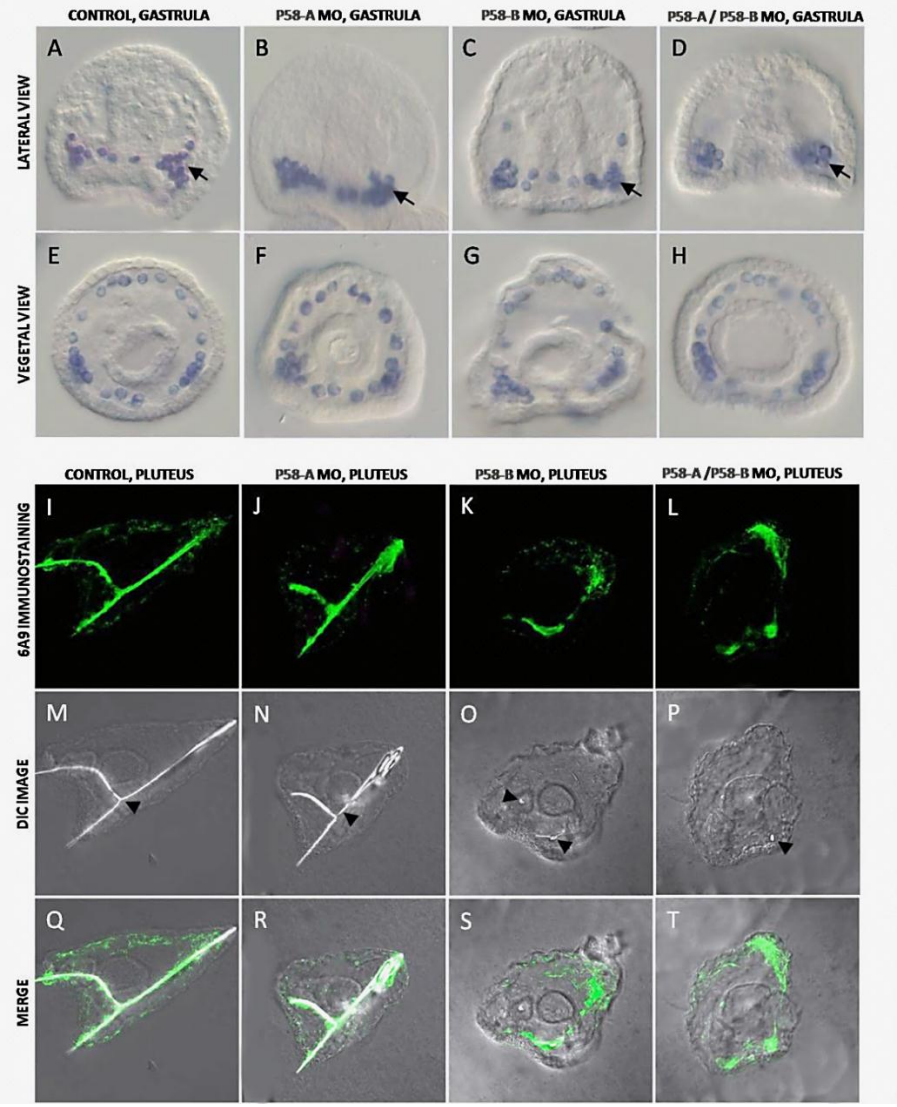

Figure 2.7: Knockdown of *p58-a* and *p58-b* does not inhibit PMC specification or migration in *S. purpuratus*. (A-H) Whole mount in situ hybridization with a *p19* probe, showing the distribution of PMCs (arrows) at the gastrula stage. (A-D) Lateral view and (E-H) ventral views of control (A, E), *p58-a* morphants (B, F), *p58-b* morphants (C, G), and *p58-a/p58-b* double knockdown embryos (D, H). The number and distribution of PMCs are similar in control and morphant embryos. The expression of *p19*, a late marker, suggests that the specification of the PMCs is unaffected. At the pluteus stage (I-T), 6a9 immunostaining which recognizes MSP130 proteins, shows comparable PMC positioning in control embryos (I, M, Q,), *p58-a* morphants (J, N, R), *p58-b* morphants (K, O, S), and *p58-a/p58-b* double knockdown embryos (L, P, T), even in the absence of well-formed skeletal elements. Skeletal elements are indicated by arrowheads.

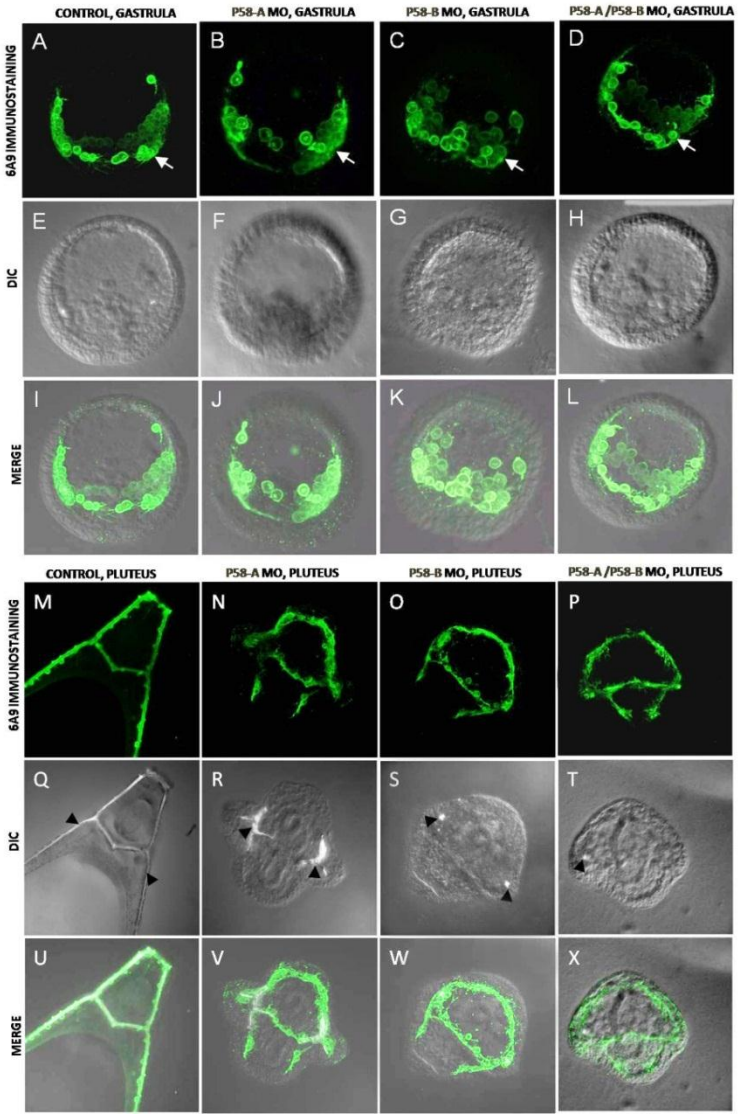

Figure 2.8: Knockdown of *p58-a* and *p58-b* does not inhibit PMC specification or migration in *L. variegatus*. 6a9 immunostaining reveals the presence and location of PMCs (arrows) at the gastrula stage (A-L). Fluorescence (A-D), DIC (E-H), and merged (I-L) images show comparable positioning of PMCs in *L. variegatus* control embryos (A, E, I), P58-A morphants (B, F, J), P58-B morphants (C, G, K), and *p58-a/p58-b* double knockdown embryos (D, H, L). At the pluteus stage (M-X), PMCs and filopodial cables (arrowheads) are present in comparable positions in control embryos (M, Q, U), *p58-a* morphants (N, R, V), *p58-b* morphants (O, S, W), and *p58-a/p58-b* double knockdown embryos (P, T, X), even in the absence of well-formed skeletal elements (arrowheads). The expression of MSP130 proteins, which are recognized by the 6a9 antibody, suggests that the specification of the PMCs is unaffected.

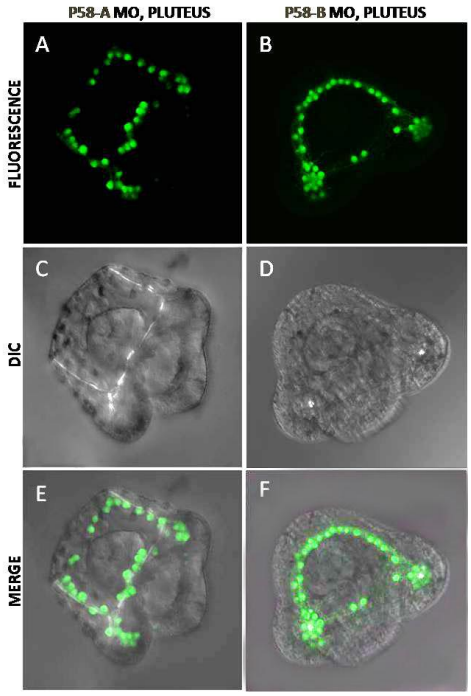

Figure 2.9: PMC fusion is not perturbed in *p58-a* (A, C, E) and *p58-b* (B, D, F) morphants. Fluorescence (A, B), DIC (C, D), and merged (E, F) images of unlabeled, morpholino-injected *L. variegatus* embryos into which a small number of PMCs from a dextran-labeled, morpholino-injected embryo were introduced. PMCs in *p58-a* and *p58-b* morphants are fusion-competent, as indicated by the diffusion of dextran throughout the PMC syncytium.

Chapter 3

VEGF Signaling Plays Multiple Roles in the Migration and Differentiation of Primary Mesenchyme Cells in the Sea Urchin Embryo

3.1 Abstract

Growth factor signaling pathways provide essential migration and differentiation cues to mesoderm cells during embryonic development in many metazoans. Recent studies have implicated the VEGF and FGF pathways in providing guidance and differentiation cues to primary mesenchyme cells (PMCs) during skeletogenesis in the sea urchin embryo, though their relative contributions to these processes and the mechanisms by which they act are presently unknown.

In this chapter, we show that in the sea urchin *Lytechinus variegatus,* FGF and VEGF ligands are expressed in distinct domains in the embryonic ectoderm. As previously shown in in *Paracentrotus lividus,* PMC migration is disrupted in *Lv-vegf*3 morphants and these embryos fail to form skeletal elements. Unlike in *P. lividus,* however, PMC migration is unaffected in *Lv-fgfa* morphants and well-patterned but shortened skeletal elements form. We show by using the VEGFR inhibitor axitinib that VEGF signaling is essential not just for the initial phase of PMC migration (subequatorial ring formation), but also for the late phase (migration toward the animal pole). However, VEGF signaling is not required for PMC fusion. Additionally, the inhibition of VEGF signaling after the completion of PMC migration causes significant defects in skeletogenesis, selectively blocking the elongation of specific skeletal rods. Nanostring nCounter analysis of ~100 genes in the PMC gene regulatory network shows a decrease in the expression of many genes with proven or predicted roles in biomineralization upon blocking the VEGF pathway. These results lead to a better understanding of the role played by growth factors in gastrulation and skeletogenesis.

3.2 Introduction

Growth factor signaling pathways play essential roles in diverse developmental processes ranging from early axis specification and patterning to germ layer formation, morphogenesis and organogenesis (Hogan, 1999; Wilson and Leptin, 2000; Wu and Hill, 2009; Dorey and Amaya, 2010). Recent studies have shown that one essential function of growth factor signaling is to regulate the migration and differentiation of the embryonic mesoderm during gastrulation. In *Drosophila* embryos, mesoderm formation is primarily regulated by the fibroblast growth factor (FGF) pathway. FGF signaling by the ligands *pyramus* and *thisbe*, which are expressed in the ectoderm, regulate the intercalation and spreading of mesoderm cells, which express the FGF receptor *heartless*. FGF signaling later regulates the directional migration of differentiated mesoderm cells (Kadam *et al*., 2009; McMahon *et al*., 2010; Winklbauer and Muller, 2011; Reim *et al*., 2012). A similar role is played by the platelet-derived growth factor (PDGF) pathway during *Xenopus* gastrulation, where the ligand PDGF-A, expressed in the ectoderm, regulates cell orientation and migration in mesoderm cells expressing the receptor PDGFR-α (Ataliotis *et al*., 1995; Nagel *et al*., 2004; Damm and Winklbauer, 2011; Winklbauer and Muller, 2011). The FGF pathway also plays a role in *Xenopus* gastrulation by regulating the migration and differentiation of the dorsal mesoderm (Amaya *et al*., 1993; Isaacs *et al*., 1994). The migration of mesoderm cells away from the primitive streak in the gastrulating chick embryo is regulated by N-cadherin through the PDGF pathway (Yang *et al*., 2008; Chuai and Weijer, 2009), while the FGF4 and FGF8 ligands directionally regulate cell migration by acting as attractants and repellants, respectively (Yang *et al*., 2002; Lunn *et al*., 2007; Chuai and Weijer, 2009). Additionally, in the mouse embryo, FGF signaling regulates the migration of ingressed mesoderm cells and the formation of paraxial mesoderm (Sun *et al*., 1999; Ciruna and Rossant, 2001; Boulet and Capecchi, 2012).

Gastrulation in the sea urchin is characterized by the directional migration of mesoderm cells known as primary mesenchyme cells (PMCs), which produce the embryonic endoskeleton (Reviewed in Wilt and Ettensohn, 2007). PMCs, after undergoing an epithelial-to-mesenchymal transition (EMT), migrate directionally within the blastocoel by means of dynamic filopodia to form two dense clusters of cells referred to as the ventro-lateral clusters (VLCs) at stereotypical locations along the blastocoel wall. The two VLCs are connected by oral and aboral chains of

PMCs to form the sub-equatorial ring. The PMCs fuse as they migrate, forming a single continuous syncytium within which the elaborate calcium carbonate endoskeleton is secreted. Specific cues from the ectoderm of the embryo regulate not only the migration and differentiation of the PMCs, but also the structure of the resulting endoskeleton (Ettensohn and McClay, 1986; Ettensohn, 1990; Hardin *et al*., 1992; Armstrong *et al*., 1993, Ettensohn and Malinda, 1993; Guss and Ettensohn, 1997). However, relatively few genes expressed in the ectoderm have been identified to directly play a role regulating PMC behavior (Di Bernardo *et al*., 1999; Cavalieri *et al*., 2003, Duloquin *et al*., 2007; Rottinger *et al*., 2008; Cavalieri *et al*., 2011).

Recent work has pointed to two pathways- mediated by VEGF and FGF, respectively- in controlling the directional migration of PMCs and the formation of the embryonic skeleton (Duloquin *et al*., 2007; Rottinger *et al*., 2008). Duloquin *et al*. (2007) identified the expression of a VEGF receptor (VEGFR-10-Ig) in migrating PMCs in the sea urchin *Paracentrotus lividus,* and a VEGF ligand (VEGF3) expressed in the ectoderm overlying the ventro-lateral clusters of PMCs. Perturbation of VEGF signaling in this system led to defects PMC migration and skeletogenesis. Rottinger *et al*. (2008) identified a similar pattern of expression of FGFA and one FGF receptor (FGFR2) in *P. lividus*, and showed that blocking the FGF pathway also led to defects in skeletogenesis. These studies suggest that FGF and VEGF signaling both have essential (and non-redundant) functions in mesoderm cell migration and skeletogenesis in the sea urchin, and further suggest that the two pathways might regulate the same specific steps in PMC morphogenesis.

In this study, we aimed to dissect the specific contributions of the VEGF and FGF pathways during the process of skeletogenesis in the sea urchin embryo. We used two-color, fluorescent in situ hybridization to show that in *Lytechinus variegatus,* FGF and VEGF ligands are expressed in transiently overlapping, but mostly distinct domains in the ectoderm. We showed that the knockdown of *Lv-vegf3* caused defects in the migration and differentiation of PMCs, while PMC migration was unperturbed in *Lv-fgfa* morphants, which formed truncated skeletal elements. Using a second-generation VEGFR inhibitor (axitinib), we found that the critical period for VEGF signaling is post PMC-ingression, and that VEGF signaling is essential for all aspects of PMC migration. Importantly, we identified a role for VEGF signaling in skeletogenesis that can

be separated from its effects on PMC migration, and we found that VEGF signaling also plays a role in regulating the expression of several genes in the PMC gene regulatory network. This study consequently expands our knowledge of the regulation of mesoderm migration and differentiation by growth factor signaling pathways.

3.3 Materials and Methods

Embryo Culture

Adult *Lytechinus variegatus* were obtained from the Duke University Marine Laboratory (Beaufort, NC, USA) or from Reeftopia, Inc. (Key West, FL, USA). Adult *Strongylocentrotus purpuratus* were obtained from Pat Leahy (California Institute of Technology, Pasadena, CA, USA). Spawning was induced by intracoelomic injection of 0.5 M KCl and embryos were cultured in artificial seawater (ASW) at 23°C (*L. variegatus*) or 15°C (*S. purpuratus*).

Cloning of *L. variegatus vegf3, fgfa, otp* and *pax2/5/8*

Partial sequences for *Lv-fgfa* and *Lv-vegf3* were obtained by polymerase chain reaction (PCR) using degenerate primers. Forward and reverse primers for *Lv-fgfa* were 5'-CAYGARGAYGGNACNATHAAYGG-3" and 5'-GGDATRAAYTGNGCYTTYTTYTG-3' respectively. Forward and reverse primers for *Lv-vegf3* were 5'-CGTGTGGTGGAYTCGTACGAGGAGCTG-3" and 5'-GGCACTTGCAGGTRCACTCGCTG-3' respectively. Full length *Lv-vegf3* and 3' *Lv-fgfa* sequences were obtained by performing RACE on *L. variegatus* late gastrula cDNA using the GeneRacer Kit with SuperScript III RT and the Zero Blunt TOPO PCR Cloning Kit for Sequencing (Invitrogen, Grand Island, NY, USA). 5' and 3' RACE primers used for *Lv-vegf3* were 5'-CTGCACCCGTGCCCTCTCATCCTCAA-3' and 5'-GGAGCTGGGCATCCCCAGAGGGTAT-3' respectively. The 3' RACE primer used for *Lv-fgfa* was 5'-GTCGCAGAGGCGGAGTATTGTTTCCAT-3'. 5' sequence for *Lv-fgfa* was obtained by screening an *L. variegatus* mid-gastrula cDNA library (a kind gift from Dr. David McClay, Duke University, NC, USA) using partial sequence obtained from degenerate PCR as a probe. Genbank accession numbers for *L. variegatus Lv-fgfa* and *Lv-vegf3* are XXXXXXXX and XXXXXXXX respectively. Comparisons of the sequences of VEGF3 and FGFA from *L. variegatus, S. purpuratus* and *Paracentrotus lividus* were carried out using ClustalW (Thompson *et al*., 1994).

Lv-pax2/5/8 primers (forward: 5'-GATAGAATTCGCCAGCACGTTGTCGA-3', reverse: 5'-GCAGTCTAGATGTGGCGATATCACCC-3') were designed using partial gene sequence available through the Baylor College of Medicine Sea Urchin Genome Project, and the gene fragment obtained by PCR was cloned into the pCS2+ vector using the EcoR1 and Xba1

restriction sites. *Lv-otp* primers (forward: 5'-GGTCGAATTCATGGAGCGAACTCTAG -3', reverse: 5'- GGCATC TAGACT AAAGATTCCCATTGA -3') were designed using full length gene sequence available on GenBank and cloned into the pCS2+ vector using the EcoR1 and Xba1 restriction sites.

Whole Mount In Situ Hybridization (WMISH)

Embryos were fixed for 1 hr at room temperature in 4% paraformaldehyde in ASW, washed twice in ASW, and stored at 4°C in 100% methanol. WMISH was carried out as described elsewhere (Lepage *et al*., 1992, Duloquin *et al.*, 2007). Fluorescent WMISH (F-WMISH) was carried out by making modifications to the conventional WMISH protocol as described in Sharma and Ettensohn (2010). *Lv-fgfa, Lv-vegf3, Lv-otp* and *Lv-pax2/5/8* WMISH probes were synthesized using sequences obtained as described above. *Sp-p19* probe was synthesized as described elsewhere (Adomako-Ankomah and Ettensohn, 2011).

Microinjection of Morpholino Antisense Oligonucleotides (MOs)

Microinjections were carried out as described in Cheers and Ettensohn (2004). Injection solutions contained 20% (vol/vol) glycerol and 0.16% (wt/vol) Texas Red dextran. MOs were obtained from Gene Tools, LLC (Philomath, OR, USA). *Lv-fgfa* splice-blocking MO was designed to be complementary to the exon 2/intron 2 boundary (sequence: 5'-TAATAAACCCTACTTACGTTTCCGT-3') as described by Rottinger *et al*. (2008), and was injected at concentrations of 2 mM and 4 mM. *Lv-fgfa* translation blocking MO was designed to be complementary to the 5' UTR of the mRNA (sequence: 5'-GTCGCACACAGACGATGTCCAACGC-3'), and was injected at a concentration of 4 mM. *Lv-vegf3* and *Sp-vegf3* translation blocking MOs were designed to overlap with the start codon of the respective mRNAs (sequences: 5'-TCGACTGAAGGTCCCATCGTGCTTT-3' and 5'-GGCTGAGTGCCCCATCGTGCTTCAA-3' respectively). Both MOs were injected at concentrations of 2 mM.

RT-PCR Analysis

RT-PCR analysis was performed as previously described (Adomako-Ankomah and Ettensohn, 2011). Forward and reverse primers for *Lv-fgfa* were 5'-

GGTTGCATAGCTGGAGCCCAATGA-3' and 5'-CCTTTTGTTGGTGCTGTCTGGCATC-3', respectively, and PCR products were cloned into the pCR4-TOPO vector (Invitrogen, Grand Island, NY, USA) for sequencing.

Axitinib (AG013736) Treatments

A stock solution of the VEGFR inhibitor axitinib (Selleckchem, Houston, TX, USA) was made to a concentration of 5 mM in DMSO, and stored at -20ºC. Embryos were cultured in ASW containing the axitinib at final concentrations of 75 nM (*L. variegatus*) or 50 nM (*S. purpuratus*). Control embryos were cultured in DMSO at concentrations commensurate to the volume of axitinib added to cultures.

Immunofluorescence

Immunofluorescence was carried out using the 6a9 monoclonal antibody as described in Ettensohn and McClay (1988). Immunostained embryos were examined using a Zeiss LSM 510 Meta/UV DuoScan Inverted Spectral Confocal Microscope.

Apoptosis Assay

The terminal dUTP nick end labeling assay (TUNEL) was carried out using the ApoAlert DNA Fragmentation Assay Kit (Clontech Laboratories Inc, Mountain View, CA, USA) as described in Voronina and Wessel (2001), with the following modifications: Prior to nuclear labeling, embryos were incubated at 4ºC overnight in full-strength 6e10 primary antibody (Ingersoll, 1993) to label the primary mesenchyme cells (PMCs). Embryos were then washed 3 times in PBS (10 min each) and incubated in a rhodamine-conjugated goat-anti-mouse IgG secondary antibody (Jackson ImmunoResearch Laboratories Inc., West Grove, PA, USA) at a 1:25 dilution in PBS for 1 hr at room temperature. Embryos were washed 3 times in PBS and treated with 0.2 mg/ml Hoechst stain in PBS for 5 min at room temperature, washed 3 times in PBS, mounted in a 1:1 2.55 DABCO (1,4-Diazabicyclo[2.2.2]octane) in PBS: glycerol solution, and observed by confocal microscopy as described above.

PMC Fusion Assay

PMC fusion was monitored by dye transfer, as described in detail in Hodor and Ettensohn (2008). One set of *L. variegatus* fertilized eggs was injected with a solution of *Lv-vegf3* MO that

contained 10% (wt/vol) fluorescein dextran, while another set of fertilized eggs was injected with a solution of the same MO that lacked the dextran. At the mesenchyme blastula stage, 2-6 PMCs were transferred from dextran-labeled donor embryos into each unlabeled host embryo. Embryos were observed by confocal microscopy 6 and 24 hr post-surgery to assess the distribution of the dextran within the PMC syncytium.

PMC Migration Assay

To assess the ability of PMCs in axitinib- and DMSO-treated (control) embryos to target to the vegetal region of the embryo, PMCs were scattered throughout the blastocoel at the mesenchyme blastula stage using microsurgical methods (Ettensohn and McClay, 1988). Embryos were cultured at 23ºC for 5 hr post-surgery and then fixed in 4% paraformaldehyde for 1 hour, washed twice in ASW, and post-fixed in 100% methanol for 20 min. The distribution of PMCs in the blastocoel was assayed by immunofluorescence as described above.

Analysis of Filopodia Extension

To analyze filopodial dynamics in vivo, embryos were treated with either 75 nM axitinib or DMSO from early cleavage. At the mesenchyme blastula stage, PMCs were scattered in the blastocoel as described above; in addition, approximately half of all PMCs were flushed out of the blastocoel. These manipulations were carried out to reduce cell density, thereby facilitating the unambiguous identification of all filopodial processes extended by individual PMCs. Embryos were cultured at 23ºC for 1.5 hours post-surgery, and then fixed and stained with the monoclonal antibody 6a9. The presence and relative lengths of filopodia were analyzed by confocal microscopy and the NIH ImageJ software.

Assay of Gene Expression using the Nanostring nCounter Analysis System

Changes in gene expression levels were assayed using the Nanostring nCounter analysis system (Nanostring Technologies, Seattle, WA, USA) as described by Geiss *et al*., (2008). For each experiment, RNA was extracted from 200 control and 200 axitinib-treated or VEGF morphant *S. purpuratus* embryos using the Nucleospin RNA II kit (Clonetech Laboratories Inc, Mountain View, CA, USA). The code set of probes used was designed to measure the levels of expression

of genes in the PMC gene regulatory network. A complete list of the probes in this code set is included in the supplementary data.

3.4 RESULTS

3.4.1 FGF and VEGF ligands are expressed in largely independent domains in the ectoderm

Previous research concerning the roles of VEGF and FGF signaling in sea urchin gastrulation was conducted in the species *P. lividus* (Duloquin *et al*., 2007; Rottinger *et al*., 2008). To further analyze the functions of these signaling pathways, we first cloned homologs of the *vegf3* and *fgfa* ligands in *L. variegatus*, a North American species. ClustalW analyses (Thompson *et al*., 1994) comparing the protein sequences of these ligands in three species of sea urchin; *L. variegatus, S. purpuratus* and *P. lividus*, showed that among these species, the VEGF3 and FGFA ligands are 70% and 80% identical, respectively (Fig. S3.1).

To characterize in detail the expression domains of *Lv-fgfa* and *Lv-vegf3* in relation to each other, we performed F-WMISH to compare their expression patterns in single embryos at different stages of development. *Lv-fgfa* and *Lv-vegf3* were detectable by F-WMISH from the hatched blastula stage (Fig. 3.1A-A’’’), at which time *Lv-fgfa* was expressed in a ring in the ectoderm in a domain spanning the equator of the embryo and in the presumptive PMCs at the vegetal pole. *Lv-vegf3* at this stage was also expressed in a ring in the ectoderm, but in a territory more vegetal to, and not overlapping with, *Lv-fgfa*. This separation of expression domains persisted at the mesenchyme blastula stage, though at this stage the expression of both genes was restricted to the ectoderm overlying the VLCs (Fig. 3.1B-B’’’). As the archenteron began to invaginate, the expression domains of *Lv-fgfa* and *Lv-vegf3* in the ectoderm overlapped slightly (Fig. 3.1C-C’’’), and this overlap persisted as the archenteron elongated (Fig. 3.1D-D’’’). At the late gastrula stage, *Lv-fgfa* and *Lv-vegf3* expression domains ceased to overlap (Fig. 3.1E-E’’’); *Lv-vegf3* continued to be expressed in the ectoderm overlying the ventro-lateral clusters of PMCs (Fig. 3.1E’), while *Lv-fgfa* was downregulated in these domains and was expressed mostly in two apical domains of ectoderm and in the PMCs (Fig. 3.1E). *Lv-fgfa* expression in prism stage embryos was largely restricted to the PMCs, while *Lv-vegf3* expression persisted in the ectoderm adjacent to these cells (Fig. 3.1 F-F’’’). At the pluteus stage, *Lv-vegf3* was expressed in the ectoderm overlying the elongating postoral rods and in the oral hood, and *Lv-fgfa* was expressed in the PMCs surrounding the postoral rods and also in the gut (Fig. 3.1G-G’’’). Additionally, we

analyzed the expression patterns of the receptors *vegfr-10-Ig* and *fgfr-2* in *L. variegatus* (Appendix Figs. 1, 2), and found that these genes were expressed selectively by PMCs in patterns identical to those reported previously in *P. lividus* (Duloquin *et al*., 2007; Rottinger *et al*., 2008).

3.4.2 VEGF signaling plays a more prominent role than FGF signaling in PMC migration and skeletogenesis in *L. variegatus*

To compare the functions of FGF and VEGF signaling in *L. variegatus*, we knocked down the *Lv-vegf3* and *Lv-fgfa* ligands using MOs. We observed that skeletogenesis was almost completely blocked in embryos injected with 2 mM *Lv-vegf3* translation-blocking MO (Fig. 3.2B, B') when compared to control embryos (Fig. 3.2A, A'), a phenotype very similar to that observed in *P. lividus* (Duloquin *et al*., 2007). However, unlike results obtained in *P. lividus* (Rottinger *et al*., 2008), skeletogenesis was not eliminated in embryos injected with 2 mM splice-blocking *Lv-fgfa* MO, and these morphants formed extensive, although truncated, skeletons (Fig. 3.2C, C'). We noted that embryos injected with as much as 4mM *Lv-fgfa* MO also formed skeletal elements (Fig. 3.2D'), even though these embryos showed effects of toxicity due to the high concentrations of MO injected (Fig. 3.2D). We designed the *Lv-fgfa* splice-blocking MO to overlap the exon 2-intron 2 boundary, leading to the exclusion of exon 2, which contained the highly conserved FGF domain (Fig. 3.2E). This was the same splice-blocking strategy used by Rottinger *et al*. (2008). We assayed the effectiveness of the MO by RT-PCR analysis on 200 control embryos and 200 embryos injected with 1 mM, 2 mM, or 4 mM *Lv-fgfa* MO, and observed a shift in the size of the *Lv-fgfa* transcript corresponding to an exclusion of exon 2 in embryos injected with all concentrations of FGF MO (Fig. 3.2F, bright bands). The exclusion of this exon was confirmed by sequencing. We also confirmed the *Lv-fgfa* knockdown phenotype by injecting embryos with an *Lv-fgfa* translation-blocking MO, and these morphants likewise formed bilaterally symmetrical, truncated skeletal elements (Fig. S3.2B, D).

We then examined the location of PMCs in *Lv-vegf3* and *Lv-fgfa* morphants by immunostaining using the 6a9 monoclonal antibody. At the late gastrula stage, PMCs in control embryos were arranged in a sub-equatorial ring with ventro-lateral clusters (VLCs) (Fig. 3.3A, arrow). PMCs in

Lv-vegf3 morphants at this stage did not form VLCs, and were located mostly in the vegetal hemisphere of the embryo (Fig. 3.3B, B'). PMCs in *Lv-fgfa* morphants at the late gastrula stage formed a well-patterned ring comparable to control embryos (Fig. 3.3C, C'). At the pluteus stage, PMCs in control embryos were aligned along a well-developed skeleton (Fig. 3.3D, D'), while PMCs in *Lv-vegf3* morphants were randomly distributed within the embryo (Fig. 3.3E, E'). Additionally, in *Lv-vegf3* morphants, PMCs appeared fragmented at the pluteus stage (Fig. 3.3E, insert), but not at earlier stages (Fig. 3.3B, insert). In contrast, in *Lv-fgfa* morphants, at the pluteus stage PMCs were arranged in a well-formed pattern similar to control embryos, though we still observed defects in the morphology of the skeleton (Fig. 3.3F, F'). Due to the apparent fragmentation of PMCs in *Lv-vegf3* morphants, we used a TUNEL assay to examine whether these cells were undergoing apoptosis. We observed a general increase in the number of apoptotic cells from the prism stage (Fig. S3.3A-A''', B-B''') to the pluteus stage in both controls (Fig. S3.3C') and *Lv-vegf3* morphant embryos (Fig. S3.3D'), but very few PMCs were apoptotic, even in the morphants (Fig. S3.3C'', D'' inserts). This indicates that the fragmentation of PMCs observed at later stages in *Lv-vegf3* morphant embryos is not due to an increase in apoptosis in these cells.

To test whether MO knockdown of *Lv-vegf3* or *Lv-fgfa* might have indirect effects on the expression of the other ligand, which might be the case if there were crosstalk between these two signaling pathways, we analyzed the expression of *Lv-vegf3* and *Lv-fgfa* in morphants by WMISH. We observed that *Lv-vegf3* expression was strongly upregulated upon blocking the VEGF pathway in both mesenchyme blastula (Fig. 3.4A) and late gastrula (Fig. 3.4A, B) embryos. Expression of *Lv-fgfa* in *Lv-vegf3* morphants was comparable to control embryos at the early blastula stage (Appendix Fig. 10). At the mesenchyme blastula stage, however, we observed a striking down-regulation of *Lv-fgfa* in the ingressed PMCs (Fig. 3.4C). *Lv-fgfa* was expressed in an expanded territory in the ectoderm in late gastrula embryos (Fig. 3.4D) as compared to control embryos (Fig. 3.4L), though this expression domain narrowed to a pattern comparable to controls by the prism stage (Appendix Fig. 10). *Lv-fgfa* was never re-expressed in the PMCs in *Lv-vegf3* morphants. Analysis of *Lv-vegf3* expression upon blocking the FGF pathway suggested that *Lv-vegf3* was slightly upregulated in *Lv-fgfa* morphants, an effect more pronounced at mesenchyme blastula (Fig. 3.4E) than at late gastrula (Fig. 3.4F) stages. Additionally, as previously described in *P. lividus* (Rottinger *et al*., 2008), *Lv-fgfa* expression

was upregulated in the PMCs and ectoderm of *Lv-fgfa* morphants at the mesenchyme blastula (Fig. 3.4G) and late gastrula (Fig. 3.4H) stages. Additionally, we assayed changes in expression of two other genes expressed in the ectoderm that have been shown to play a role in regulating skeletogenesis: *Lv-otp* (Di Bernardo *et al*., 1999; Cavalieri *et al*., 2003) and *Lv-pax2/5/8* (Cavalieri *et al*., 2011). We noted that *Lv-pax2/5/8* expression was slightly downregulated in *Lv-vegf3* morphants (Fig. S3.4A, A'), and strongly downregulated in *Lv-fgfa* morphants (Fig. S3.4C, C'). On the other hand, *Lv-otp* was unaffected by the knockdown of either *Lv-vegf3* or *Lv-fgfa* (Fig. S3.4B, B', D, D'). As *Lv-fgfa* knockdown led only to minor defects in skeletogenesis and no effect on PMC migration, we focused our attention on further elucidating the role of VEGF signaling in PMC morphogenesis.

3.4.3 VEGF signaling extensively regulates PMC migration and filopodia extension

Although MOs are highly effective at knocking down all zygotic expression of target genes, it is difficult to use these reagents to perturb gene expression selectively at late stages of embryonic development. Therefore, to determine the temporal requirements for VEGF signaling during development, we used a second-generation VEGFR inhibitor, axitinib, which has been shown in other systems to specifically block VEGF signaling at low (nM) concentrations (Hu-Lowe *et al*., 2008; Bhargava and Robinson, 2011). We observed that *L. variegatus* embryos cultured in 75 nM axitinib from early cleavage developed no skeletal elements (Fig. 3.5B, B') a phenotype identical to VEGF morphants (See Fig. 3.2B). As in VEGF morphants, PMCs in axitinib-treated embryos were located mostly in the vegetal hemisphere, and did not form ventro-lateral clusters (Fig. 3.5C, D, D'). At the pluteus stage, PMCs in axitinib treated embryos showed the same fragmented phenotype observed in VEGF morphants (Fig. 3.5F). These findings confirmed that axitinib phenocopied VEGF knockdown, and made it possible for us to use this drug to assess the temporal requirements for VEGF signaling during skeletogenesis.

PMC migration can be considered to occur in two phases. During the initial phase (early gastrulation), PMC disperse from the site of ingression and arrange themselves in the subequatorial ring and ventro-lateral clusters. During the second phase (late gastrulation), chains of PMCs migrate from the animal-most portion of each ventro-lateral cluster towards the animal

pole. These PMCs produce the dorsoventral, anterolateral, and recurrent rods of the early larval skeleton. To test whether VEGF signaling might play a role in the second phase of PMC migration, we cultured embryos in axitinib starting at the early gastrula stage, when the PMCs were in the process of forming the sub-equatorial ring (Fig. 3.6A, A'). We then fixed control and axitinib treated embryos 4.5 hours later, at the late gastrula stage, and assayed PMC location by immunostaining. PMCs in DMSO-treated control embryos migrated normally and formed two chains of cells that extended from the ventro-lateral clusters towards the animal pole (Fig. 3.6C, C'). No strands of PMCs migrated towards the animal pole in axitinib-treated embryos, however, though ventro-lateral clusters were visible in many embryos (Fig. 3.6B, B'). Based on these observations, and the phenotype of VEGF morphant embryos (Duloquin *et al*., 2007; Fig. 3.33), we conclude that VEGF signaling is required for both phases of PMC migration.

We noted that upon VEGF knockdown or VEGFR inhibition by axitinib treatment, PMCs did not disperse randomly through the blastocoel, but remained mostly in the vegetal hemisphere. We wondered whether this behavior might be the result of unidentified, VEGF-independent, directional cues in the blastocoel. To test this hypothesis, we displaced PMCs throughout the blastocoel in control (Fig. 3.7A, A') and axitinib-treated embryos at the mesenchyme blastula stage, and observed the location of PMCs by immunostaining 5 hours post-displacement. We observed that in 28/30 cases, PMCs in control embryos migrated back towards the vegetal pole, formed a sub-equatorial ring with ventro-lateral clusters, and began migrating in two chains from the VLCs towards the animal pole (Fig. 3.7C, C'). On the other hand, in 30/30 axitinib-treated embryos, many PMCs remained in the animal half of the embryo (Fig. 3.7B, B'). We also obtained comparable results for identical experiments conducted on *Lv-vegf3* morphant embryos (data not shown). We therefore find no evidence for a VEGF-independent mechanism that targets PMCs to the vegetal hemisphere. It seems more likely, instead, that PMCs remain relatively close to the site of ingression because PMC motility is compromised in some general way after blocking VEGF signaling.

As PMCs motility is mostly dependent on the extension and retraction of several filopodia, (Malinda *et al*., 1995), we analyzed the effect of blocking VEGF signaling on filopodial dynamics by observing the number and lengths of filopodia extended by PMCs in control and axitinib-treated embryos 1.5 hours after PMCs were displaced within the blastocoel. PMCs in

control embryos showed a stereotypical elongated morphology with filopodia extending mostly from the two ends of each cell (Fig. 3.8A). On the other hand, PMCs in axitinib-treated embryos appeared more rounded and had very few filopodia (Fig. 3.8B). Our analysis of the length and number of filopodia extended by both samples of embryos (Fig. 3.8C, D) showed that PMCs in control embryos (n=57) extended on average 5 filopodia per cell, and these filopodia were of an average length of 11.5µm. PMCs in axitinib-treated embryos (n=63) extended approximately 2 filopodia per cell, of average length of 4.8µm. Blocking VEGF signaling therefore severely inhibited filopodial dynamics during skeletogenesis.

Apart from migration, filopodia are also crucial for PMC fusion, another essential step in skeletogenesis (Wilt and Ettensohn, 2007). We therefore tested whether VEGF signaling played a role in PMC fusion by a dye transfer assay in which a few dextran-labeled PMCs from *Lv-vegf3* morphants were transplanted into unlabeled, *Lv-vegf3* morphant host embryos. In 20/21 embryos, dextran spread to all PMCs by the late gastrula stage (Fig. 3.9A, A'), demonstrating that PMC fusion occurred normally. At the pluteus stage, the dextran label was still visible in the fragmented PMCs of *Lv-vegf3* morphant embryos (Fig. 3.9B, B').

3.4.4 Blocking VEGF signaling at any point during development inhibits skeleton secretion

Why do PMCs fail to secrete skeletal elements when VEGF signaling is blocked? One possibility is that VEGF has a direct effect on biomineralization- for example, by directly regulating the expression of biomineralization genes. Alternatively, VEGF might regulate biomineralization indirectly, by affecting the ability of PMCs to migrate directionally and accumulate at the sites of the ventro-lateral clusters, where local, ectodermal cues other than VEGF might induce skeletogenesis. To distinguish between these possibilities, we treated embryo cultures with axitinib at various stages of development (Fig. 3.10). The frequencies of morphant phenotypes we observed upon drug addition at each stage of development are given in Table 3.1. Embryos treated with axitinib beginning at the hatched blastula (Fig. 3.10B, B'), mesenchyme blastula (Fig. 3.10C, C'), and early gastrula (Fig. 3.10B, B) stages had developed no skeletal elements when control embryos reached the pluteus stage (Fig. 3.10A, A'). Embryos treated with axitinib from the mid-gastrula (Fig. 3.10E, E'), late gastrula (Fig. 3.10F, F') or prism (Fig. 3.10G, G')

stages developed truncated skeletal elements. Thus, no skeletal elements were formed when VEGF signaling was blocked prior to the initiation of skeletogenesis, but blocking the pathway post-initiation inhibited the elongation of the skeletal rods. Interestingly, we noted that in embryos cultured in axitinib from the mid-gastrula or late gastrula stages, specific skeletal rods were affected to different degrees. In particular, the body rods extended normally (Fig. 3.10E', F', arrow) while other rods, most noticeably the postoral and anterolateral rods, were severely truncated (Fig. 3.11). The postoral and anterolateral rods extend by a plug of PMCs at their growing tips, and these PMCs are visible in both control and axitinib-treated embryos (Fig. S3.5).

We also assayed the reversibility of the effects of VEGF inhibition on skeletogenesis. Embryos were cultured in axitinib from early cleavage, and the inhibitor was washed out of the cultures at different stages of development (Fig. S3.6, schematic diagrams). We observed that embryos maintained the ability to recover fully from the effects of blocking the VEGF pathway if inhibition was alleviated prior to the end of gastrulation (Fig. S3.6B'-E', Table S1), while embryos cultured in axitinib post-gastrulation had limited, if any, ability to form skeletal elements (Fig. S3.6G', H', Table S3.1).

3.4.5 VEGF signaling regulates the expression of genes in the PMC GRN

Because we observed that the VEGF signaling pathway controlled biomineralization independently of its effects on PMC patterning, we tested the role of this pathway in regulating the expression of genes in the PMC GRN. To this end, we used the Nanostring nCounter analysis system, which measures the number of transcripts of specific genes in an RNA sample (Geiss *et al*., 2008). Embryos of the species *S. purpuratus* were used in this experiment since the availability of a sequenced genome facilitated the design of the Nanostring probe set (Table S3.2). The knockdown of *Sp-vegf3* using a translation-blocking MO led to a complete inhibition of skeletogenesis, as is observed in *P. lividus* and *L. variegatus* (Fig. S3.7 A, B, D, E). Skeletogenesis was also blocked in *S. purpuratus* embryos cultured in 50 nM axitinib from early cleavage (Fig. S3.7C, F). Likewise, PMC migration was disrupted in *Sp-vegf3* morphants (Fig. S3.7H, K) and axitinib-treated embryos (Fig. S3.7I, L). Differences in gene expression levels

between control embryos and both VEGF morphants and embryos cultured in axitinib from early cleavage were measured at the late gastrula stage (48 hr post-fertilization). Three trials were conducted for both *Sp-vegf3* morphants and axitinib-treated embryos, and Table S3.3 shows results obtained for each gene measured. We observed that 19 out of 90 genes measured showed a change of greater than 50% in *Sp-vegf3* morphants, most of which were morphoeffector genes with proven or predicted roles in biomineralization (Fig. 3.12A, Supplementary Table 3.3). Similar results were obtained in axitinib-treated embryos, in which 21 out of 90 genes measured showed a change of 50% or more (Fig. 3.12B, Supplementary Table 3.3). Interestingly, most regulatory genes showed little to no change in both sample sets, an observation which correlates with the fact that VEGF signaling does not regulate the specification of PMCs.

3.5 Discussion

The mechanisms regulating cell migration during gastrulation have long been of interest to researchers, and the importance of growth factor signaling pathways in this process is becoming evident. Studies regarding the role of growth factors in directional cell migration have typically been conducted using *in vitro* cell migration assays and tissue explants (Ataliotis *et al*., 1995; Ciruna and Rossant, 2001; Montero *et al*., 2003; Smith *et al*., 2009; McLennan *et al*., 2010; Damm and Winklbauer, 2011, among several others), and though these experiments have yielded a wealth of information, they can be less reliable than experiments conducted *in vivo*. The sea urchin embryo, which is optically clear and amenable to a wealth of experimental manipulations, therefore serves as an excellent model to study the factors regulating mesoderm migration and differentiation *in situ*.

There are some similarities and differences in the aspects of mesoderm cell migration regulated by growth factor signaling in different systems. For example, the initial migration of mesoderm cells away from the primitive streak in the chick embryo is regulated by the PDGF pathway. The migration path of these mesoderm cells is then fine-tuned by two FGF ligands; FGF8 which acts as a repellent for migrating cells, and FGF4 which acts as an attractant for cells migrating anteriorly. Additionally, cells in the posterior streak migrate in response to VEGF signaling (Chuai and Weijer, 2009). Unlike gastrulation in the chick embryo where multiple pathways contribute to mesoderm cell migration, our results have shown that PMC migration is fully reliant on VEGF signaling in the sea urchin embryo, though VEGF signaling is a common thread in both of these systems. During gastrulation in the *Xenopus* embryo, PDGF signaling is responsible for both the orientation and migration of prechordal mesoderm cells (Winklbauer and Muller, 2011), an observation similar to our results detailing the multiple functions of VEGF signaling in the sea urchin embryo. Conversely, PDGF signaling also regulates cell polarization and the extension of cellular processes but not the directional migration of mesendoderm cells during zebrafish gastrulation (Montero *et al.,* 2003). The mesoderm of the *Drosophila* embryo is formed by a series of migration events culminating in the flattening of the mesoderm cells into a monolayer. FGF signaling plays multiple roles during these migration events, including the intercalation and spreading of mesoderm cells post ingression, and attachment of mesoderm cells to the epithelium prior to migration. The FGF receptor Heartless is expressed in migrating

mesoderm cells, and the FGF ligands Pyramus and Thisbe are expressed in the ectoderm. These two FGF ligands play slightly different but overlapping roles in regulating mesoderm formation (Wilson and Leptin, 2000; Winklbauer and Muller, 2011). There are no comparable intercalation events during sea urchin gastrulation, though the movement of PMCs away from the site of ingression may be analogous to mesoderm spreading. In most of the above-mentioned systems, growth factors have been proven to act as chemoattractants, though a role in regulating the mechanics of cell migration has not been ruled out. However, as described below, VEGF signaling clearly regulates the mechanics of cell migration during gastrulation in the sea urchin embryo.

Previous research into the roles of receptor tyrosine kinases during sea urchin gastrulation led to the identification of two pathways, FGF (Rottinger *et al*., 2008) and VEGF (Duloquin *et al*., 2007) signaling, as important factors regulating mesoderm migration and differentiation during gastrulation in the sea urchin species *P. lividus*. ClustalW comparisons of the protein sequences of the *fgfa* and *vegf3* ligands in three species of sea urchin demonstrate high levels of similarity amongst *S. purpuratus, P. lividus* and *L. variegatus* (Fig. S3.1A, B) which point to important conserved functions of these signaling molecules during development. Furthermore, our analyses of the expression patterns of *vegf3* and *fgfa* show a high level of similarity among the aforementioned species (Duloquin *et al*., 2007; Rottinger *et al*., 2008, Fig. 3.1, data not shown). We noted, however, that *fgfa* was expressed in the PMCs prior to their ingression in *L. variegatus* (Fig. 3.1A), an earlier stage than in *P. lividus* (Rottinger *et al*., 2008). Throughout embryonic development, *Lv-fgfa* showed a highly dynamic pattern of expression, while *Lv-vegf3* expression was steadily maintained in the ectoderm overlying the VLCs and areas of rapid skeletal growth (Fig. 3.1). These expression patterns are consistent with the hypothesis that VEGF might play a more direct role in the regulation of directional PMC migration and later skeletogenesis. Our observation that *Lv-vegf3* is initially expressed in a ring of ectoderm at the vegetal pole of the blastula after which it resolves to the ectoderm overlying the ventro-lateral clusters might explain two features of PMC guidance: the existence of "vegetal" directional cues even prior to PMC ingression (Ettensohn and McClay, 1986) and the gradual emergence of the two PMC clusters during gastrulation (Malinda *et al*. 1995; Gustafson and Wolpert, 1999). The expression pattern of *vegf3* has been studied in embryos of two other groups of echinoderms: sea stars (*Patiria pectinifera*) and brittlestars (*Amphipholis kochii*). Morino *et al*. (2012) showed that

in brittlestars, which form an embryonic endoskeleton, a *vegf3* homolog is expressed in a similar ring-like pattern during early embryogenesis, which then resolves into two domains of ectoderm as seen in *L. variegatus* embryos. In contrast, *vegf3* is not expressed in embryonic stages of the seastar, which do not form an embryonic endoskeleton, though this gene is expressed in larval stages in patterns that correlate with adult skeletogenesis (Morino *et al*., 2012). These comparative studies point to an important, conserved role of VEGF signaling in echinoderm skeletogenesis and suggest that evolutionary modifications in VEGF expression played an important role in the appearance of new patterns of skeletogenesis within the phylum.

Knockdown of *vegf3* blocks directed PMC migration and differentiation in three species of sea urchin (Figs. 3.2B, 3.3B, S3.6, Duloquin *et al.*, 2007). In contrast, we saw a difference in the severity of skeletal defects observed upon the knockdown of *fgfa* between *P. lividus* and *L. variegatus* (Fig. 3.2C, 3.2D, Rottinger *et al*., 2008). The lack of visible effects on PMC migration (Fig. 3.3C) and the presence of skeletal elements in *Lv-fgfa* morphants (Fig. 3.2C, 3.2D, 3.3F) might reflect interspecies variation in gene function. We conclude, however, that, at least in *L. variegatus*, VEGF signaling plays a more prominent role than FGF signaling in the regulation of directed PMC migration and differentiation. Our analyses of the interactions between VEGF and FGF signaling showed that though VEGF signaling has a strong influence on the expression of *Lv-fgfa* in the PMCs, FGF signaling does not significantly regulate *Lv-vegf3* expression. The VEGF and FGF pathways have been shown to function synergistically in other systems. For example, FGF and VEGF function are interdependent in embryonic coronary vasculogenesis and angiogenesis in quail explants and mouse embryonic hearts (Tomanek *et al*., 2010). We have also analyzed the effects of blocking the VEGF and FGF pathways on the expression patterns of two other genes expressed in the ectoderm with direct roles in regulating PMC migration: *otp* (Cavalieri *et al*., 2003) and *pax2/5/8* (Cavalieri *et al*., 2011), and found that while *Lv-otp* expression is not regulated by either FGF or VEGF signaling, *Lv-pax2/5/8* expression is dependent on the FGF pathway (Fig S3.4). Cavalieri *et al*. (2011) showed that the tripartite motif-containing protein *strim1* regulates the expression of *otp*, *pax2/5/8*, and *fgfa* in the ectoderm but not in the PMCs. These results are complementary to our observation that VEGF signaling regulates the expression of *Lv-fgfa* specifically in PMCs (Fig. 3.4C, D), and neither VEGF nor FGF signaling regulates *Lv-otp* expression (Fig. S3.4B, B', D, D'). Research on *strim1* function, together with our observations, have shed some light on the complex

interactions between genes expressed in the ectoderm overlying the VLCs, indicating that at least two pathways may be at play in regulating gene expression in this territory.

Individual signaling pathways often play multiple roles during development. The PDGF pathway, for example, functions in the orientation, radial intercalation, and migration of mesoderm cells during gastrulation in *Xenopus* embryos (Nagel *et al*., 2004; Damm and Winklbauer, 2011). PDGF signaling also regulates both cell polarization and the extension of cellular processes but not the directional migration of mesendoderm cells in zebrafish embryos (Montero *et al*., 2003). We have made similar observations concerning the functions of VEGF signaling during sea urchin development. During skeletogenesis, PMCs undergo a complex but highly coordinated pattern of migration (Malinda and Ettensohn, 1994; Gustafson and Wolpert, 1999), and we have shown that VEGF signaling independently regulates all phases of PMC migration by controlling the number and length of their filopodia, which are essential to their migration and differentiation (Okazaki, 1965; Malinda *et al*., 1995; Miller *et al*, 1995; Wilt and Ettensohn, 2007). PMCs usually have about of 5-7 filopodia, each being on average 5-10 µM in length (Ettensohn *et al*., 1997). These dimensions were comparable with our measurements for control embryos, while axitinib treated embryos had obviously shorter and fewer filopodia (Fig. 3.8). VEGF signaling is a known regulator of filopodial dynamics during development, often controlling endothelial cell migration and angiogenic sprouting (Hellström *et al*., 2007; Gerhardt, 2008). Filopodia extension is regulated by cytoskeletal dynamics (Le Clainche and Carlier, 2008; Mattila and Lappalainen, 2008; Yang and Svitkina, 2011), and Ras, Rho and Cdc42 proteins are usually associated with regulating actin polymerization during growth factor-related directed cell migration (Lauffenburger *et al*., 1996; Motell, 1999). These proteins often function by activating the Arp2/3 complex through proteins of the WASP family (Le Clainche and Carlier, 2008; Kurosaka and Kashina, 2008; Yang and Svitkina, 2011). *cdc42*, *arp3* and *wasp* are specifically expressed by the PMCs and the non-skeletogenic mesenchyme cells (Rafiq *et al*., 2012). We observed no change in the expression levels of these genes upon blocking VEGF signaling (Fig. 3.12, Table S3.3), but it is more likely that as in other systems, the VEGF signaling cascade regulates the activity of these proteins by post-translational modifications rather than their expression.

Surprisingly, we observed no defects in PMC fusion upon blocking the VEGF pathway (Fig. 3.9), though PMCs fuse through connections made between their filopodia (Okazaki, 1965). These results are supported by observations from experiments conducted on cultured PMCs. Okazaki (1975) showed that horse serum is essential for the secretion of skeletal rods in cultured PMCs, as it is thought to provide the cells with factors necessary for skeleton secretion including VEGF (Duloquin *et al*. 2007; Knapp *et al*., 2012). Fusion however occurs in PMCs cultured in the absence of serum or other external factors (Hodor and Ettensohn, 1998). Our results therefore indicate that PMC migration and PMC fusion are regulated by separate mechanisms, in which the migration of PMCs is fully reliant on VEGF signaling, but PMC fusion is independent of the VEGF pathway.

Our time-course experiments (Fig. 3.10, Table 3.1) have led to the identification of a critical period prior to the mid-gastrula stage during which continuous VEGF signaling is essential to the synthesis of all skeletal elements. Blocking VEGF signaling after this critical period led to the formation of truncated skeletal rods. The PMCs are known to possess some information regulating skeletogenesis independent of ectodermal signals. Armstrong and McClay (1994) and Okazaki (1975) have shown by interspecies transplantation experiments that the specific pattern of skeleton synthesized is an intrinsic characteristic of the PMCs. Upon blocking VEGF signaling at later stages of development, the PMCs have already received essential positional information from the ectoderm, and may now possess the ability, if limited, to synthesize significant skeletal elements. On the other hand, the PMCs in these embryos may have built up enough proteins prior to blocking VEGF signaling to proceed with biomineralization to some extent, after which point skeletogenesis ceases. At the pluteus stage, the *vegf3* ligand and *vegfr-10-Ig* receptor are expressed in regions of rapid skeletal rod elongation: *vegfr-10-Ig* is expressed in the PMCs at the tips of the elongating postoral and anterolateral rods, while *vegf3* is expressed in the ectoderm overlying these rods (Fig. 3.1, Duloquin *et al*., 2007). We have observed a parallel inhibition in the elongation of exactly these rods when VEGF signaling is blocked after the formation of the triradiate spicule rudiments (Fig. 3.11). Because the postoral and anterolateral rods are laid down by a small plug of PMCs that originates from the VLCs (Ettensohn and Malinda, 1993), and because treatment with axitinib even after the formation of the VLCs blocked the formation of these rods, the truncation of these rods cannot be an indirect effect of blocking the directional migration of PMCs during gastrulation or their arrangement

into the subequatorial ring. The growth of these rods must be regulated by VEGF signals from the ectoderm directly influencing the secretion of the calcium carbonate biomineral at their growing tips. This conclusion is supported by observations that the photoablation of the ectoderm overlying the postoral rods brings skeletal growth in these rods to a halt (Ettensohn and Malinda, 1993).

Knapp *et al*. (2012) have described in detail the complex patterns of skeletal growth in PMC cultures under the influence of recombinant VEGF. They showed that the effects of VEGF on skeletal growth are concentration-dependent; relatively high levels of VEGF favor growth in the a-axis (i.e., the formation of triradiate spicules), while lower levels of VEGF favor growth in the c-axis (i.e., the formation of linear rods of the kind that ordinarily extend perpendicular to the plane of the triradiate spicule). These observations may be recapitulated in vivo, as *vegf3* mRNA is expressed at higher levels during gastrulation when the triradiate spicules are synthesized, while levels are visibly lower by the prism and pluteus stages, when additional skeletal rods (e.g., the postoral and anterolateral rods) form by branching and extend in the direction of the c-axis. Results from our experiments adding or removing axitinib from embryo cultures closely mirror previous work examining the effects of horse serum on PMC cultures. PMCs in culture synthesize skeletal rods in response to the presence of serum during a critical window between the mesenchyme blastula and early gastrula stages and become insensitive to horse serum after sibling control embryos reach the late gastrula stage (McCarthy and Spiegel, 1983; Page and Benson, 1992). Our results therefore provide further evidence that VEGF is an essential component provided by horse serum to induce biomineralization in cultured PMCs.

The secretion of the endoskeleton is regulated by complex interactions between upstream transcription factors, particularly *alx1* and *ets1*, and a battery of downstream morphoeffector genes (Rafiq *et al*., 2012). VEGF signaling does not significantly regulate the expression of most upstream transcription factors, but controls the expression of several morphoeffector genes (Fig 3.12, Table S3.3). The onset of expression of many of these genes preceeds or coincides with the expression of the VEGF receptor in the PMCs (Zhu *et al.*, 2001; Illies *et al*, 2002; Rafiq *et al*., 2012; Duloquin *et al*., 2007), suggesting that VEGF signaling is not required for the initial activation of morphoeffector genes. Additionally, the expression of most of morphoeffector genes was not fully blocked by inhibiting VEGF signaling, showing that VEGF is not solely

responsible for their expression. VEGF signaling most likely maintains the expression of these morphoffector genes at levels compatible with skeletal growth. A vast majority of genes regulated by VEGF signaling have predicted or proven roles in biomineralization, though not all genes encoding biomineralization proteins were regulated by VEGF signaling. For example, *p16* which is essential to biomineralization (Cheers and Ettensohn, 2005) is not regulated by VEGF signaling, though interestingly, other members of the *p16* family appeared to be affected by VEGF knockdown. Also, members of the *msp130* gene family were, in general, not regulated by VEGF signaling. Likewise, blocking FGF signaling perturbs the expression of *sm30* and *sm50,* but not *msp130* (Rottinger *et al*., 2008). An analysis of the cis regulatory machinery of these genes and gene families could reveal important differences in regulatory modules which may explain the variances in their responses to the absence of ectodermal signals.

The question still remains as to what the downstream components of the VEGF signaling pathway are. The two most likely candidates known to mediate signaling though receptor tyrosine kinases are the MAPK and PI3K pathways (Schlessinger, 2000), both of which are essential for skeletogenesis in the sea urchin embryo. Bradham *et al*. (2004) proposed that the external signals regulating skeletogenesis might be signaling through PI3K. Their experiments showed that inhibiting this kinase blocked the elongation of skeletal rods, but not PMC specification, cell migration, the extension of filopodia, cell fusion or skeletal initiation. The MAPK pathway, on the other hand, regulates PMC specification, ingression, migration and differentiation, and the expression of several genes not regulated by VEGF signaling such as the transcription factors *alx1*, *ets1*, *tbr* and *deadringer* and the morphoeffector gene *msp130* (Rottinger *et al*. 2004; Fernandez-Serra *et al*., 2004). Noticeably, the perturbation of neither of these pathways gives phenotypes identical to VEGF knockdown. However, wash-in experiments blocking the MAPK pathway using the inhibitor U0126 post-PMC specification show that these embryos form truncated skeletal elements in a manner similar to axitinib treatments (Rottinger *et al*., 2004; Fernandez-Serra *et al*., 2004; Adomako-Ankomah and Ettensohn, unpublished observations). Additionally, the spicule matrix genes *sm50* and *sm30* are downregulated upon blocking both the MAPK and VEGF pathways (Fernandez-Serra *et al*., 2004; Fig. 3.12). The MAPK pathway is therefore a more likely candidate for the mediation of VEGF signaling.

Interestingly, it has been suggested that two pathways are utilized in the regulation of skeletogenesis by MAPK signaling: a Ras-independent pathway necessary for PMC ingression, and a Ras-dependent pathway necessary for PMC migration and skeletogenesis (Rottinger *et al*., 2004; Fernandez-Serra *et al*., 2004). As the VEGF pathway does not regulate PMC ingression, VEGF signaling might function by a Ras-dependent mechanism. Further research is essential to confirm this hypothesis on the downstream mediators of VEGF signaling regulating its influence on PMC migration and differentiation during skeletogenesis in the sea urchin embryo.

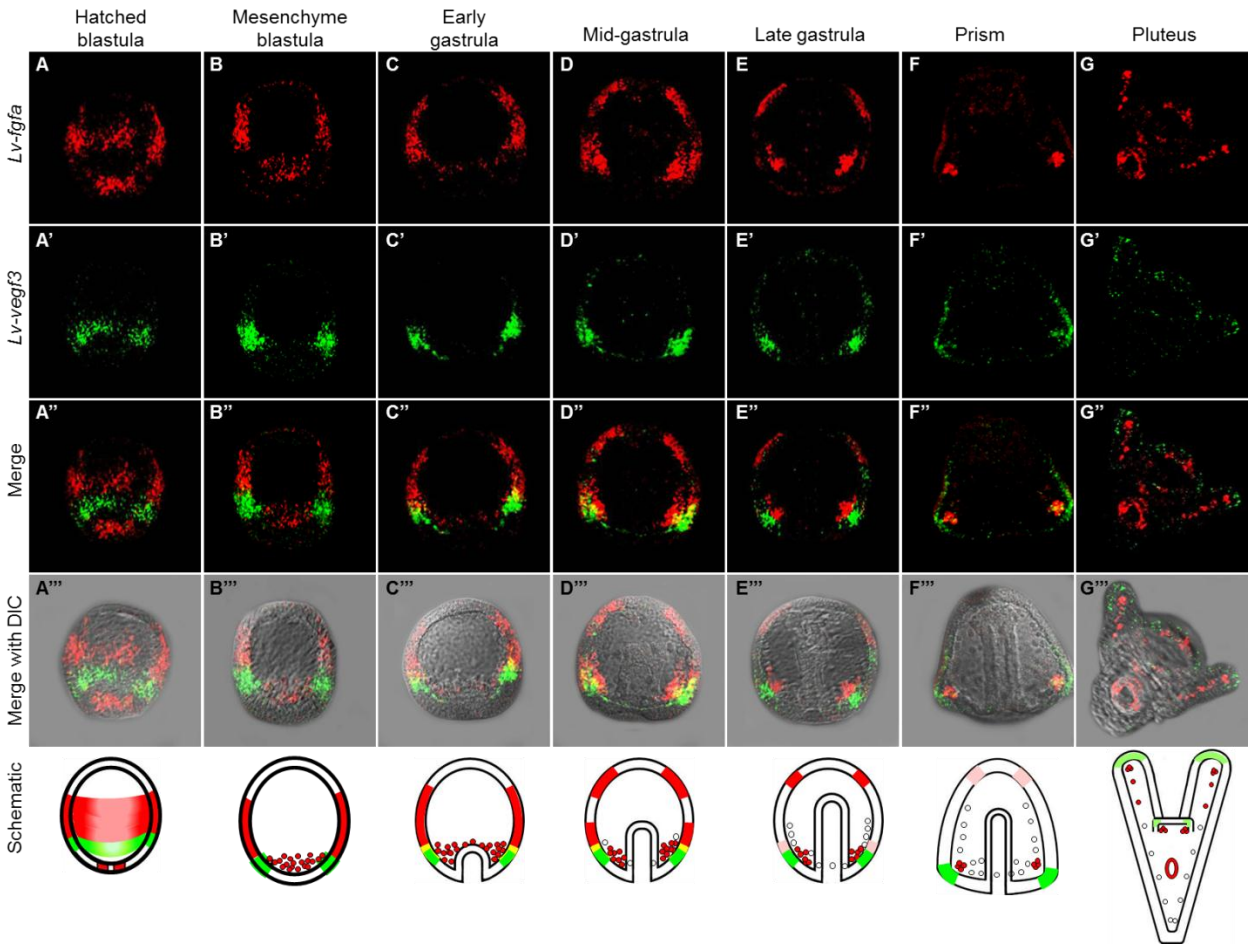

Figure 3.1: FGF and VEGF ligands are expressed in mostly independent domains in the ectoderm. Double fluorescent in situ hybridization analyses of *Lv-fgfa* (A-G) and *Lv-vegf3* (A'-G') expression show that their expression domains are entirely separate at hatched blastula (A-A''') and mesenchyme blastula (B-B''') stages. Their expression domains overlap at early gastrula (C-C''') and mid-gastrula (D-D''') stages. At late gastrula (E-E'''), prism (F-F''') and pluteus (G-G''') stages, *Lv-fgfa* and *Lv-vegf3* are once again expressed in independent domains. Schematic diagrams illustrate expression patterns.

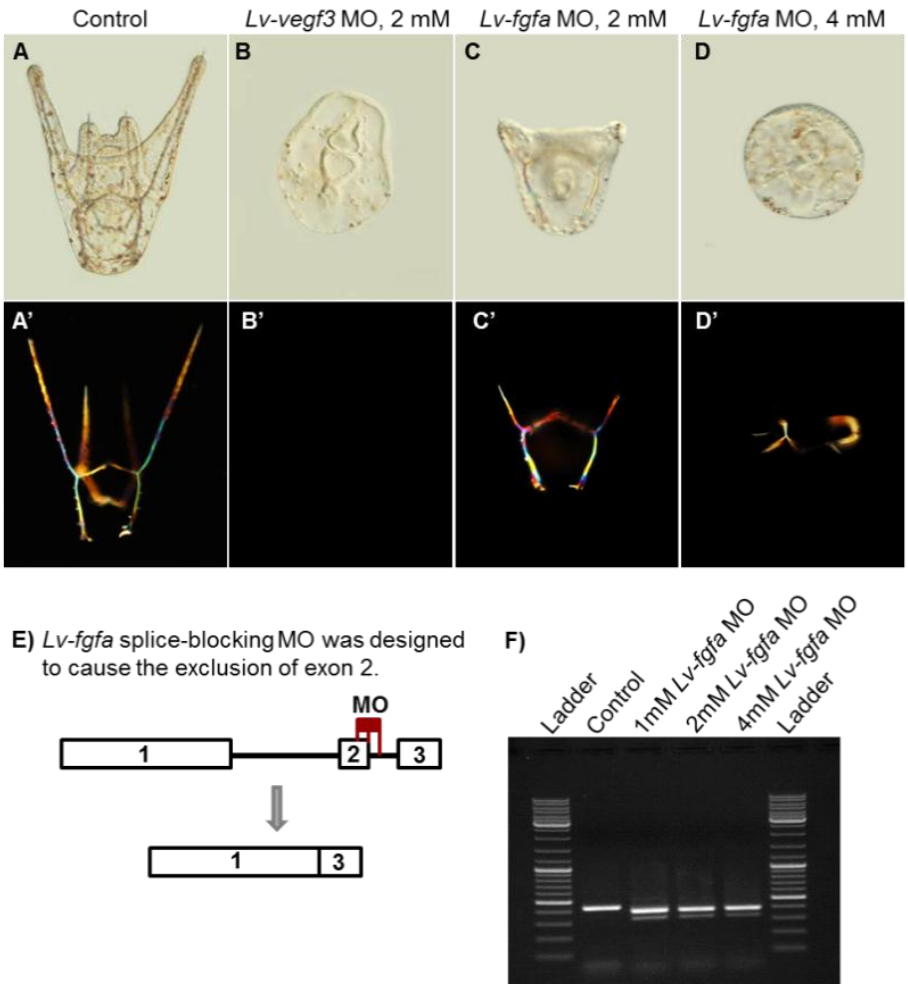

Figure 3.2: Knockdown of *Lv-vegf3*, but not *Lv-fgfa*, inhibits skeletogenesis. DIC (A-D) and polarized light (A'-D') images of a control embryo (A, A'), an embryo injected with 2 mM *Lv-vegf3* translation-blocking MO (B, B'), and embryos injected with 2 mM (C, C') and 4 mM (D,D') *Lv-fgfa* splice-blocking MO. No skeletal elements form in *Lv-vegf3* morphants (99% of embryos scored), but shortened skeletal elements form in *Lv-fgfa* morphants (90% of embryos scored). (E) Schematic of design of *fgfa* splice-blocking MO. (F) Agarose gel showing shift in band size of the *Lv-fgfa* transcript in MO-injected embryos. Brighter band in morphant embryo samples was sequenced, and showed the exclusion of exon 2.

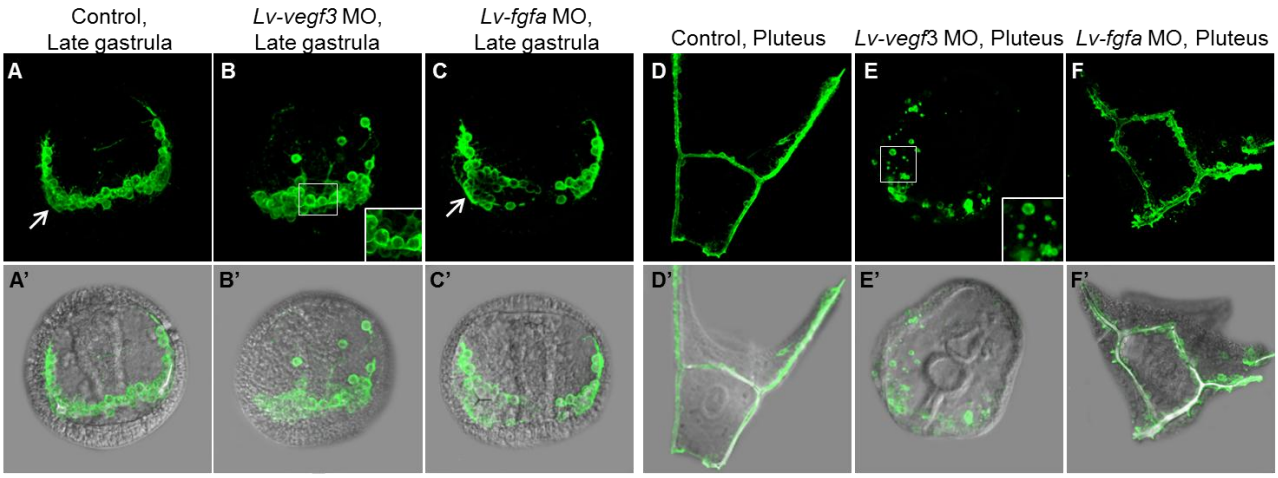

Figure 3.3: PMC migration is perturbed in *Lv-vegf3*, but not *Lv-fgfa* morphants. Fluorescence (A-F), and merged images with DIC (A'-F') of control embryos (A, A', D, D'), *Lv-vegf3* morphants (B, B', E, E') and *Lv-fgfa* morphants (C, C', F, F') at late gastrula (A-C) and pluteus (D-F) stages. 6a9 immunostaining shows that directed PMC migration is abolished in *Lv-vegf3* morphants, but is unperturbed in *Lv-fgf*a morphants. Additionally, in *Lv-vegf3* morphants, PMCs appear fragmented at the pluteus stage (E, insert) when compared to the late gastrula stage (B, insert). Arrows indicate well-formed ventro-lateral clusters at the late gastrula stage.

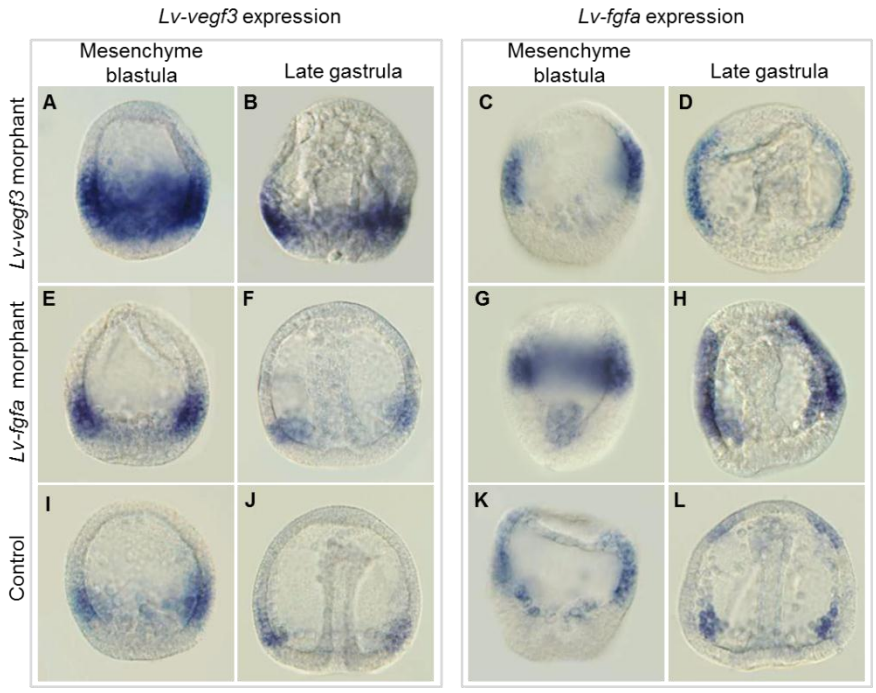

Figure 3.4: Complex interactions between VEGF and FGF signaling and expression of *Lv-vegf3* and *Lv-fgf*. WMISH analysis of *Lv-vegf3* (A, B, E, F, I, J) and *Lv-fgf*a (C, D, G, H, K, L) expression in *Lv-vegf3* morphants (A-D), *Lv-fgfa* morphants (E-H) and control embryos (I-L) at the mesenchyme blastula (A, C, E, G, I, K) and late gastrula (B, D, F, H, J, L) stages. In *Lv-vegf3* morphants, *Lv-vegf3* is strongly upregulated (A, B), and *Lv-fgfa* is downregulated in the PMCs and upregulated in the ectoderm (C, D). In *Lv-fgfa* morphants, *Lv-vegf3* expression is slightly upregulated (E, F), while *Lv-fgfa* is strongly upregulated both in the PMCs and in the ectoderm (G, H).

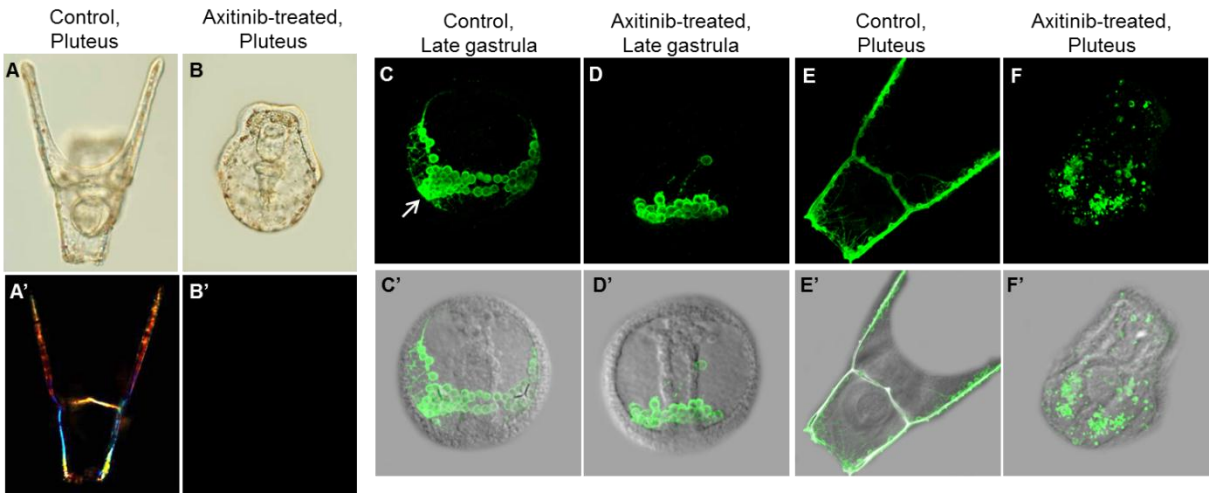

Figure 3.5: VEGFR inhibition with axitinib phenocopies *Lv-vegf3* morphants. DIC (A, B) and polarized light (A', B') images of control embryo (A, A') and embryo treated with 75 mM axitinib from the 2-cell stage (B, B') show that axitinib treatment inhibits skeletogenesis. Fluorescence (C-F), and merged images with DIC (C'-F') of control embryos (C, C', E, E') and axitinib-treated embryos (D, D', F, F') at late gastrula (C-D) and pluteus (E-F) stages. 6a9 immunostaining shows that PMC migration is perturbed in axitinib-treated embryos.

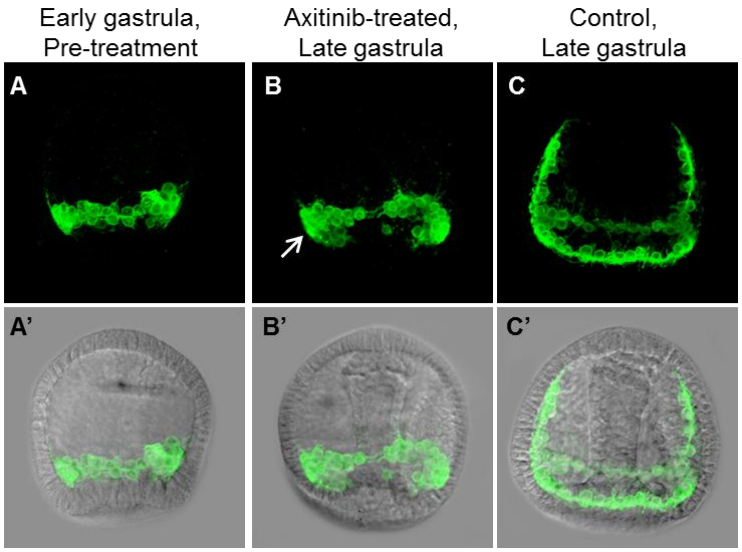

Figure 3.6: VEGF signaling regulates later stages of PMC migration. Fluorescence (A-C) and merged images with DIC (A'-C') of early gastrula embryos immediately prior to axitinib treatment (A, A'), late gastrula embryos treated with axitinib from the early gastrula stage (B, B') and control late gastrula embryos treated with DMSO from the early gastrula stage (C, C'). 6a9 immunostaining shows that PMC migration toward the animal pole is inhibited by axitinib treatment, even when ventro-lateral clusters (arrow) form.

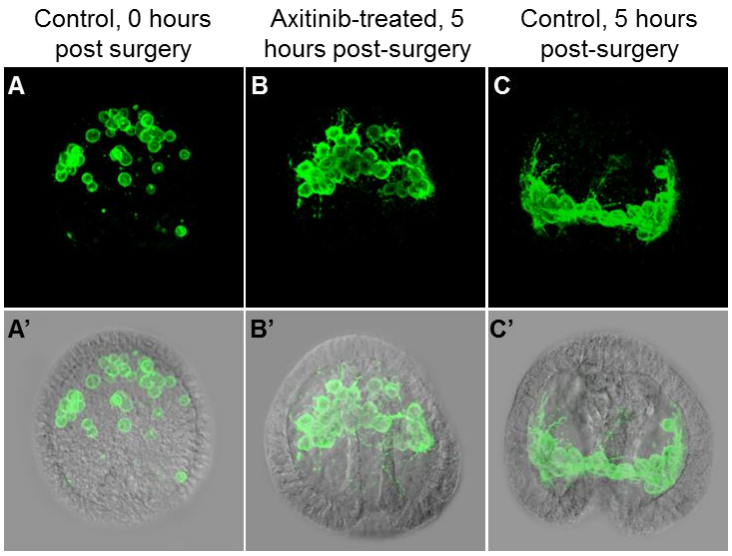

Figure 3.7: VEGF signaling is required for the targeting of PMCs to the vegetal hemisphere. At the mesenchyme blastula stage, a micropipette was used to scatter the PMCs, redistributing most of the cells into the animal hemisphere. 6a9 immunostaining (A-C), and merged images with DIC (A'-C') of a control embryo 0 hr post-surgery (A, A'), and axitinib-treated (B, B) and DMSO-treated control (C, C') embryos 5 hr after surgery. In control embryos, almost all PMCs migrate to the vegetal hemisphere and form a sub-equatorial ring pattern, while in axitinib-treated embryos, most PMCs remain in the animal hemisphere. This suggests that the restriction of PMCs to the vegetal region in VEGF morphants and axitinib-treated embryos is not a consequence of VEGF-independent guidance cues.

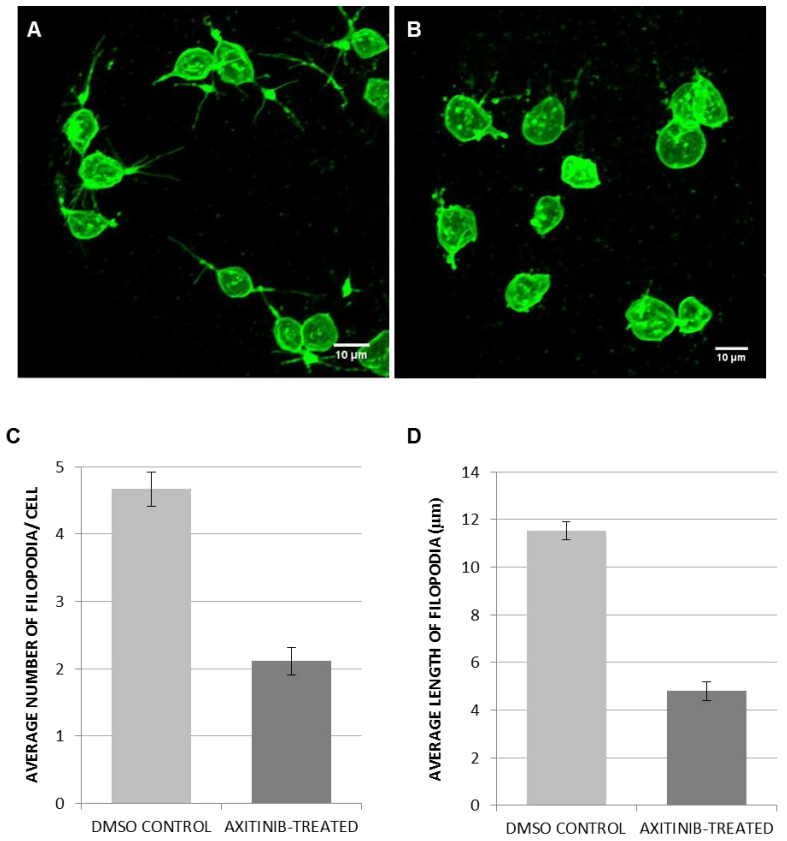

Figure 3.8: VEGF signaling regulates the number and length of filopodia extended by PMCs. Fluorescence images of control embryo (A) and axitinib-treated embryo (B) 1.5 hr after PMCs were scattered within the blastocoel. PMCs in control embryos extend more filopodia than PMCs in axitinib-treated embryos, and these filopodia are longer in control embryos. Graphs show a comparison between the average number of filopodia per cell (C) and the average length of filopodia (D) extended by PMCs in control embryos (n=57) and axitinib-treated embryos (n=63).

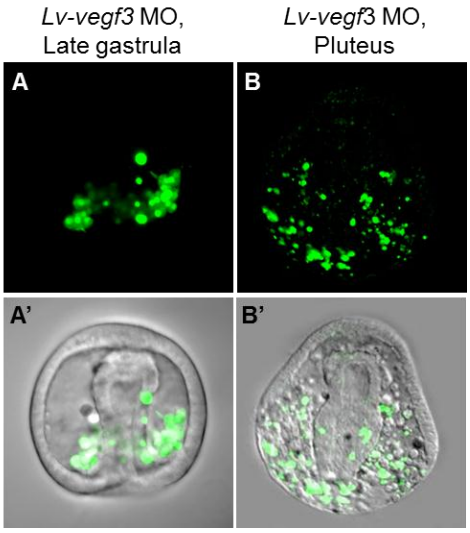

Figure 3.9: VEGF signaling does not regulate PMC fusion. Fluorescence (A, B), and merged images with DIC (A', B') of *Lv-vegf3* morphant hosts 6 hr (A, A') and 24 hr (B, B') after a few FITC-dextran labeled PMCs were transferred from *Lv-vegf3* morphant donors. PMCs are fusion competent, as shown by the spread of dextran through the syncytium 6 hr post-surgery (A) and in the scattered, fragmented PMCs 24 hr post-surgery (B).

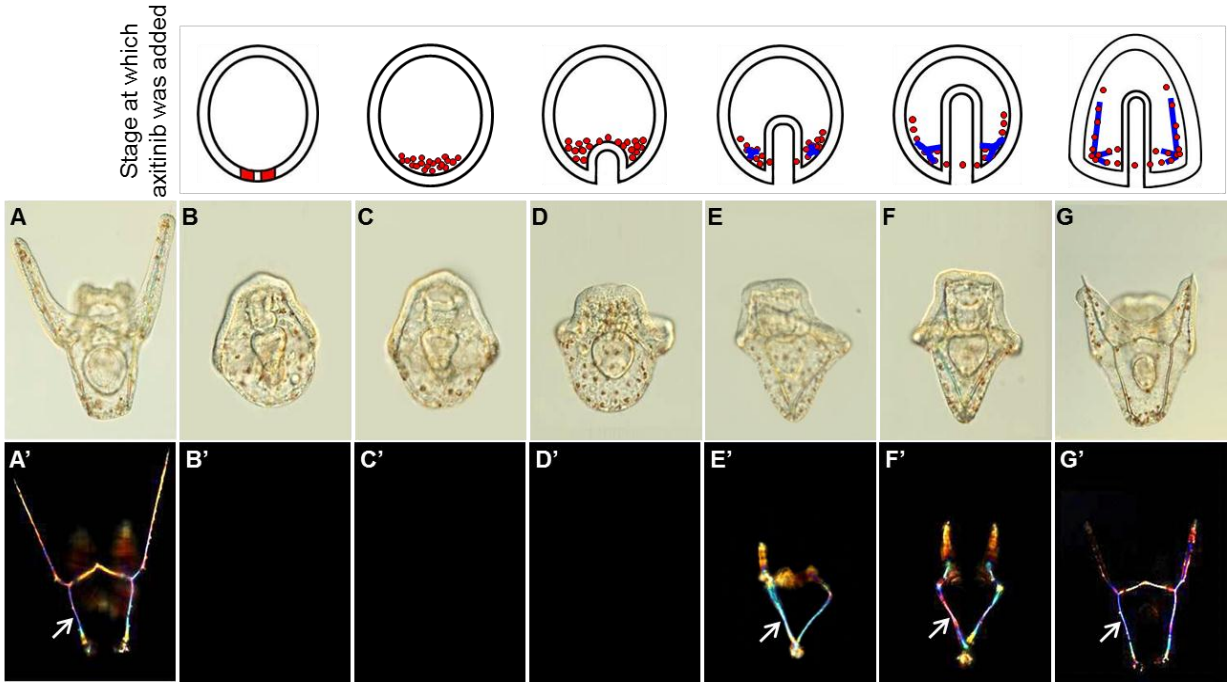

Figure 3.10: VEGF signaling regulates biomineralization independent of its role in PMC guidance. DIC (A-G) and polarized light (A'-G') images of control embryo (A- A'), and embryos treated with axitinib at the hatched blastula (B, B'), mesenchyme blastula (C, C'), early gastrula (D, D'), mid-gastrula (E, E'), late gastrula (F, F') or prism (G, G') stages. Inhibition of VEGF signaling prior to the mid-gastrula stage completely eliminates biomineralization (B'-D'), whereas VEGFR inhibition at or after mid-gastrula leads to the formation of truncated skeletal elements (E'-G'). Schematic diagrams indicate the stage of development at which axitinib was added to embryo cultures (PMCs are represented in red, and skeletal elements are represented in blue). Inhibition of VEGF signaling at the late gastrula or prism stages (at which PMC migration is completed) still led to defects in skeletal elongation (F', G').

OBSERVED PHENOTYPE	STAGE AT WHICH AXITINIB WAS ADDED															
	2-CELL		HATCHED BLASTULA		MESENCHYME BLASTULA		EARLY GASTRULA		MID-GASTRULA		LATE GASTRULA		PRISM		DMSO CONTROL	
	#	%	#	%	#	%	#	%	#	%	#	%	#	%	#	%
NO SKELETON	**202**	**100**	**228**	**100**	**206**	**99.0**	**148**	**63.2**	15	7.4	1	0.5	0	0	0	0
TINY SKELETAL DEPOSITS (SPECKS)	0	0	0	0	2	1.0	68	29.1	11	5.4	4	1.9	2	0.9	0	0
BRANCHED SKELETAL RUDIMENTS	0	0	0	0	0	0	18	7.7	13	6.4	3	1.4	1	0.4	2	0.9
EXTENDED RODS, WITH PROMINENT BODY AND DORSOVENTRAL CONNECTING RODS	0	0	0	0	0	0	0	0	**163**	**80.3**	**171**	**82.2**	21	9.1	0	0
SHORT PLUTEUS SKELETON	0	0	0	0	0	0	0	0	1	O.5	29	13.9	**208**	**89.6**	11	5.1
WILD TYPE SKELETON	0	0	0	0	0	0	0	0	0	0	0	0	0	0	**204**	**94**
TOTAL	202	100	228	100	208	100	234	100	203	100	208	100	232	100	217	100

Table 3.1: Distribution of phenotypes in axitinib wash-in experiments. Bold type indicates the prevalent phenotype at each stage of development.

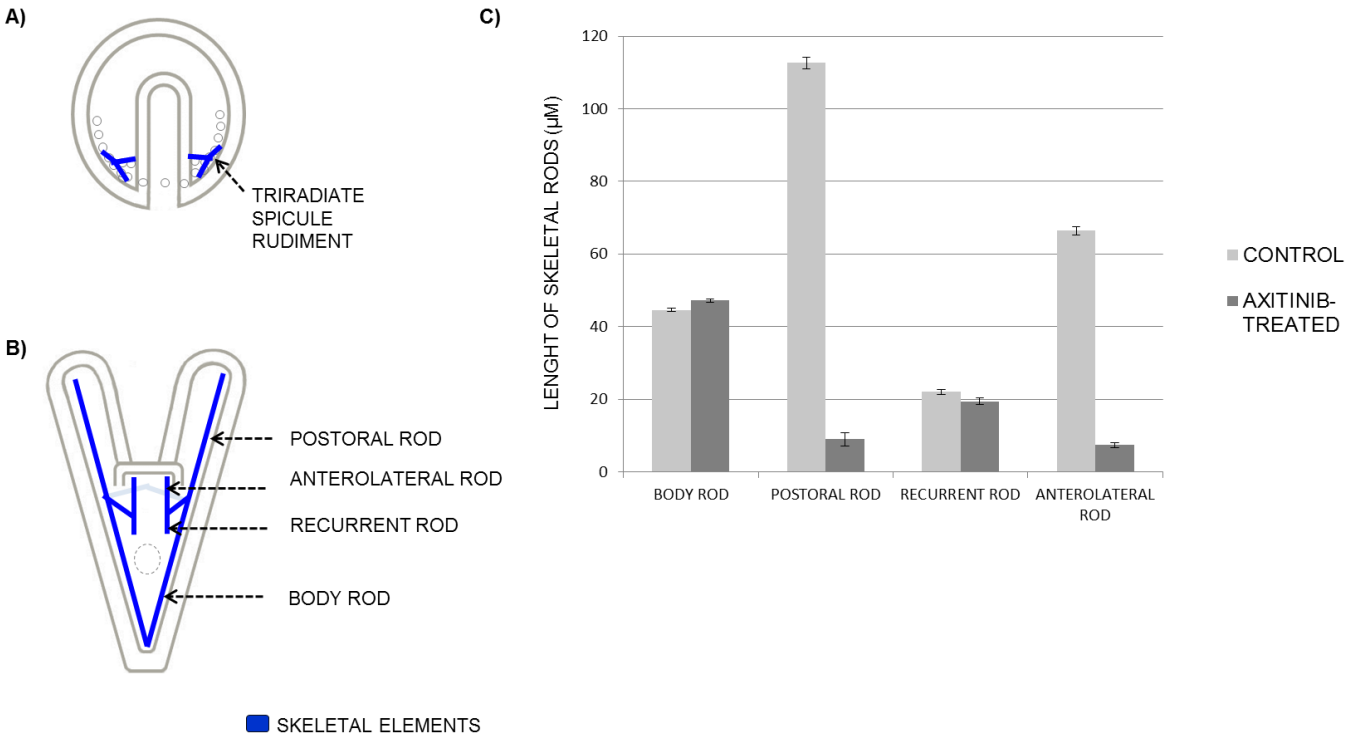

Figure 3.11: VEGF signaling selectively inhibits the elongation of specific skeletal rods. Schematic diagrams showing (A) the stage at which axitinib was added to embryo cultures and (B) the stage at which skeletal rods were measured using an ocular micrometer (skeletal elements are represented in blue). Graph (C) shows that the body rods and recurrent rods are of comparable length in control and drug-treated embryos while the postoral rods and anterolateral rods are significantly shorter in drug-treated embryos.

A)

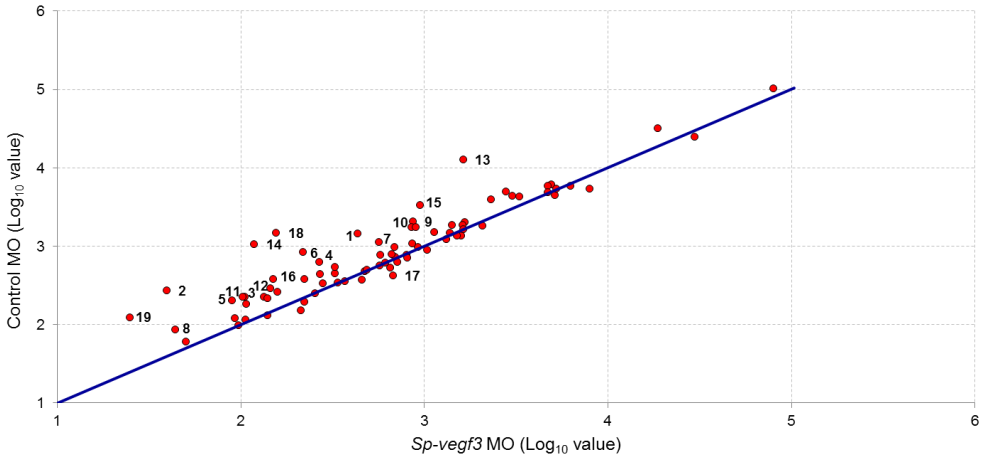

LEGEND

1- sm27/pm27	8- Sp-p16rel1	15- Sp-sm37
2- Sp-can1	9- Sp-p19	16- Sp-sm49
3- Sp-casc	10- Sp-p58A	17- Sp-tsp
4- Sp-Clectin	11- Sp-p58B	18- Spu_000164
5- Sp-fgfr2	12- Sp-sm29	19- Spu005989
6- Sp-frp (ficolin)	13- Sp-sm30B	
7- Sp-msp130rel2	14- Sp-sm32	

B)

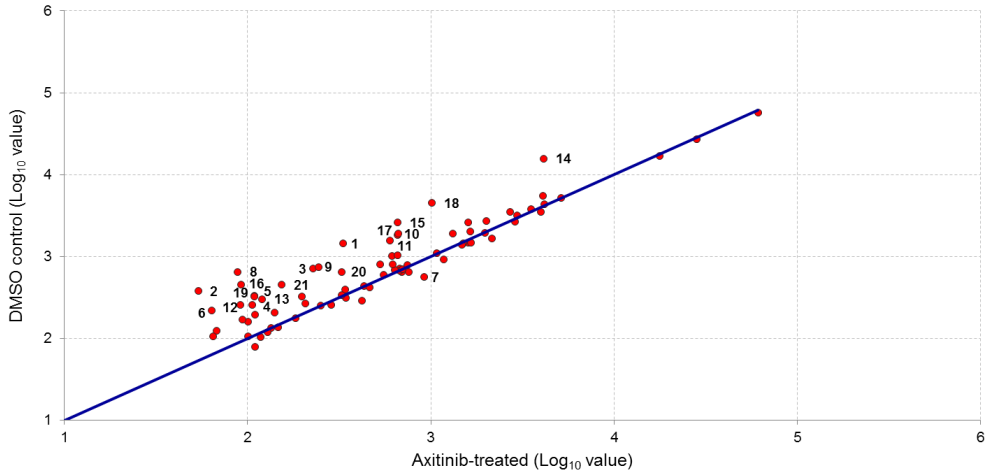

LEGEND

1- sm27/pm27	8- Sp-frp (ficolin)	15- Sp-sm37
2- Sp-can1	9- Sp-p16rel2	16- Sp-sm49
3- Sp-Clectin	10- Sp-p19	17- Sp-sm50
4- Sp-egf-rich	11- Sp-p58A	18- Spu_000164
5- Sp-ets1/2	12- Sp-p58B	19- Spu005989
6- Sp-fgfr2	13- Sp-sm29	20- Spu005991
7- Sp-fos	14- Sp-sm30B	21- Sp-vegfr

Figure 3.12: VEGF signaling regulates the expression of genes in the PMC GRN. Analyses of changes in gene expression by the Nanostring nCounter system in *Sp-vegf3* morphants (A) and axitinib-treated embryos (B) show changes in the expression of many genes with proven or predicted roles in biomineralization. Legends list genes with changes of 50% or more between control and axitinib-treated or *sp-vegf3* morphant embryos (n=3 for both axitinib-treated embryos and *Sp-vegf3* morphant embryos).

Supplementary Information

A)

```
Lv-vegf3    1 MGPSVDSKPGDRLSRVGLLD-ISGTN-VLCETTTRARDACHCSRDVADGN  48
Sp-vegf3    1 MGHSAEATPMDRLSPVGSPD-LSGTN-VLSGTSTGVRDSCKCSHYDADGR  48
Pl-vegf3    1 MGQSPEARPMDRISRVGSPDNLRGSNGPNSGTKSAARDSCQCSYLDDQAR  50
              ** * .. * **.* **  * . *.*   . * .  **.*.**

Lv-vegf3   49 RVTERVDHAHFDKLSSTTSYPCASHATHNQVNSLSRPDLRHSRSMRTPLS  98
Sp-vegf3   49 RVFERVDRAQFTDVSSSTSYPCASHMTHNQTNSLSRPDVRHSRSRRTPSS  98
Pl-vegf3   51 RVIERVDHAHIT---TTTSHPCASHTTHTHMNSTLRPDVCHARSCRTPAS  97
              ** ****.*.     ..** ***** **.. **  ***. *.** *** *

Lv-vegf3   99 S---------SSAHHSDSVLSSQ---KATTTTTTDLLRNSHASWSLSCWF 136
Sp-vegf3   99 ATTSLSSSTSSSSSHTDSVFSSK---KAATATTPDLRRNSNASLSC-CWF 144
Pl-vegf3   98 TSSS-----SSSSSHRDSVLSSKRVTTTTTTTTPDLRRNSHASSLSCSWF 142
              .         **. * *** **.    ..*.** ** ***.**    .**

Lv-vegf3  137 SRRMYTGNIKPWTLSFMFYLFVLILSHQVESTHSVPALSR--RVDQRTNN 184
Sp-vegf3  145 SRRMYMGNITPWTLSFMFYLFVIILSHQVESTHSVPALSRRVTVEQRMRK 194
Pl-vegf3  143 SRRMYMGNIKPWTLSFIFYLFVIVLSHQVESTHSVPMLSQR-VIEERMRK 191
              ***** *** ******.*****..************ **.   ...*

Lv-vegf3  185 MNALEDYLNALSLNGTNTPRSRYFVNRSPSALNKRSYRRLGRAGSYSGSR 234
Sp-vegf3  195 VNSLEDYLNALSLNDTDTPRSRYFLNRSPSALNKRSYRRLGRAGSAGGSS 244
Pl-vegf3  192 VNSLEEYLSALSLNGTSTLRSRYYLNRSPTALNKRSYRRLGRAGSAGG-L 240
              .*.**.** ***** * * ****..****.***************  *

Lv-vegf3  235 INNAFMAKIEDERARVQCQPRDRVVDSYEELGIPRGYGDFLLPECIVVRR 284
Sp-vegf3  245 SDSAFFARLEDENARVQCQPRDRVVDSYEELGIPRGYGDFLYPECIVVRR 294
Pl-vegf3  241 QNSAFLARLEDENARVQCQPRDRVVDSYEELGIPRGYGDFLYPECIVVRR 290
                 ** *..*** ***************************** ********

Lv-vegf3  285 CKQGGCCGDDQECVPSRTTNVTMNFLQVRQQIPIEIVHETVHDLECECQD 334
Sp-vegf3  295 CKQGGCCGDERECVPSRTTNITMNFLKTR----LQITREIVHDLECECQD 340
Pl-vegf3  291 CKQGGCCGDERECVPSRTTNITMNFLKTG----REITREIVKDLECECQD 336
              *********..*********.*****.       .* .* *.********

Lv-vegf3  335 KPSFCPEPVVDCPDDKVWSYSECTCKCRNRCPKPFLQDEDTCGCDCLSQD 384
Sp-vegf3  341 KPSFCPEPVVDCPDNKVWSYSECTCKCRNRCPKPFLQDEDTCGCDCLSQD 390
Pl-vegf3  337 KPSFCPEPVVDCPNNKVWSYSECTCKCRNRCPKPFLQDEDTCGCDCLSQD 386
              *************  **********************************

Lv-vegf3  385 RHCKNIYKGRRNGKLSQEECDCVRKGLCGKPPCINGAFSISDCKCINSNS 434
Sp-vegf3  391 RNCKNIYRGRRNGKLSREECDCVRKGLCGKPPCINGGFSISDCKCINSNS 440
Pl-vegf3  387 RNCKNIYRGRRNGKLSREECDCVRKGLCGYPPCINGGFSISDCKCINSNS 436
              *.*****.********.************ ****** *************
```

Supplementary Figure 3.1: Analysis of VEGF3 and FGFA proteins in *L. variegatus, S. purpuratus* and *P. lividus*. ClustalW alignment of the of VEGF3 (A) and FGFA (B) protein sequences in *L. variegatus, S. purpuratus* and *P. lividus* show that VEGF3 proteins are 70% identical (A) and FGFA proteins are 80% identical among the three species of sea urchin. Asterisks show identical amino acids, and dashes show conserved amino acids.

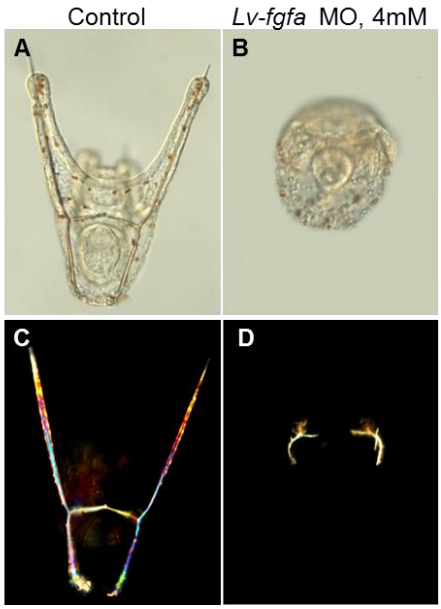

Supplementary Figure 3.2: Knockdown of *Lv-fgfa* using a translation-blocking MO leads to the formation of truncated skeletal elements. DIC (A-B) and) polarized light (C-D images of control embryo (A, C) and embryos injected with 4 mM Lv-*fgfa* translation-blocking MO (B, D) show that shortened skeletal elements form in *Lv-fgfa* morphants.

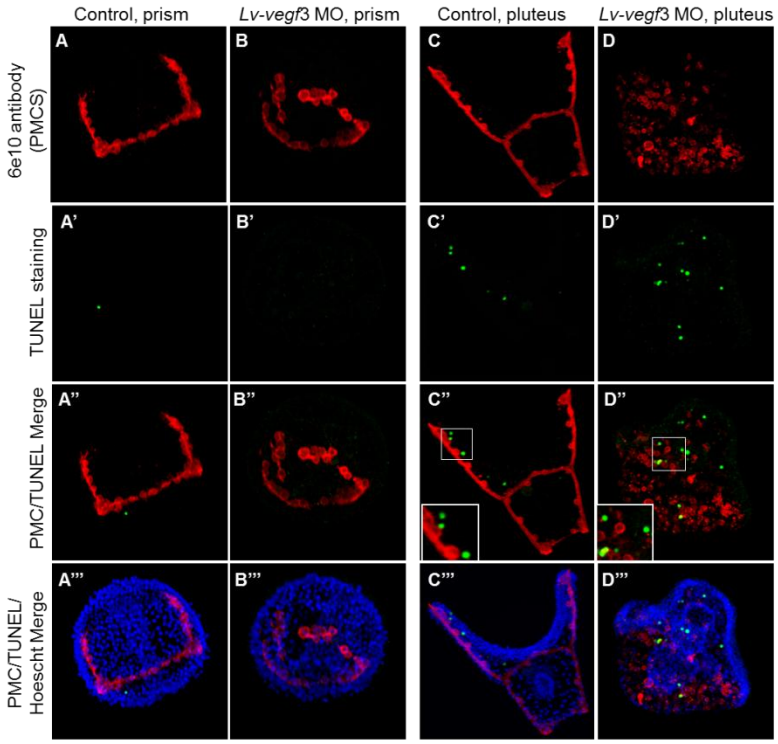

Supplementary Figure 3.3: PMCs in VEGF morphants are not undergoing apoptosis. Fluorescence images of 6e10 antibody labeled-PMCs (A-D), TUNEL staining (A'-D'), 6e10/TUNEL merged images (A''-D'') and 6e10/TUNEL/Hoechst merged images (A'''-D'''). There is no apparent correlation between the position of apoptotic cells and PMCs, either in control embryos (A-A''', C-C''') or in *Lv-vegf3* morphants (B-B''', D-D'') (see inserts in C'' and D'').

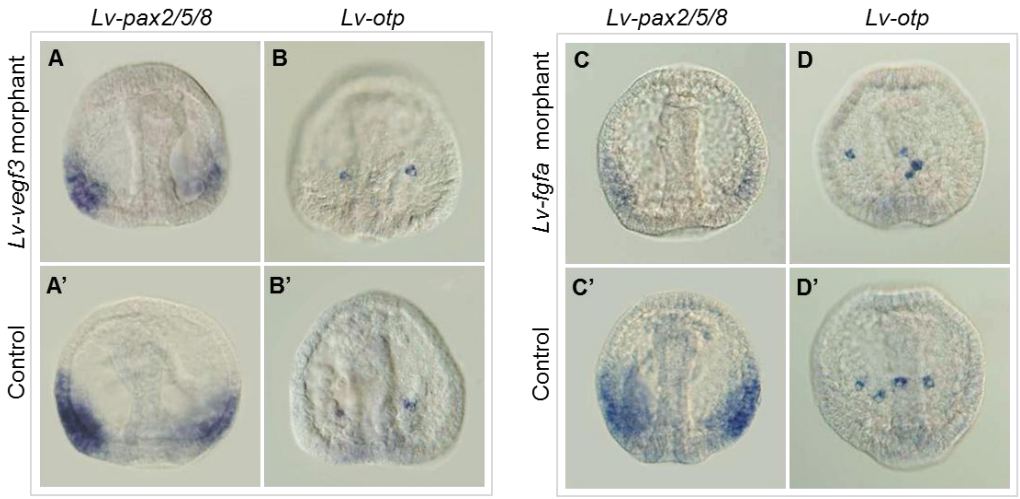

Supplementary Figure 3.4: WMISH analysis of *Lv-pax2/5/8* (A, A', C, C') and *Lv-otp* (B, B', D, D') expression in *Lv-vegf3* morphants (A, B), *Lv-fgfa* morphants (C, D) and controls (A'-D') at the late gastrula stage show that *Lv-pax2/5/8* expression is not strongly affected in *Lv-vegf3* morphants (A), while its expression is downregulated in *Lv-fgf* morphants (C). *Lv-otp* expression is not affected in either *Lv-vegf3* (B) or *Lv-fgfa* (D) morphants

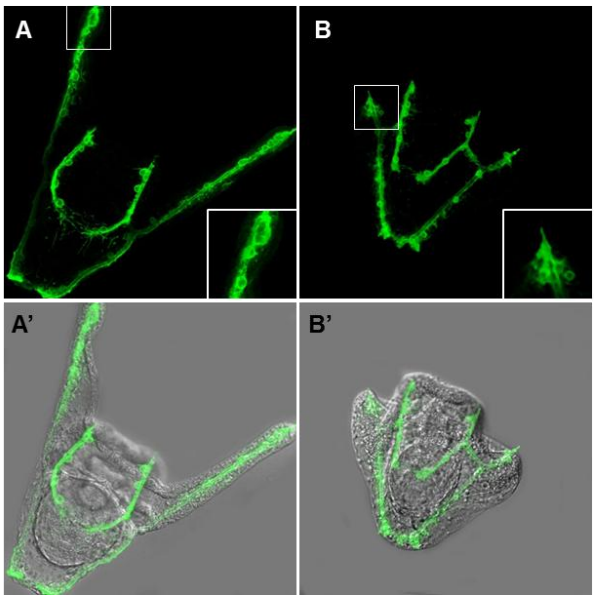

Figure 3.5: Blocking VEGF signaling at later stages does not affect the location of PMCs along the skeletal rods. Fluorescence (A,B) and merged images with DIC (A', B') of pluteus embryos treated with DMSO (A, A') or axitinib (B, B') from the late gastrula stage. PMCs are visible along the skeletal rods and at the tips of the body rods (A, B, inserts) in both control and axitinib-treated embryos.

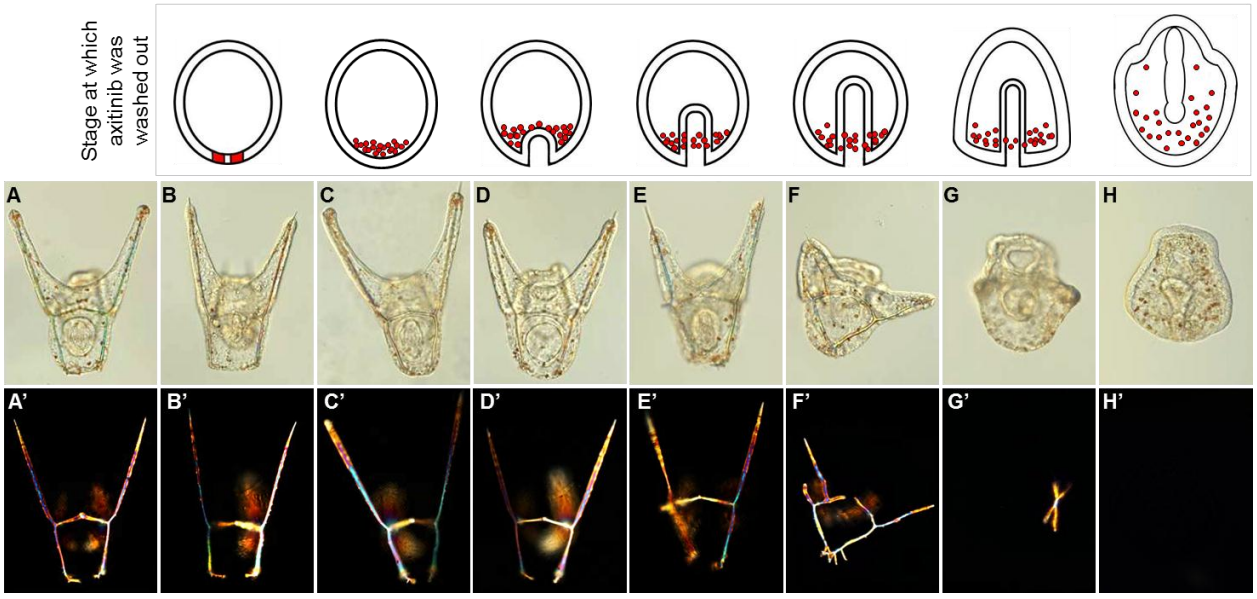

Supplementary Figure 3.6: The effects of VEGFR inhibition are reversible early in development. DIC (A-H) and polarized light (A'-H') images of control embryo (A- A'), and embryos treated with the VEGFR inhibitor axitinib at the 2-cell stage and washed out of the drug at hatched blastula (B, B'), mesenchyme blastula (C, C'), early gastrula (D, D'), mid-gastrula (E, E'), late gastrula (F, F'), prism (G, G') and pluteus (H, H') stages. Embryos are able to recover and secrete skeletal elements comparable to controls if VEGFR inhibition is alleviated prior to the late gastrula stage (B'-E'), and truncated skeletal elements are secreted if the inhibitor is washed out at late gastrula or prism (F', G'). Embryos do not form skeletal elements if axitinib is washed out at the pluteus stage (H'). Schematic diagrams indicate the stage of development at which axitinib was washed out of embryo cultures (PMCs are represented in red).

OBSERVED PHENOTYPE	STAGE AT WHICH AXITINIB WAS WASHED OUT															
	DMSO CONTROL		HATCHED BLASTULA		MESENCHYME BLASTULA		EARLY GASTRULA		MID-GASTRULA		LATE GASTRULA		PRISM		PLUTEUS	
	#	%	#	%	#	%	#	%	#	%	#	%	#	%	#	%
NO SKELETON	0	0	0	0	0	0	0	0	0	0	3	1.3	42	16.3	**236**	**100**
TINY SKELETAL DEPOSITS (SPECKS)	0	0	0	0	0	0	0	0	0	0	0	0	15	5.8	0	0
BRANCHED SKELETAL RUDIMENTS	2	0.9	9	3.6	5	2.3	11	4.3	5	2.1	**116**	**49.8**	**183**	**70.9**	0	0
EXTENDED RODS, WITH PROMINENT BODY AND DORSOVENTRAL CONNECTING RODS	0	0	0	0	2	0.9	1	0.4	0	0	0	O	7	2.7	0	0
SHORT PLUTEUS SKELETON	10	4.4	31	12.4	26	11.9	28	11.0	61	26.0	114	48.9	11	4.3	0	0
WILD TYPE PLUTEUS SKELETON	**214**	**94.7**	**211**	**84.0**	**185**	**84.9**	**215**	**84.3**	**169**	**71.9**	0	0	0	0	0	0
TOTAL	226	100	251	100	218	100	255	100	235	100	233	100	258	100	236	100

Supplementary Table 3.1: Distribution of phenotypes in axitinib washout experiments. Bold type indicates prevalent phenotype for drug washout at each stage of development.

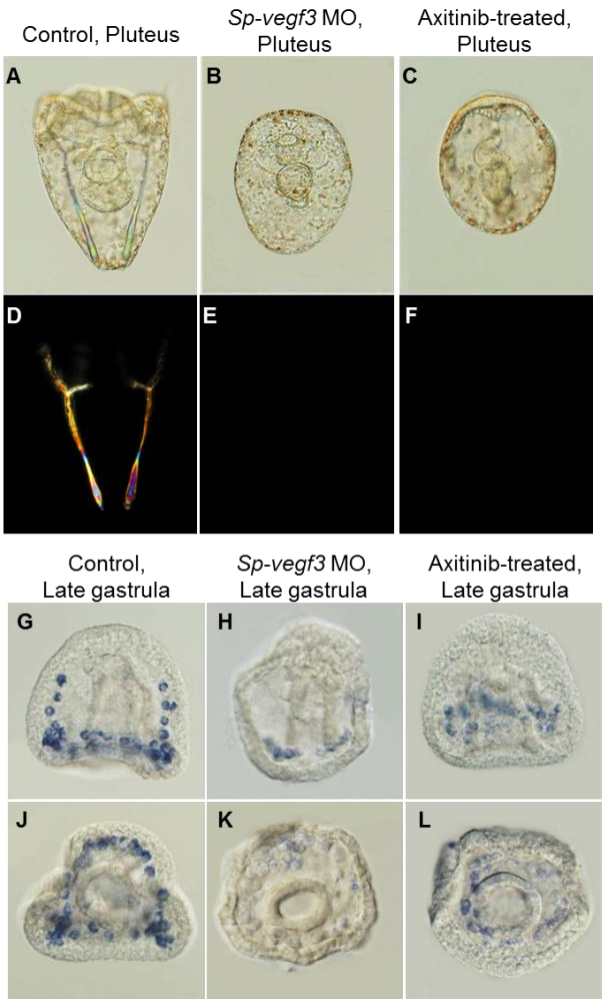

Supplementary Figure 3.7: Perturbation of VEGF signaling in *S. purpuratus* inhibits PMC migration and skeletogenesis. DIC (A-C) and polarized light (D-F) images of *S. purpuratus* control embryo (A, D), *vegf3* morphant (B, E) and embryo treated with 50n M axitinib from the 2-cell stage (C, F) show that skeletogenesis is inhibited in *Sp-vegf3* morphants and axitinib-treated embryos. WMISH analysis of PMC position show that PMC migration is perturbed in *Sp-vegf3* morphants (H, K) and axitinib-treated embryos (I, L) as compared to controls (G, J) at the late gastrula stage. Lateral (G-I) and blastoporal (J-L) views of embryos are shown.

	Gene Name	Accession Number	Targeted Region	Target Sequence
1	Sp-alx1	NM_214644.1	600-700	AAGAAGAGGAGAAATAGGACGACGTTCACCAGCTATCAACTTGAGGAGATGGAGAAGGTATTTCAAAGAACGCACTATCCCGATGTGTACTGCAGAGAAC
2	Sp-alx1(intron)	SP_PMC_003.1	920-1020	TCGCCTCATTTTCTCGCCTTTGTTTGTAGAGAGGGAGGAGAAAGGAAAAAAAAAGCAAGTTTGAGCGCGAGTCGGATATCGTGACTGAAATTGAAGATAACCC
3	Sp-pmar1	SP_PMC_007.1	334-434	TCGGTCGTAAGCGGAAGAGATCGTGCGACACCGTTGAGGTCGACCAGACGACACCACCTACCAAGAAGATGAATTCCGTTTCTTCCACGTTCTCTGTTGA
4	Sp-tbr	tbr_742649.1	305-405	TCGAATTCACGTCCTAGAGTTGAGCGAGAGCCGCTCTATCCAAACCCATAGCTTTCCCGAGACGCAATTCTTCGGCGTGACGGCCTACCAAAATACTGAT
5	Sp-tbr(intron)	SP_PMC_015.1	1811-1911	GAGGAAATTCGATGGGACTCCTTTGTTTCTAGTTTCTGCAGTGAGGGGAGGGGGGGGGGCTCTCTCGATGTGTTATATTTGTGTCTGATATTAAAAAAA
6	Sp-dri	NM_214634.2	855-955	GACGTGAAACCAGCCACGCCCATATTGATCTGAACATGATGCGAGCCAATGCCCACCTCAAGGAGATGATGGATAAGAACCGTCGATTTGTTTCTACCCG
7	Sp-dri(intron)	SP_PMC_009.1	664-764	TGCCCATCATGTGTTGAAACATGCCCCATGTGCTCTATTATCATTATCACAGCTTCTAGTTAGACGAAAATGAAAGCAATGAACCACTTTTGTGAAGTAC
8	Sp-erg	NM_214668.1	355-455	TGTATAGGAAGCATTATCGGTAGTCTCGGACGACCAGACGCTATTTGAGAACACATACCGTGAGGTGAATAAGTCCAACACTATCGTCTCGTCGCCACAC
9	Sp-ets1/2	SP_PMC_049.1	23-123	ACGTCAGCTCTGGCTATCTCAACACAACATCGTGTATGCCCAGATTAGATGACTTCTTAGCACAAGGTTTCTCTGTAGATCAACCACAAGCCGTACCCGT
10	Sp-ets1/2(intron)	SP_PMC_018.1	18-118	GTCAGGGTTTCGGTAAAAGAAGAAAACGTCCACAGAGAAAGATGACGGACAGGCTTTGGGCTATTTGCCGCAGAAACTGTAAAGAGGAGCAATTAAGATT
11	Sp-fos	SP_PMC_013.1	518-618	AGCTCCAACAGCAGAAAGAACAACTGGAGTTCATTCTGGAGGCTCACAAGGCTATGTGCCGTAAGAACAAGGTCAACAAGGAGACAACTACAACAGCCTC
12	Sp-foxB	NM_214632.1	625-725	ACAGTGATGCCAAGCCGCCATATTCCTACATCTCCCTAACGGCTATGGCTATCCAGAGCTCGCAGGAGAAGATGCTACCCTTGAGTGATATCTATAAATT
13	Sp-foxN2/3	XM_790403.2	650-750	ATGATCCAATGGACCCGCACCGACACATCAATAGCAAACCTCCTTTCTCATTTAGCTGCCTCATATTCATGTCGATAGAGGACTGCCCTCTTAAGCGTCT
14	Sp-foxO	XM_001183650.1	685-785	AGGCAAGTCATCAAGGAGAAGAGCATCCAGCATGGACACCACAAATTCAAAGTTTGAAAGGAAGCGGGGGCGCGTGAAGAAGAAGGTCCTGGAAGAGCGT
15	Sp-hex	hex_742618.1	290-390	CACGTTCCCGGGGCATTCGTTCGGACCGTCGCCGTACGGACAGCCTCAGCATCCGACCGGAGCTTACTACGATCCCGCCGCCTTACCTGGTGGGCTGGCT
16	Sp-jun	GLEAN3_03102.1	655-755	AAAACCAGGAGCGCATCAAGGCTGAGAGGAAAAGGCTCAGGAATCGAATCGCCGCCAGCAAGTGCCGCAAGCGCAAGCTTGAGCGTATTGCCAGGTTAGA
17	Sp-smad1/5/8	SP_PMC_048.1	0-100	AACCGAGAAGGCAATAAGTAGTTTCCTCAGCGTCCATCCTGAGTTGATAGGTGTTGATTAAGGTGCTGGGCAGGCTCTCTTCAACAAGTCGAGAGATCTA
18	Sp-smad1/5/8(intron)	SP_PMC_046.1	1292-1392	TTCACACCTTTCTCTTGTTGGTCCACACAGGCAGTGGATGATTAATGGTGAAGCAATGAATAGAATATAAACAGGAATCAATAGCAGAACAGCATTCAGT
19	Sp-snail	AY372519.1	365-465	CCCGTCAACATTCCGCATCCAGTTATCCCACAAACCCGAGCCTCTCCAGGCCATTCCCAACCCATCGGCCTACTGGCGACACCATCCGAATGTGATCTACA
20	Sp-snail(intron)	SP_PMC_016.1	1143-1243	GCTTAAGTATGATCAGAATGGTTCGTTGGACGTGGGGGATTCGAGAAAACATAATTACGACGCCCAAAGTGAATATTACATGAGGATAAAGGCAATAGCT
21	Sp-tel	XM_791264.2	290-390	CAGCGCATGTTCGAGAAACAACCCTTGCGACTTCCCGGCGGGAAAAACCTCCACGACAACTTCAGCGAGTCGGTGATGGATTCCTCTCAGGTTCCGCCGT
22	Sp-tel(intron)	SP_PMC_041.1	348-448	ACACTGATTCCACCAGAACAAATTCAGGTTTTGGAAATCCATGTGATGTCTACTAACTGAAATTACTGCTAAACTTGGAGACCAAATTGAGGTTACCTGT
23	Sp-tgif	XM_775847.2	590-690	AGCTCTACCTATCTCGCTTGGCTAACCTCACTCTTCTCCAGGTGTGCAATTGGTTCATCAACGCTCGAAGACGTATCCTGCCAGAGATGATTCGTCGCGA
24	Sp-hesC	GLEAN3_21608.1	525-625	GCAACATCGCCAGTCCAGCAGTTTGCTACAACACCAAACGGCATGGTTCTCCTCCTCCCAGCCCACACCGTCCAACACAACTCGGTCATCTCGGTTCGAG
25	Sp-hesC(intron)	SP_PMC_025.1	303-403	ATTGTTTGTGGTAGGGCGTCGTTTGTATAGAGGGTTACGGGGGAGAAGGAACGTGCGAACAATGTTTACTCGGTGGAACAACGGGCGAGCTTCGCCGTCT
26	Sp-can1	XM_779235.2	949-1049	ACGACGGTCATACACTTAAAGTCAGTACGGAAGGCATGTACGTGCTGAAAGGAGGTGGACTGCCTTTTGATGCCAAGCCAGCTCAACTTCATTTCACTG
27	Sp-msp130	SP_PMC_012.1	7-107	CCCATGATTCCGACTACACCTTTACCCGGTACAATCTGCAATGGAACATCTACTATGAGCTACGTTGTCAGTCAGATCAACTTCCACAAATTCAACGCAC
28	Sp-msp130rel1	NM_214641.1	708-808	GTACGGATCGGACGTCAGGCACATTGACTTCCGACTCTTCAACGATCCTGCACTAGCACCTCTGATGGAACAGCAGTTTATCCGCAACACATACAAAGGT
29	Sp-msp130rel2	NM_214642.1	319-419	ATTCTTGGTCGCCTGGATTACCCGCGGTGTCAAAATAACCGATCCGGGAACCGTCCATGTGTGGGATATGTACAGGCGGGTCAGTAAGAAATGGAATCTT
30	Sp-msp130rel3	XM_001195507.1	409-509	GACAAGTTCGATTCACCACGCCCTGTCACGGATATCGCCGAGTGCGGGCGCTATGTAGCATGGGCTGTAGAAGGTCAGGAGATTACAGACAGTGGATCGG
31	Sp-msp130rel5	XM_791451.2	1156-1256	AATCACTGGCATTTGCTGAGGTCAACGGGACCAGACTTCTCTTTGTAGGAATCGAGAGATTGTCCGCCATTGCTATCTTCACATTCCCTTCCGGGTCAGC
32	Sp-p16	AF519415.1	539-639	TCGGATACTTCGTCTACAGGAAACGTCAAAATGGCGCTACCATGCTTCAAAACGCATAAGAACTACTCACGCGCACTTAGATTAAAAAACTCTTGCCGTC
33	Sp-p16rel1	XM_794764.2	273-373	ACGAGGTGTTTGAAGGGAACGTCTGACTGGCTAATTACAGGCAGTTAAACTCTTTATCGGACTACCGCGAAGTAATAGGAAGAGACCAATTGCACCAATA
34	Sp-p16rel2	SP_PMC_045.1	395-495	AAGACATCTTGGAAATAATATCGCTGAGGTGAAAGGCCGCAACTTCGGTAAAAAGATCGGTATGGGCTTTGGTGCACTTATGGCTGTTGTTGTAATAGGA
35	Sp-p19	SP_PMC_002.1	388-488	TCAATGACTTGGAGAAGGAAGTTGGTGATATGAAGGGTGAGCTTGACACACTCAAGGTCTGTGTTGCGAGACCGGAGGAGATCGACACTAAGGTCCCGGA
36	Sp-p58A	SP_PMC_001.1	367-467	CCATGACAAACGATGCCTTTTTGGCTATCCCAACTCATGGTCTTGGGCAAGAATACTATGTTGCATCTTACGACCCGGTGCCCATCGAAATGTCACAGTT
37	Sp-p58B	XM_794812.2	263-363	CCCAGCAAGCGCCTTACCTACCTTCAAACTCGCCAACGTTCACTGTTGGATCACCGGACACACGTGGGACGAAGTTCATGTTTGCGATGCCGAGTAACTT
38	sm27/pm27	XM_777844.1	202-302	CAAAATGCAAGGGAGGCTGGTTCCTCATCGGGCAGCAATGCTTTAAGATGATGTCCAGAGCGCTGAAATGGAACGACGCTGAGTTGATGTGTGAGCAGAA
39	Sp-sm29	SP_PMC_028.1	287-387	CCCGAAAGCAACCGATACTTCTGGGCTGATGGAACCGAATTCTTTTTCACACGCAACTTCGTCTTCAACCGCTTCAAGCCCGACCAACCGCAGCAGAACG
40	Sp-sm30B	SP_PMC_019.1	751-851	TGAATAGTCTCACTGGAGGACGTTTTGGAGGGTCACTCCTTCCAGGAGATACCACGAAGACAACGAATGAGGCCTTCCAATTACAGAAAGAATCCTTACTT
41	Sp-sm30E	SP_PMC_023.1	245-345	ACCCGGTGGAAGACAACCTGGGTTTGGTAACCCTGGAACACCCGGTGGTAGACAACCTGGATGGGGTCAACCTGGTGTCGGACAGCCTGGTGCCGGACAA
42	Sp-sm32	SP_PMC_021.1	829-929	GAGATATCACTCAAAGAAAACAGAGGTTATCCAATACATGGCACTTCCGCATTCTGGGCATCAACTGTGCCAATGCGTGTAGCATCCACATGTTGATAGT
43	Sp-sm37	SP_PMC_037.1	147-247	AAGACGTTTACAGGATGCGATGGAATTTCACCCGGCCATCTTGCCGCACCAACAACATTCGAGGAACGCGAAGCAGTCCTGAAAATTAGGTTCGATCTGT
44	Sp-sm49	XM_794872.2	393-493	CTTTCTACCAGCCTCCAACTGGTCAGCAGCTTGACTTCATACCACCTGAAAAAGCTATTTGGACAGCCTTGGCTTTCGATTGGAACCTTGAGCAATGGAC
45	Sp-sm50	SP_PMC_004.1	6-106	GCGCGTTCCCTACAGGATGGCCTCCGAATTCTGTGAAATGGTTACACCTTGTGGAAATGGACCAGCAAAAATGGGTGCTCTGGCTTCAGTTTCGTCGCCT
46	Spu005991	XM_776670.2	477-577	TACTGCTATAAATTCTTCAACCAAAGAATGAACTGGCTCCAGGCGCAACGAGAATGCAATAAATATTCTGCCCTCAACGGTACCACGCCTAGAGGCTATC
47	Spu005989	XM_776543.2	693-793	TCGATGGCGTCTTCACATTCGACAATTATCCATACCAAACATGGGTCACTTCAAGCCACGAGACGCAGATGTCTTTCACATGCCAATATCAGTATCTACC
48	Sp-Clectin	NM_214640.1	204-304	TGGTCCTCTTTTCAGTAGTGGCCCTACACACAAATAAAGTCGCTGGACAGTTTTATATCGGAACACAATGCAGTTGCCCTACCTTTTGGACCGGCTATGG
49	Sp-vegfr	XM_779931.2	1209-1309	TTCAATGTTACCTGCAATGTAGAATCACCCCTTGGAATCCAAATCAGGTGGAAATGGGACTATCCAGGTCTTCATAACCCCAACGCTAATCCCAATAATT
50	Sp-fgfr2	XM_786393.1	1253-1353	CAAGCAGAGACCAACTTTCGACCAACTGAGACATCGATTAGAGACGATATTGATCGAATCTGGGAACTACCTCGTACTTGACGATTTTGATGAGCGTCTA
51	Sp-egf-rich	SP_PMC_014.1	8-108	GTGTGGGCGGTGAGTGCGTCAACCTGATTGGTGACTACCAATGTCATTGTCTGACAGGGTTTCTTTCCTTCCTCGGAGATGGAAACTGTGAAGACGTGGA
52	Sp-frp (ficolin)	XM_781185.2	636-736	CGACTTTAGAATGACAATCGAGGAGTTTCTAGGAGGGAACGCGACGGATGCACTGACCTATCACAGCGGGAGTAAGTTTACGACGACGGATAAAGACAAT
53	Sp-net7	SP_PMC_047.1	604-704	TGGAATCGAAGGCTCACGTCGTTGGGATTGCTTGTATAATCGTCGCTATCTTTCAGATCTTTGGTATTGGGCTCGCATATACGATGTGGAAAAGCGTGAG
54	Sp-p133 (lam/EGF)	SP_PMC_011.1	309-409	ATGCATCTCGGTGGCAGTGGAGTTCTTCCATCAGGTTTCCATGGGATGAGTGGCTGTCTTGCAGGAGTGCTCATCAATGGCAAATATCAATTCATCTATG
55	Sp-stomatin	SP_PMC_005.1	354-454	ATCTCTGTGGATGCTGTGGTCTTCTACCGTGTCAAGAATGCTACCATCAGCATCGCTAATGTGGAAGATGCCCACAAGTCTACCAAACTTCTGGCTCAGA
56	Sp-casc	XM_782734.2	217-317	GTCTCTCCTTGGACTCAGTGCCTCGTATGTAGGGTGTGTGAGATCCAGTGAAACATTTAGACTAGGTCCAGACTGTGATCTTATCGGCTGACTGACTCCA
57	Sp-cyp1	NM_001033647.1	515-615	CAAGACCAAGTGGCTGAACGGTGCCCATGTTGTCTACGGTAAAGTCCTGGATGGCCTTGATGTTCTGGCCACCATTGAGAACTCTGCTACAGATGAGAAC
58	Sp-cyp2	SP_PMC_032.1	6-106	ATTTCAAGTTGTGAAGTGATTAAAGACAAGGTGACTGGAGACTCCCTGAGCTATTCCTTCATTGAATTTGAAAGGGAGGAAGACTGCGAAGAAGCCTACT
59	Sp-pks2	SP_PMC_035.1	374-474	CGCCAACAGAGGCTAAGGGAGTGATCTTTGCAACACTGTCAACTCATTTGGTCGAACGTTTGGGTCTAAGTGGAGATGTGTCTCAAGACGCGACACCCAT
60	Sp-scp	SP_PMC_008.1	212-312	CATAAAGCGCTAGAAGATTGAGCTTGGCTTCAGCGCCCTATATGGAACCTCCGCCCAAATCGACTAGTTCCTCAAAATGATTGATATTGACTGGACGTGC
61	Sp-lasp1	SP_PMC_043.1	273-373	CTTCAGGGCACAAGGAGAATTTGGGGAAGTTCACCACTGTGTCCGATGATCCAGAAAGCTTACGACTTAAGAAAAATACTCACCAGGCTTCTGATGTGAC
62	Sp-delta	NM_001032370.1	1650-1750	GAAAATGGAGGAACCTGTCTGCAAGATGTAATGGGAGGATTCATGTGCGAGTGTGCTGAAGGATGGATAGGTACAACATGTACGCAATCGACTGGTAAAG
63	Sp-fgfA	NM_001124764.1	364-464	ATACCCGGCGAGTAAGAGAGCCTCGCACGTCATCATCATCGGGTTCTTATGCGTAACCCTGGCGGCAGGTTTATCAGACGATGGCGGGTTGCAAACGAGAA
64	Sp-wnt8	NM_214667.1	650-750	CAGTGACAATGTACGATTCGGTGAACGAATGGCGAGCGATATCATGGACGACGCAGAGAGTTCACAGGGCGCCATCTCCGTTATGACTCTACATAACAAC
65	Sp-coll (colp3alpha)	NM_214466.1	4672-4772	GTTTATCTGCACTTGGCATCAAGGGAGAACCTGGTTTCCCTGGACTTAAGGGAGACTCCGGTCAACCTGGTCTAAATGGTGGATCTGGATCAATCGGTCT
66	colp4alpha	NM_214511.1	2-102	ATGGTAGCTCAGGAAGTTCTCTGTGCGATTCTGTTCAGCAATTGAAGAGCCCTGATGCCTCGCTAACCGGCCAGTAGCCCTCGGTTTGAATGCTAATATT
67	Sp-fn3-rich	SP_PMC_017.1	146-246	AGATGTAGGGGATGTATATGCCAATTCAAGAGAAATGACTGCTGATGTGGAGGGACTAACACCAGATACTCTATATGACGTTCAGGTTGCTATGGTTTAC
68	Sp-p11	SP_PMC_040.1	117-217	CCGGATGATCTTGTCTACAATAGCTGCGGGGCGTGTGAGGTCTTAACATGTGGAAAACCAATGCCCAGGTGCAATCGCATGTGCTATCCAGGATGCTTTT
69	Sp-tsp	SP_PMC_027.1	4-104	GATTCAGTCACCAGGATCTATAGTCCAAAGCTATTTTGTCTAGTTTGTATTTTCTCTTTTTGCGAAAGGATTCTGTACTCCAGTTTGCTGTTCGTGGAGA
70	Sp-alpha actinin	SP_PMC_024.1	431-531	CTTGGCTAACGGCAAGGCTTATATCCTCACCTGATGAGCTTCGTATGGAACTTCCTCCCGAGCAAGCAGAGTACTGCATCGCTCGTATGGCACCATTCAAT
71	Sp-arp1	XM_791369.2	482-582	CTCAATGCAAGCCATTCTTAGTTTATATGCTACAGGTAGAACCACAGGAGTAGTCTTAGATTCAGGAGACGGTGTGACGCACGCCGTCCCGATCTACGAA
72	Sp-arp3	XM_775172.2	190-290	TACATCATTCCCTCAGCCATTGCGATCAAAGAATCAGCTAAAGTTGGAGATCAAGCTTCTCGAAGATTAGGGAAGGGTGTGGAAGATCTGGATTTCTTCA
73	Sp-advillin	SP_PMC_006.1	475-575	GTTCCAATGCTTCAGGTAACTTTAGGGTAGAGGAGATCAACAATTACACGCAGCAAGACCTCATACAAGATGATGTCATGCTCCTAGATGCTTACAATGA
74	Sp-cdc42	XM_784336.2	141-241	AGATTCGAAGGGGCGTCGATTTACATCGAAAAGGTCATCCTTGGTGGATAAAACCAATCACGTAGCAGCAGGTTACCAAAGCTAAATCAAAATGCAGACG
75	Sp-cofilin	SP_PMC_036.1	411-511	CAATTTGGGTGTAAAGAGCAAGATGGGATACGCATCCAGTGTGGAAGAGTTGAAGAAGGAGTGTCTTGGGCCGACGGTAGTGTACGTGCAAAACGAATTA
76	Sp-p21-arc	XM_782276.2	12-112	AAGTACCGACTCTCCCTCCCTCTTTCTCCCTCGAAGAGAGACTTCATTTCTAACTTTCCTACCGTTAGTCCTCACAGTATTTAGTGACAAGATGCCGGCC
77	Sp-profilin	SP_PMC_042.1	364-464	CTTAAGGGAAGAAGACTCAAAGTTGGTGTTGGGGAAAAAGAAAGGTGAAGGATCACTCACATTGCAAAGCAGCAAGACAGCGATTGTAATCGGTCATTGC
78	Sp-alpha spectrin	SP_PMC_044.1	233-333	AAGTCTTGTCTGAGATCCTTGGGTTATGATCTACCCATGGTGGAAGAAGGCCAGGATGAACCAGTCTTCCTCTCTATACTCGACGTTGTTGATCCTAACC
79	Sp-beta spectrin	SP_PMC_026.1	543-643	AAGGAGAACGGTGAACGCATCACCGAGGGACAGACAGACACACAGTACATGTTCCTCAGACAGCGTCTGCAAGCCTTGGATGATGGATGGCTGGAACTGC
80	Sp-talin	SP_PMC_022.1	84-184	CCACCCAGGGCCTGTGCGAGTCGGCCAACTCCGTGGTACAAGGTCATGCCAGTCAGGAACGTCTGATTGGATCAGCCAAGCAAGTCGCTAGCTCCACCGC
81	Sp-wasp	XM_791919.2	158-258	CCTCAGGTCAAAGGTTGGTTCAACACTATTGGTGTGTCCGATGACCAGCTCAAGGATCAGAACACAGCCAAGTTCATCAGGAACTTCATCGACCAGCATG
82	Sp-elav	SP_PMC_029.1	5-105	TTATCTCAAACCCGCAGATGCCCTGAAAGCCGTCAAGACATTAAATGGATTGCGTCTTCAATGTAAGACGATTAAGGTGTCATTTGCCCGCCCATCTAGC
83	Sp-calumenin	SP_PMC_010.1	453-553	AAGAAGCTAACAAAGGCTGAAATCCTGGACAAGTATGACCTCTTCGTGGGAAGCCAGGCGACCGACTTCGGCGAAGCCCTTACTAGACATGACGAGTTTT
84	Sp-cdi	SP_PMC_034.1	589-689	GTAAACCGTCCGCCCATCGCGAGGAATTAACCTCTGAGGATATTAACCATGGATGCAAATAGTGTTGAGACCAGTAATAATGGAATATCATCTCGACCGTC
85	Sp-vigilin	XM_787409.2	370-470	AGTGGACGCGGGCCGTCCTATGCCAGAATGGCAGTCAAGTCTTCCGTTGTAACTCAGGTGTTCCATGTGCCTTTAGAGGAACGTCGCTACAAAGAAATGA
86	Sp-alx4 (alx1-like)	SP_PMC_020.1	165-265	CAACGCGGTGCGCGCCGCAGCGGCCCACGGCGTCGGCGTTGGTGTGATGGAGGAAGCGCATCGACGTCTAACCGCGATGCAGTCGCCGATTGCGTCAAGC
87	Spu_000164	XM_781455.1	54-154	ATGCCCTTCGCTCAAGCTAACCTCTTCTGCGGTCAATGTCACCCAGGTGCGCATCTAGTAGTCATCAGTGATGCAGCCGAGCATGAGTTCCTCTACAATA
88	Sp-pks	pks_742571.1	40-140	CCGTGGTAGGCATTGGAACTCGCCATGCTTGTGGCGCAAACACTACCGATGACTTCTGGAAGGTTCTCAAGGAAGGTAAGGAGTGCATCCTGGACATTCC
89	Sp-endo16	NM_214519.1	30-130	TTCGCGGTTTTGGCCGTGGCGCGGTCAATGCCCACAGAGTTGCAATGTGACATCGACGAGGCCCATACGAATGTTGGAACACCACGAGTAGTCGACGATG
90	Sp-spec1	NM_214603.1	310-410	TCAGTCCTCAAGAGCTGCGTGAAGCGTTGTCAGCAAGCAAACCACCGATGAAGAGGAAGAAAATCAAAGCAATCATCCAGAAAGCCGACGCCAATAAGGA
91	Sp-ubq	GLEAN3_21496.1	10-110	TTGTCAAGACCCTCACCGGCAAGACCATCACACTCGAGGTCGAGCCAAGTGACTCCATCGAGAACGTAAAGGCCAAGATCCAGGACAAAGAAGGCATCCC
92	Sp-spz12	NM_214616.1	780-880	GAGTGTCTTCATGGAGTGAGGCCCTACGAATGCAAAACTGCGGGAAACGGTTCGCCCAGAAGAGCTGTCTTACGCGTCACACCAAGTCACACCCGGAGA
93	Sp-tatabp	GLEAN3_12621.1	70-170	AAGAGATTTGCAGCAGTGATCATGAGGATACGTGAGCCAAGAACCACAGCTCTAATCTTCAGCTCAGGGAAGATGGTCTGTACTGGTGCAAAGAGTGAAG

Supplementary Table 3.2: List of probes used in Nanostring nCounter analyses.

	VEGF MORPHANTS										
	TRIAL 1			TRIAL 2			TRIAL 3				
GENES	VEGF MO	CONTROL MO	% CHANGE	VEGF MO	CONTROL MO	% CHANGE	VEGF MO	CONTROL MO	% CHANGE	AVERAGE % CHANGE	
colp4alpha	2130.408985	2048.448266	4.001112434	1071.583698	1768.912248	-39.42131956	1743.952708	2231.197988	-21.83783251	-19.08601321	
sm27/pm27	728.8220489	1435.555164	-49.23064837	243.5702589	1332.041632	-81.71451605	325.4849379	1576.365647	-79.35219291	-70.09911911	
Sp-advillin	256.720472	158.6945328	61.77020559	136.0979263	144.6151803	-5.889598885	244.2614722	157.5622431	55.02538389	36.96866353	
Sp-alpha actinin	1524.715115	1255.684362	21.42503017	1064.701234	1409.453221	-24.45998079	2140.652824	1453.103089	47.31596398	14.76033779	
Sp-alpha spectrin	1571.132776	1212.382132	29.59055854	1118.17269	1239.82087	-9.811754544	1231.891729	1216.849853	1.236132487	7.004978829	
Sp-alx1	255.5883339	180.9008047	41.28645498	148.2745945	261.7422793	-43.35091951	356.0908815	311.6404408	14.26337369	4.066303054	
Sp-arp1	866.942894	884.839622	-2.022595687	521.5159466	699.2860399	-25.42165625	685.693351	623.6487913	9.948637847	-5.831871363	
Sp-arp3	2166.637403	1564.35154	38.50067247	1787.360022	2099.426074	-14.86435059	2238.356413	1842.150539	21.50779026	15.04803738	
Sp-beta spectrin	474.0909822	439.6038716	7.845042518	437.8675301	407.8145809	7.369267952	509.1205995	585.1292419	-12.99006048	0.741416664	
Sp-calumenin	5831.368349	6587.410231	-11.47707301	3531.8001	5794.314846	-39.0471489	5402.54012	6025.373608	-10.33684429	-20.28702207	
Sp-can1	71.04982783	291.9321639	-75.66221313	18.0371865	279.2440297	-93.54070828	28.84271531	256.4290866	-88.75216705	-85.98502949	
Sp-casc	93.69258932	204.2173901	-54.12115037	42.39052295	141.2494591	-69.98889537	177.1638266	339.8881104	-47.87583879	-57.32862818	
Sp-cdc42	7296.355017	6202.131414	17.64270264	5029.530292	6495.058007	-22.56373559	6338.375703	4999.469608	26.78096279	7.286643281	
Sp-cdi	1859.827985	2454.823041	-24.23779825	1134.0553	1259.342053	-9.948588048	1242.486094	1853.706403	-32.97287576	-22.38642069	
Sp-Clectin	333.705861	754.9329318	-55.79662153	91.62661621	591.5829603	-84.51162012	377.2796117	564.5854822	-33.17582127	-57.82802097	
Sp-cofilin	30141.76922	23446.41181	28.5560002	22483.99006	27736.79787	-18.93804696	35827.20236	24091.0423	48.71586675	19.44460667	
Sp-coll (colp3alpha)	2039.837939	1581.006244	29.02149794	860.8743959	1334.061065	-35.46964089	1230.714577	1591.773467	-22.68280615	-9.710316366	
Sp-cyp1	3781.066297	4830.894128	-21.73154293	2205.602104	3743.244325	-41.07779475	2987.024879	4530.81509	-34.07312326	-32.29415365	
Sp-cyp2	74.44624206	136.488261	-45.45593773	71.50864262	116.3431219	-38.53642447	132.4320629	113.9067537	16.26357399	-22.57626273	
Sp-dri	3071.215724	5864.596082	-47.63124892	2345.369079	3349.45494	-29.97758978	2923.458689	5663.289843	-48.37879096	-41.99587655	
Sp-egf-rich	365.4057271	432.9419901	-15.59937924	312.9243257	512.8250834	-38.98030034	293.7018426	402.8033745	-27.08555559	-27.22174506	
Sp-elav	485.412363	577.282757	-15.91427995	424.6320212	487.245602	-12.8505174	546.7894531	443.8908939	23.18104756	-1.861249931	
Sp-endo16	4828.294016	2912.272241	65.79130026	4320.636433	6033.281053	-28.3866209	6226.546294	4609.138174	35.09133507	24.16533814	
Sp-erg	777.5039861	491.7886104	58.0971925	393.9256404	475.8021498	-17.20809993	775.1568784	630.0687162	23.02735535	21.30548264	
Sp-ets1/2	641.6474172	367.4334881	74.62954194	235.0995331	338.4807234	-30.54271134	492.640476	413.0752544	19.26167709	21.11616923	
Sp-fgfA	159.3565976	165.3564144	-3.628414882	68.33212048	187.0232679	-63.46330526	91.23175419	196.0817925	-53.47260293	-40.18810769	
Sp-fgfr2	153.6959072	190.893627	-19.48609826	38.68458045	204.5250183	-81.0856487	74.75163071	212.7735973	-64.86799506	-55.14658068	
Sp-fn3-rich	196.7171541	211.9895852	-7.204330887	289.1004096	481.8604481	-40.00329125	351.3822748	315.4923958	11.37583012	-11.94393067	
Sp-fos	2753.084926	2850.09468	-3.403737955	1650.240149	2195.685701	-24.84169532	450.2630156	609.5249565	-26.12886301	-18.12476543	
Sp-foxN2/3	871.4714463	744.9401094	16.98543752	528.3984113	721.4998	-26.76388666	985.8670286	848.3461631	16.21046591	2.144005589	
Sp-foxO	123.1281792	128.7160658	-4.341250292	134.5096652	125.7671414	6.951357646	161.8608548	142.1544233	13.86269315	5.490933502	
Sp-frp (ficolin)	423.1447689	858.1920958	-50.693467	82.62647013	780.7364938	-89.41685565	146.557883	881.7297726	-83.37836744	-74.49623003	
Sp-hesC	968.8353207	1260.125616	-23.11597286	504.0450748	940.2716803	-46.39367692	580.9268518	752.0472894	-22.75394647	-30.75453208	
Sp-hesC(intron)	318.9880661	464.0307706	-31.25713072	187.9811213	429.3551968	-56.21780691	299.587601	447.7428489	-33.08936106	-40.18809956	
Sp-hex	160.4887357	210.8792716	-23.8954429	95.86197907	203.851874	-52.97468835	141.8492763	262.8490115	-46.03393201	-40.96802109	
Sp-jun	9928.57604	8469.391769	17.22891455	4161.280905	5817.20175	-28.46593458	1512.053828	2158.010844	-29.93298285	-13.7233343	
Sp-lasp1	855.6215132	825.9930016	3.587017269	876.2275862	1203.471081	-27.19163758	1025.890186	895.8536074	14.51538256	-3.029745918	
Sp-msp130	7746.945971	6848.333925	13.1216155	2231.014281	4174.729787	-46.5590734	4086.484545	6633.982489	-38.40073361	-23.94606384	
Sp-msp130rel1	196.7171541	254.1815017	-22.60760412	66.21443904	174.2335272	-61.99672926	155.9750964	224.3294621	-30.47052538	-38.35828626	
Sp-msp130rel2	1003.931601	1416.679833	-29.13489852	196.9812674	761.2153106	-74.12279225	494.9947793	1193.738123	-58.53405619	-53.93058232	
Sp-msp130rel3	275.9668193	303.0352998	-8.932451282	118.0976341	282.6097509	-58.21176244	272.5131124	559.4495422	-51.28906329	-39.47775901	
Sp-msp130rel5	875.9999986	756.0432453	15.8663878	676.106691	700.6323284	-3.50050038	571.5096383	447.7428489	27.64238218	13.33608987	
Sp-net7	243.1348151	261.9536969	-7.184048933	70.97922226	165.482652	-57.10775636	160.6837031	355.2959302	-54.77468514	-39.68883014	
Sp-p11	1885.867161	1765.318301	6.828732258	1382.882868	1715.060709	-19.36828466	1593.277294	1527.574218	4.301138031	-2.746138124	
Sp-p133 (lam/EGF)	1386.59427	1125.777671	23.16768267	479.6917384	892.4784388	-46.25172805	708.0592329	1274.629177	-44.4497862	-22.51127719	
Sp-p16	2764.406306	4364.56242	-36.66246371	1716.947114	3277.428506	-47.61298039	2387.854676	4198.262979	-43.12279418	-42.46607943	
Sp-p16rel1	64.25699939	85.41383574	-24.76980008	17.50776614	73.26189011	-76.10249187	50.0314455	101.0669039	-50.49670706	-50.456333	
Sp-p16rel2	631.4581746	491.7886104	28.40032509	286.4533078	566.003479	-49.39018602	788.1055469	633.9206712	24.32242436	1.110854476	
Sp-p19	1288.098258	2564.744087	-49.77673351	559.6342124	1379.161729	-59.42214749	738.6651765	2323.644907	-68.21092696	-59.13660266	
Sp-p21-arc	815.9966807	689.4244298	18.35911891	635.8707439	793.5262345	-19.86770994	952.9067816	671.1562356	41.97987459	13.49042785	
Sp-p58A	1231.491354	1688.706663	-27.07488037	712.6366957	2318.871098	-69.26794697	595.0526719	1295.172937	-54.05612215	-50.13298316	
Sp-p58B	162.7530118	189.7833134	-14.24271769	48.74356724	210.5833165	-76.85307267	94.76320922	284.6767562	-66.71199628	-52.60259554	
Sp-pks	11507.90865	7104.816365	61.97334403	4913.587234	4310.704925	13.98570115	7342.486084	4951.962164	48.27427676	41.41110732	
Sp-pks2	303.138133	139.8192018	116.8072262	117.5682137	133.8448723	-12.16083838	240.7300171	314.2084108	-23.38524085	27.08704899	
Sp-profilin	24799.20964	34803.80955	-28.74570351	13773.43692	36582.58642	-62.34974542	17467.16766	25616.41645	-31.81260272	-40.96935055	
Sp-scp	1654.910994	1474.416139	12.24178503	1262.175027	1223.665408	3.147070954	1583.86008	1412.01557	12.17015692	9.186337634	
Sp-sm29	235.2098486	334.1240804	-29.60404161	34.44921759	236.8359421	-85.45439629	164.2151582	309.0724709	-46.86839702	-53.97561164	
Sp-sm30B	3122.161938	11014.23052	-71.65338122	981.5822374	15980.33359	-93.85756103	761.0310583	11561.91685	-93.41777779	-86.30957335	
Sp-sm32	254.4561959	1122.446731	-77.33022077	48.21414689	805.6428309	-94.01544394	51.20859717	1272.061207	-95.9743606	-89.1066751	
Sp-sm37	1806.617496	3489.635309	-48.22904586	453.2207205	3006.824519	-84.92693146	584.4583068	3655.137332	-84.00994946	-72.38864226	
Sp-sm49	129.9210077	241.9680522	-46.30654481	157.8041609	458.9735437	-65.61802677	159.5065514	441.322924	-63.85717968	-58.59391709	
Sp-sm50	1614.154023	1645.404433	-1.899254007	384.9254943	1591.202167	-75.80913964	688.0476544	2027.044376	-66.05660623	-47.92166663	
Sp-smad1/5/8	1185.073693	767.1463813	54.47817024	831.2268558	1074.227385	-22.62095837	1074.153404	880.4457876	22.00108394	17.95276527	
Sp-smad1/5/8(intror	126.5245935	77.6416406	62.95971144	70.44980191	125.0939971	-43.68250794	92.40890586	94.64697898	-2.364653519	5.63751666	
Sp-snail	65.38913746	38.78066487	68.61272924	42.91994331	65.85730339	-34.82887835	41.79138376	77.95517422	-46.39049406	-4.202214388	
Sp-spec1	63786.64851	78027.20737	-18.25076066	89651.55084	151567.7404	-40.85050645	85592.46665	81399.14397	5.151556241	-17.98323696	
Sp-stomatin	4263.357117	5260.585488	-18.95660424	2478.253588	3787.671845	-34.57053067	3069.425497	3897.810494	-21.2525724	-24.9265691	
Sp-talin	381.2556602	352.9994114	8.004616388	271.6295378	366.7527818	-25.93661145	354.9137298	323.1963057	9.813671622	-2.706107814	
Sp-tbr	895.2463458	641.6809454	39.51580646	312.9243257	388.966542	-19.54980906	617.4185537	843.2102231	-26.77762475	-2.270542449	
Sp-tel	117.4674889	112.0613619	4.824255954	99.56792158	125.7671414	-20.83153001	99.47181592	111.3387837	-10.65843134	-8.888568466	
Sp-tgif	480.8838107	753.8226182	-36.20729876	513.5746412	844.012053	-39.150793	729.247963	741.7754096	-1.6888463	-25.68231269	
Sp-tsp	780.9004004	426.2801085	83.18950023	651.7533546	437.4329278	48.99503746	591.5212168	409.2232994	44.54729672	58.91061147	
Spu_000164	278.2310954	1239.029658	-77.54443619	70.97922226	2068.461438	-96.56850155	117.1290911	1202.726018	-90.26136549	-88.12476774	
Spu005989	17.83933835	59.87662312	-70.20650562	19.62544757	193.0815661	-89.83566999	37.08277705	115.1907387	-67.8075013	-75.9498923	
Spu005991	145.7709407	291.9321639	-50.06684471	53.50835046	405.7951482	-86.81395017	906.9978662	384.8275848	135.6894106	-0.397128102	
Sp-vegfr	515.980091	450.7070075	14.48237599	160.4512627	535.7119878	-70.04896916	297.2332976	658.3163858	-54.84947602	-36.80535639	
Sp-vigilin	4830.558292	4287.950782	12.6542383	4243.870481	5372.926547	-21.01380051	4982.296972	5111.176301	-2.521519942	-3.627027383	
Sp-wasp	607.683275	739.3885415	-17.81272755	592.4582745	849.397207	-30.24956173	778.6883335	777.7269891	0.123609494	-15.97955993	
Sp-wnt8	1294.891086	1272.339066	1.772485102	1062.583552	1838.91925	-42.21695422	1014.118669	1455.671059	-30.33325335	-23.59257416	
Sp-spz12	571.4548566	472.9132794	20.83713475	436.279269	349.9241756	24.67823014	498.5262344	416.9272093	19.57152789	21.69563093	
Sp-tatabp	40.48209983	45.44254643	-10.91586406	46.09646545	53.0675627	-13.13626798	54.7400522	54.84344456	-0.188522724	-8.080218256	
Sp-ubq	21277.1281	22578.14658	-5.762290909	23439.59381	25240.10585	-7.133536034	16992.77553	21657.89076	-21.54002566	-11.47861753	

AXITINIB TREATED EMBRYOS

	TRIAL 1			TRIAL 2			TRIAL 3			
GENES	AXITINIB	DMSO	% CHANGE	AXITINIB	DMSO	% CHANGE	AXITINIB	DMSO	% CHANGE	AVERAGE % CHANGE
colp4alpha	2127.208393	3282.411804	-35.19373801	1179.49539	1798.836034	-34.43007766	1500.922835	2833.894517	-47.03674303	-38.8868529
sm27/pm27	223.6986005	1305.583214	-82.8660021	456.8878171	1501.527342	-69.57179505	315.1979259	1501.968609	-79.01434663	-77.15071459
Sp-advillin	256.2186995	255.1345499	0.424932503	109.9052451	112.3170857	-2.147349758	183.1133329	167.4514051	9.353118191	2.543566979
Sp-alpha actinin	1587.37475	1258.712802	26.11095624	1168.856774	1133.430866	3.125546367	2048.997985	2015.045126	1.684967691	10.30715676
Sp-alpha spectrin	1613.390829	1272.498217	26.78924086	1476.5583	1376.763873	7.248478018	1888.067332	1791.329944	5.400310974	13.14600995
Sp-alx1	206.3545478	255.1345499	-19.11932435	265.3927184	250.3532641	6.007293076	281.7972242	247.7815669	13.72808227	0.205350333
Sp-arp1	600.9317485	674.2111824	-10.86891405	526.4480025	507.8438275	3.663365385	532.3024868	612.290473	-13.06373197	-6.756426878
Sp-arp3	1394.422163	1371.753209	1.652553386	1265.422678	1121.927852	12.79002267	1866.81234	1836.245734	1.664625036	5.369067032
Sp-beta spectrin	939.1407777	773.4661744	21.41976066	489.622022	429.9772654	13.87160704	840.4998703	748.7653715	12.25143447	15.84760072
Sp-calumenin	3063.787243	3210.727643	-4.576545132	1917.651711	2253.647545	-14.90897875	3893.627646	4107.084393	-5.19728174	-8.227601874
Sp-can1	82.77817171	365.4178742	-77.3469834	41.16341475	346.8016194	-88.13055867	37.36481657	420.534603	-91.1149246	-85.53082222
Sp-casc	95.78621129	131.06581	-26.91746893	62.44064794	109.6625438	-43.06109839	143.6397764	236.5526195	-39.27787538	-36.41881423
Sp-cdc42	4193.31868	4705.066688	-10.87653038	4948.02073	4622.383759	7.044784433	6278.741388	6227.627911	0.820753546	-1.003664132
Sp-cdi	2634.521937	2438.744372	8.0278018	1879.18902	1873.163207	0.321691852	1393.129662	1508.87873	-7.67119758	0.226098691
Sp-Clectin	167.330429	497.7578635	-66.38316714	237.5686442	776.8374058	-69.41848546	275.7243694	869.6924968	-68.29633803	-68.03266354
Sp-cofilin	12739.60069	13345.76515	-4.541998584	16984.38787	16211.22881	4.769281067	23320.69031	21628.56108	7.823586713	2.683623065
Sp-coll (colp3alpha)	2096.856301	2717.209766	-22.83053275	878.3407052	1322.788188	-33.59929328	966.5116085	1694.588244	-42.96481096	-33.13154566
Sp-cyp1	2012.304043	2298.133134	-12.43744699	1151.671316	1630.715047	-29.37629919	1772.68309	2141.154842	-17.20901942	-19.6742552
Sp-cyp2	152.1543828	186.2074721	-18.28771366	92.71978748	116.7413222	-20.57671977	157.3036998	100.077721	57.18153671	6.105701092
Sp-dri	6148.860631	7693.744778	-20.07974259	4115.75357	6046.987907	-31.93712913	1994.342292	2803.662736	-28.86654068	-26.96113747
Sp-egf-rich	108.7942509	379.2032898	-71.3097819	136.9109641	230.8866235	-40.70208052	72.28373195	157.9499881	-54.23631694	-55.41605979
Sp-elav	436.1632471	365.4178742	19.36012928	474.8916298	555.6255815	-14.53027983	381.9993293	383.3927002	-0.363431791	1.488805887
Sp-endo16	1908.239727	2813.707675	-32.18059773	1187.678942	1938.641907	-38.73654864	2953.853358	3421.25484	-13.66169735	-28.19294791
Sp-erg	514.2114846	500.5149466	2.736489312	193.3774676	290.1713924	-33.35750091	315.1979259	392.030352	-19.59859121	-16.7398676
Sp-ets1/2	126.1383037	329.5757938	-61.72707279	81.26281576	373.3470383	-78.23397338	119.348357	296.152417	-59.70036029	-66.55380215
Sp-fgfA	334.266937	266.1628823	25.58735993	279.3047554	259.201737	7.755742166	246.8783089	239.1439151	3.234200533	12.19243421
Sp-fgfr2	56.76209254	241.3491343	-76.48133576	95.17485284	195.4927316	-51.31540081	38.88303028	221.8686115	-82.47474935	-70.09049531
Sp-fn3-rich	707.1640718	453.6445337	55.88506401	370.9605292	383.0803586	-3.163782523	316.7161396	419.6708378	-24.53224978	9.396343903
Sp-fos	414.4831811	368.1749573	12.57777664	1065.744028	501.6498964	112.447772	1271.672565	805.7738734	57.82002949	60.94852605
Sp-foxN2/3	780.8762961	721.0815953	8.292362635	618.1037762	629.9527545	-1.880931257	627.9499506	774.6783269	-18.94055522	-4.176374614
Sp-foxO	193.3465082	147.6083086	30.98619582	98.44827333	101.6989182	-3.196341594	148.1944176	158.8137533	-6.686660017	7.034398071
Sp-frp (ficolin)	48.09006615	685.2395149	-92.98200628	137.7293192	628.1830599	-78.07497081	78.3565868	639.0671936	-87.73891265	-86.26529658
Sp-hesC	941.3087843	908.5632467	3.604101056	610.7385801	549.4316505	11.158245	527.7478456	467.1779227	12.96506534	9.242470464
Sp-hesC(intron)	308.2508578	222.0495526	38.82075162	399.6029585	342.3773829	16.71418101	319.752567	367.844927	-13.07408541	14.15361574
Sp-hex	221.5305939	197.2358046	12.31763645	91.90143235	207.8805938	-55.79124021	107.2026473	211.5034293	-49.31399094	-30.92919824
Sp-jun	1257.837748	1302.826131	-3.453137969	1949.567561	1204.21865	61.89481539	3275.714665	2453.837838	33.49352653	30.64506799
Sp-lasp1	1164.613464	1203.571139	-3.236840291	1179.49539	1061.758235	11.08888549	890.6009228	1019.987638	-12.68512583	-1.611026875
Sp-msp130	5468.10656	4619.597112	18.36760712	2820.297411	3135.8403	-10.06246678	4183.606465	5236.889249	-20.11275652	-3.93587206
Sp-msp130rel1	63.26611233	169.6649735	-62.71115303	67.35077867	94.62013978	-28.81982754	72.28373195	105.2603121	-31.32859813	-40.9531929
Sp-msp130rel2	676.8119794	974.7332413	-30.56438924	585.3695713	888.3281652	-34.10435532	571.7760433	1203.105856	-52.47500124	-39.04791527
Sp-msp130rel3	351.6109898	434.344952	-19.0479852	109.9052451	240.6199438	-54.32413319	131.4940667	309.9726599	-57.57881783	-43.65031207
Sp-msp130rel5	1329.381965	974.7332413	36.38418275	1388.994302	1085.649112	27.94136575	816.208451	679.6641571	20.08996538	28.13850463
Sp-net7	58.93009913	175.1791397	-66.36009331	136.092609	165.4079235	-17.72304128	85.94765536	171.770231	-49.96359098	-44.68224186
Sp-p11	618.2758013	1151.18656	-46.292302	450.3409761	894.5220963	-49.65569012	898.1919914	1057.993306	-15.10418958	-37.0173939
Sp-p133 (lam/EGF)	746.1881905	1027.11782	-27.35125653	545.2701703	652.9587842	-16.49240603	290.9065065	742.7190152	-60.83222584	-34.8919628
Sp-p16	3271.915877	3141.800565	4.141424917	3111.631835	3698.603181	-15.87008168	1714.990969	3606.964353	-52.45334302	-21.39399993
Sp-p16rel1	145.650363	144.8512255	0.551695383	33.79821864	95.50498708	-64.61104317	14.59161089	79.34735671	-81.6104638	-48.55660386
Sp-p16rel2	321.2588974	726.5957615	-55.78574574	237.5686442	717.5526369	-66.89181644	170.9676232	788.4985698	-78.3173198	-66.99829399
Sp-p19	590.0917155	1584.048608	-62.74787829	659.8398875	1585.587835	-58.38515705	728.1520556	2348.458486	-68.99446764	-63.37583433
Sp-p21-arc	668.139953	784.4945068	-14.83178694	524.8112922	503.419591	4.249278655	840.4998703	716.8060598	17.25624509	2.224578936
Sp-p58A	681.1479926	1239.41322	-45.04270394	804.6887442	2325.320176	-65.39449695	304.5704299	1117.593104	-72.7476459	-61.0616156
Sp-p58B	52.42607934	211.0212201	-75.15601544	136.092609	250.3532641	-45.63977047	85.94765536	315.155251	-72.72847109	-64.50808567
Sp-pks	4024.214166	4092.994238	-1.680434124	3318.675681	3556.142766	-6.677658925	3224.095399	3727.891479	-13.51423675	-7.290776599
Sp-pks2	119.6342839	109.0091451	9.747015963	100.9033387	104.35346	-3.30618778	131.4940667	100.077721	31.39194754	12.61092524
Sp-profilin	23844.13048	22973.49937	3.789719176	28812.89282	26078.16102	10.48667426	32281.18764	32860.09972	-1.761747789	4.17154855
Sp-scp	1444.286315	1178.757391	22.52617251	1379.17404	1305.091242	5.676445889	1593.533872	1724.820025	-7.611585661	6.86367758
Sp-sm29	117.4662773	313.0332952	-62.47482965	106.6318246	291.0562397	-63.36384176	134.5304942	305.653834	-55.98599487	-60.60822209
Sp-sm30B	3675.165104	14539.58214	-74.72303489	5071.592354	18085.33538	-71.95743266	3582.393835	14367.75097	-75.0664259	-73.91563115
Sp-sm32	108.7942509	166.9078904	-34.81779044	146.7312256	213.1896776	-31.17339112	73.80194567	208.0483686	-64.5265444	-43.50590865
Sp-sm37	568.4116495	2637.254356	-78.44684005	809.5988749	2662.446996	-69.59192516	589.9946078	2537.62306	-76.75010851	-74.92962458
Sp-sm49	128.3063103	765.194925	-83.2322058	104.9951143	306.0986438	-65.69892861	43.43767142	291.8335911	-85.11560261	-78.01557901
Sp-sm50	661.6359332	1923.169831	-65.59659357	696.665868	1762.557295	-60.47414345	635.5410192	2040.094316	-68.84746876	-64.97273526
Sp-smad1/5/8	778.7082895	823.0936703	-5.392506644	537.9049742	652.9587842	-17.62037862	596.0674627	603.6528212	-1.256576341	-8.089820535
Sp-smad1/5/8(intron)	156.490396	75.92414778	106.1141292	83.71788113	80.46258303	4.045729055	88.98408279	81.93865226	8.598421305	39.58609317
Sp-snail	147.8183696	139.3370593	6.086902065	99.26662846	114.0867803	-12.99024463	54.06516741	62.07205311	-12.89934085	-6.600894471
Sp-spec1	38139.96598	41244.68913	-7.527570736	68760.07977	62571.91809	9.889678748	75653.51697	68660.57515	10.18479936	4.182302458
Sp-stomatin	2903.354755	2380.845627	21.94636738	3648.472795	2897.816377	25.90420927	5448.278487	5210.976293	4.553891253	17.46815597
Sp-talin	462.1793263	445.3732844	3.773473275	240.8420647	238.8502492	0.833918108	275.7243694	322.0653724	-14.38869465	-3.260434422
Sp-tbr	590.0917155	437.1020351	35.00090783	388.9643419	232.6563181	67.18408725	286.3518654	199.4107168	43.59903519	48.59467676
Sp-tel	180.3384686	147.6083086	22.17365694	72.26090941	107.8928492	-33.02530249	133.0122804	103.5327818	28.47358892	5.873981125
Sp-tgif	930.4687513	883.7494987	5.286481365	627.9240377	634.376991	-1.017211117	539.8935553	591.5601087	-8.733948182	-1.488225978
Sp-tsp	197.6825214	266.1628823	-25.72874187	158.1881973	206.9957465	-23.5790107	266.6150871	335.0218501	-20.41859746	-23.24211668
Spu_000164	1429.110269	3230.027225	-55.75547296	742.4937549	4245.43881	-82.51078892	864.7912897	6107.564551	-85.84065248	-74.70230479
Spu005989	110.9622575	188.9645553	-41.27879838	89.44636699	374.2318856	-76.09867827	126.9394256	404.9868297	-68.65591267	-62.01112978
Spu005991	132.6423234	483.9724479	-72.59300111	124.6356373	593.6740153	-79.00604809	719.0427734	871.4200271	-17.48608582	-56.36171167
Sp-vegfr	171.6664422	577.7132736	-70.28518297	129.545768	347.6864667	-62.74063549	158.8219136	425.717194	-62.69309397	-65.23963748
Sp-vigilin	3419.340325	3064.602238	11.57533864	2308.007104	2223.562736	3.797705667	2894.643023	2777.74978	4.208199155	6.527081155
Sp-wasp	770.0362631	773.4661744	-0.443446837	659.0215324	600.7527937	9.699287175	797.9898864	975.935614	-18.23334706	-2.99250224
Sp-wnt8	652.9639068	1054.688651	-38.08941569	655.7481119	686.5829815	-4.491062328	541.411769	686.5742785	-21.14301599	-21.24116467
Sp-spz12	507.7074648	434.344952	16.89037999	519.9011615	447.6742113	16.13381972	362.262551	356.6159796	1.583375871	11.53585853
Sp-tatabp	41.58604636	53.86748291	-22.79935109	42.80012499	58.3414006	-26.63850276	44.95588513	49.1155754	-8.469187694	-19.30234718
Sp-ubq	22554.16655	19631.91464	14.88521098	21504.98157	18494.13483	16.28000858	28541.82726	27172.206	5.040522875	12.06858081

Supplementary Table 3.3: Complete table of results obtained from Nanostring nCounter analysis of changes in gene expression between control and either axitinib-treated embryos or *Sp-vegf3* morphants.

Chapter 4

Signals Transmitted by Primary Mesenchyme Cells Regulate Gene Expression in the Ectoderm of the Sea Urchin Embryo

4.1 Abstract

The study of skeletogenesis in the sea urchin embryo provides insights into the interactions between different cell types during embryonic development. The sea urchin embryonic endoskeleton is formed by the primary mesenchyme cells (PMCs), which undergo a sequence of directional migration and differentiation events under the influence of signals from the ectoderm. Though the importance of ectoderm-to-PMC signaling has been well documented, there is currently no evidence of reciprocal signals transmitted from the PMCs to the ectoderm. In order to understand the mechanisms regulating the process of skeletogenesis, it is necessary to fully comprehend the nature of this communication between the PMCs and the ectoderm.

The work described in this chapter details the expression patterns of *Lv-fgfa*, *Lv-vegf3*, *Lv-pax2/5/8* and *Lv-otp*, four genes expressed in the ectoderm that regulate PMC behavior during skeletogenesis. We observed that *Lv-vegf3* and *Lv-pax2/5/8* are expressed in similar, overlapping domains in the ectoderm, while the domain of *Lv-fgfa* transiently overlaps this shared domain. *Lv-otp* is expressed in a domain largely independent of the other three genes. Additionally, we identify that there are signals transmitted from PMCs regulating gene expression in the ectoderm during skeletogenesis. We assayed the expression of *Lv-fgfa*, *Lv-vegf3*, *Lv-pax2/5/8* and *Lv-otp* upon the knockdown of *Lv-alx1*, a transcription factor essential for the specification of PMCs. In *Lv-alx1* morphants, which lack PMCs, we observed a downregulation of *Lv-otp*, *Lv-pax2/5/8* and *Lv-vegf3*, and an upregulation of *Lv-fgfa*. Additionally, we found that *Lv-vegf3* was upregulated and *Lv-fgfa*, *Lv-pax2/5/8* and *Lv-otp* were downregulated in embryos in which PMCs were surgically removed, and subsequent changes in the expression of these genes correlated with the respecification of PMCs which has been shown to occur under such conditions. Our findings therefore show that the signaling between PMCs and the ectoderm represents a complex, reciprocal tissue interaction.

4.2 Introduction

The sea urchin embryo is a valuable model organism for the study of a wide variety of developmental processes, including cell signaling. The formation of the endoskeleton is arguably the most intensively studied aspect of sea urchin embryogenesis, and this process is regulated by interactions between the mesoderm cells which form the skeleton, and the ectoderm of the embryo. As reviewed in Wilt and Ettensohn (2007), the sea urchin embryonic endoskeleton is formed by the primary mesenchyme cells (PMCs), progeny of the large micromeres which form at the vegetal pole of the embryo during early cleavage. The PMCs undergo an epithelial-to-mesenchymal transition (EMT), ingressing into the blastocoel. This ingression event is followed by the directed migration of PMCs to specific regions within the blastocoel. The PMCs form two ventro-lateral clusters (VLCs) of cells, linked by two chains of PMCs, one located orally and the other aborally, to form the sub-equatorial ring. The PMCs fuse as they migrate, forming a continuous single syncytium within which the calcite endoskeleton is secreted.

Although the endoskeleton is secreted solely by the PMCs, the ectoderm of the embryo has an essential function in regulating the migration patterns and differentiation of these cells. The VLCs and subequatorial ring of PMCs are formed at consistent locations along the blastula wall, regions which appear to be thickened prior to PMC migration (Gustafson and Wolpert 1961; Galileo and Morrill, 1985; Ettensohn and McClay, 1986). Additionally, several mRNAs in the PMC gene regulatory network are enriched in the VLCs and expressed in lower levels elsewhere in the sub-equatorial ring (Guss and Ettensohn, 1997). Moreover, treatments which block ectodermal patterning, such as nickel chloride, lead to the disruption of skeletogenesis (Hardin *et al.*, 1992; Armstrong *et al*. 1993).

The hypothesis of an ectodermal influence on skeletogenesis has been confirmed by the identification of a handful of genes which regulate this process. The homeobox gene *orthopedia (otp),* which is expressed in the ectoderm, has been shown to regulate PMC migration and biomineralization (Di Bernardo *et al.,* 1999, Cavalieri *et al.* 2003). Also, Duloquin *et al.* (2007) and Rottinger *et al.* (2008) have shown that ligands of the vascular endothelial growth factor (VEGF) and fibroblast growth factor (FGF) pathways expressed in the ectoderm provide migration and differentiation cues to PMCs, and the work described in Chapter 3 characterizes in detail the functions of VEGF signaling in regulating skeletogenesis. Likewise, Cavalieri *et al*.

(2011) detailed the roles of *strim1* and *pax2/5/8,* which are expressed in the ectoderm overlying the VLCs. In light of the essential functions the ectoderm throughout skeletogenesis, we hypothesize that there exists some reciprocal communication from the PMCs that regulates gene expression in the ectoderm.

In this chapter, we use florescent whole mount *in situ* hybridization (F-WMISH) to characterize in detail the expression domains of *Lv-fgfa, Lv-vegf3, Lv-pax2/5/8* and *Lv-otp* in relation to each other in the ectoderm of the developing embryo. We have identified a significant region of overlap between the expression domains of *Lv-vegf3* and *Lv-pax2/5/8* throughout embryonic development and a transient overlap between the expression of *Lv-pax2/5/8* and *Lv-fgfa*. *Lv-otp,* however, was expressed in a domain only significantly overlapping with *Lv-pax2/5/8.* We observed that the expression patterns of these genes were altered in the absence of PMCs: the expression of *Lv-fgfa* was upregulated, while *Lv-otp, Lv-pax2/5/8* and *Lv-vegf3* expression was downregulated in *Lv-alx1* morphants, in which PMC specification is blocked (Ettensohn *et al.,* 2003). Additionally, we observed changes in the expression of *Lv-fgfa, Lv-vegf3, Lv-pax2/5/8* and *Lv-otp* in embryos from which the PMCs had been removed by microsurgery (Ettensohn and McClay, 1988). In these embryos, there was an upregulation of *Lv-vegf3,* while *Lv-fgfa, Lv-pax2/5/8* and *Lv-otp* were downregulated. We, however, noticed a recovery of normal gene expression patterns that corresponded to the respecification of PMCs in these embryos.

4.3 Materials and Methods

Embryo Culture

Adult *Lytechinus variegatus* were obtained from Reeftopia, Inc. (Key West, FL, USA) or from the Duke University Marine Laboratory (Beaufort, NC, USA). Spawning was induced by intracoelomic injection of 0.5 M KCl, and embryos were cultured in artificial seawater (ASW) at 23°C.

Whole Mount *In Situ* Hybridization (WMISH)

Conventional and fluorescent WMISH were carried out as described in Chapter 3. *L. variegatus fgf, vegf, otp* and *pax2/5/8* WMISH probes were synthesized as described in Chapter 3.

Microinjection of Morpholino Antisense Oligonucleotide (MO)

Microinjections were carried out as described in Cheers and Ettensohn (2004). MOs were obtained from Gene Tools, LLC (Philomath, OR, USA). Design of *L. variegatus alx1* MO used was described in Ettensohn *et al.* (2003), and was injected at a concentration of 4 mM. Injection solution contained 20% (vol/vol) glycerol and 0.16% (wt/vol) Texas Red dextran.

Microsurgical Methods

PMC removal by microsurgery was carried out at the mesenchyme blastula stage as described by Ettensohn and McClay (1988).

4.4 Results

4.4.1 *Lv-vegf3, Lv-fgfa, Lv-otp* and *Lv-pax2/5/8* are expressed in diverse domains in the ectoderm of the developing embryo

Several ectodermal mRNAs that play a role in skeletogenesis have been reported to be expressed in localized patterns that correlate with sites of skeletal rod growth. We used two-color F-WMISH to directly compare the patterns of expression of four such genes (*Lv-vegf3*, *Lv-fgfa*, *Lv-otp* and *Lv-pax2/5/8*) during embryonic development. A comparison of the expression patterns of *Lv-pax2/5/8* and *Lv-fgfa* showed that both genes were expressed at the hatched blastula stage but in different territories. *Lv-pax2/5/8* was expressed in a ring in the ectoderm close to the vegetal pole, while *Lv-fgfa* was expressed in a non-overlapping ring in the ectoderm in a domain above *Lv-pax2/5/8* expression, and in the presumptive PMCs prior to ingression (Fig. 4.1A-A'''). At the mesenchyme blastula stage, we observed a small region of overlap between the *Lv-pax2/5/8* and *Lv-fgfa* expression domains, and at this stage both genes were restricted to the ectoderm overlying the VLCs (Fig. 4.1B-B'''). This narrow overlap persisted through the early gastrula (Fig. 4.1C-C'''), mid-gastrula (Fig. 4.1D-D''') and late gastrula (Fig. 4.1E-E''') stages, although in mid-gastrula and late gastrula embryos, *Lv-fgfa* expression was downregulated in the ectoderm overlying the VLCs and remained strongly expressed in the PMCs and in two domains of ectoderm near the animal pole of the embryo. At the prism stage, *Lv-pax2/5/8* was still expressed mostly in the ectoderm overlying the VLCs while *Lv-fgfa* was mostly expressed in the PMCs, though both genes were expressed at low levels in the same two domains near the animal pole (Fig. 4.1F-F'''). At the pluteus stage, *Lv-pax2/5/8* was expressed in the ectoderm overlying the postoral rods and in the oral hood, and *Lv-fgfa* was expressed in the PMCs lining the postoral rods and also in the endoderm (Fig. 4.1G-G'''). No regions of co-expression were observed at this stage.

Because the expression pattern of *Lv-pax2/5/8* seemed similar to that of *Lv-vegf3*, we compared the expression of these two genes directly using two-color F-WMISH. We confirmed that from the hatched blastula stage (when expression of these two genes was first detectable) to the pluteus stage, *Lv-pax2/5/8* and *Lv-vegf3* were expressed in the same general territories of the embryo but in a nested pattern, with *Lv-pax2/5/8* expressed in a broader domain (Fig. 4.2). Both

mRNAs were restricted to the vegetal hemisphere, and limited to the ectoderm overlying the VLCs from the mesenchyme blastula stage onward.

Similarly, we directly compared the expression domains of several other pairwise combinations of genes. A comparison of *Lv-otp* and *Lv-fgfa* expression showed that *Lv-otp* was expressed in the oral ectoderm of the embryo from the late gastrula stage in two small clusters of cells (Fig. 3A) that were located near, but did not directly overlie, the VLCs of PMCs (Fig. 4.3A'', A'''), which at this stage expressed *Lv-fgfa* (Fig. 4.3A'). At the prism stage, *Lv-otp* was expressed in a chain of cells that spanned the oral ectoderm, while *Lv-fgf* was expressed in the PMCs and ectoderm at the animal pole (Fig. 4.3B-B'''). In pluteus stage embryos, *Lv-otp* was expressed in a row of single cells in the ectoderm along the growing postoral rods, independent of *Lv-fgfa* expression in the PMCs and endoderm (Fig. 4.3C-C'''). A comparison of *Lv-otp* and *Lv-vegf3* expression showed that at the late gastrula stage, there was no overlap between the few cells in the oral ectoderm that expressed *Lv-otp* in the oral ectoderm and the domains of *Lv-vegf3* expression (Fig. 4.4A-A'''). At the prism stage, a few *Lv-otp* expressing cells were located within the *Lv-vegf3* expression domains (Fig.4.4B-B'''), an observation that persisted at the pluteus stage (Fig. 4.4C-C'''). We observed that the expression domain of *Lv-otp* correlated more closely with that of *Lv-pax2/5/8* than with *Lv-fgfa* or *Lv-vegf3*. At the late gastrula stage, a few *Lv-otp* expressing cells were located within the *Lv-pax2/5/8* expression domain overlying the VLCs, and these cells appeared to be coexpressing both genes (Fig. 4.5A-A'''). This expression pattern persisted at the prism stage (Fig. 4.5B-B'''). At the pluteus stage, several cells appeared to be co-expressing *Lv-otp* and *Lv-pax2/5/8* in the ectoderm surrounding the postoral rods (Fig. 4.5C-C'''). Our results therefore show a surprising diversity in the patterns of expression of these four genes which have been implicated in the local control of skeletogenesis, with a wide variety in the degrees of overlap among their expression domains.

4.4.2 Expression patterns of *Lv-vegf3, Lv-pax2/5/8, Lv-otp* and *Lv-fgfa* are dependent on the presence of PMCs

vegf3, pax2/5/8, otp and *fgfa* have been shown to regulate PMC behavior during skeletal morphogenesis, in some instances influencing gene expression in the PMCs (Di Bernardo *et al.*,

1999; Cavalieri *et al.*, 2003; Duloquin *et al.*, 2007; Rottinger *et al.*, 2008; Cavalieri *et al.*, 2011; Chapter 3). As yet, however, there is no evidence that the PMC-ectoderm interaction is bi-directional; i.e., there is no evidence of PMC-to-ectoderm signaling. To assay for a reciprocal role for the PMCs in regulating the expression of these four genes in the ectoderm, we adopted a two-fold approach: 1) we analyzed the expression of *Lv-vegf3, Lv-fgfa, Lv-otp* and *Lv-pax2/5/8* in *Lv-alx1* morphants (Fig. 4.6). The transcription factor *Lv-alx1* is essential for the specification of PMCs, and as such these morphants completely lack PMCs at all stages of development (Ettensohn *et al.*, 2003). 2) We observed the expression patterns of *Lv-vegf3, Lv-pax2/5/8, Lv-otp* and *Lv-fgfa* in PMC-depleted embryos, in which PMCs were surgically removed from the blastocoel (Fig. 4.7). In these embryos, the blastocoelar cells with time are respecified into a new set of PMCs which undergo directed migration and differentiation to form the embryonic endoskeleton (Ettensohn and McClay, 1988; Ettensohn *et al.*, 2007; Sharma and Ettensohn, 2011). We observed that *Lv-vegf3* was downregulated in *Lv-alx1* morphants (Fig. 4.6A-C) in comparison to control embryos (Fig. 4.6A'-C') at all stages tested. Conversely, we found that in *Lv-alx1* morphants, *Lv-fgfa* was strongly and progressively upregulated in the ectoderm (Fig. 4.6D-F), while in control embryos, *Lv-fgfa* was progressively downregulated in the ectoderm and expressed strongly in the PMCs at later stages (Fig. 4.6 D'-F'). *Lv-pax2/5/8* (Fig. 4.6G-I, G'-I') and *Lv-otp* (Fig. 4.6J, K, J', K') showed a similar pattern of downregulation in *Lv-alx* morphants (Fig. 4.6 G-K) when compared to controls (Fig. 4.6 G'-K'). These results show that signals from PMCs regulate the expression of genes in the ectoderm and point to the reciprocal nature of the interaction between these tissues.

In embryos where PMCs were surgically removed from the blastocoel, we observed an upregulation of *Lv-vegf3* expression within 3 hr of PMC depletion (Fig. 4.7A) when compared to control embryos (Fig. 4.7A'), and though *Lv-vegf3* was upregulated 6 (Fig. 4.7 B) and 12 (Fig. 4.7C) hr post-PMC depletion in comparison to control embryos (Fig. 4.7 B', C'), the strength of this upregulation of *Lv-vegf3* appeared to reduce with time. On the other hand, we observed a downregulation of *Lv-fgfa* 3 hr post-PMC depletion (Fig. 4.7D) in comparison to control embryos (Fig. 4.7D'). At 6 hr post-depletion, we observed comparable levels of this gene between PMC-depleted (Fig 4.7E) and control embryos (Fig. 4.7E'), though *Lv-fgfa* was expressed in a wider domain at the animal pole in PMC-depleted embryos than it was in controls. At 12 hr post-depletion, the expression domains of *Lv-fgfa* at the animal pole narrowed down to

areas comparable to control embryos, but diffuse staining was visible throughout the embryo at this time point. We observed that *Lv-pax2/5/8* expression was also altered in response to PMC depletion and respecification. At 3 hr post-depletion, *Lv-pax2/5/8* was expressed at lower levels in PMC-depleted embryos (Fig. 4.7G) than in controls (Fig. 4.7G'), a difference which persisted at 6 hr post-depletion (Fig 4.7H, H'). We observed a rebound of *Lv-pax2/5/8* expression in the ectoderm overlying the VLCs in embryos 12 hr post-depletion (Fig. 4.7I), though the domains of expression near the animal pole visible in control embryos at this stage (Fig. 4.7I') were not yet present. Similarly, *Lv-otp* was downregulated 6 hours post-depletion (Fig. 4.7J) in comparison to controls (4.7J'), and a recovery of gene expression was observed 12 hours-post depletion (Fig. 4.7K, K'). These experiments show that gene expression in the ectoderm responds to the removal and subsequent respecification of the PMCs.

4.5 Discussion

Epithelial-mesenchymal communication is a hallmark of embryogenesis, and the development of the sea urchin embryonic endoskeleton is no exception. Signals from the embryonic ectoderm exert a great influence on migratory and differentiation activities of the PMCs during skeletogenesis. Here, we have studied in detail the expression domains of four genes known to play a role in this process: *Lv-fgfa*, *Lv-vegf3*, *Lv-pax2/5/8*, and *Lv-otp*. We observed a wide variation in the patterns of expression among these four genes in the ectoderm, some more closely matched than others. The expression domains of *Lv-pax2/5/8* and *Lv-fgfa* overlap only slightly (Fig. 4.1), an observation reminiscent of the overlap between *Lv-fgfa* and *Lv-vegf3* (Fig. 3.1). *Lv-pax2/5/8* and *Lv-vegf3* show the greatest degree of overlap, as these two genes are co-expressed in the ectoderm overlying the VLCs at all stages of development tested (Fig. 4.2). *Lv-pax2/5/8* and *Lv-vegf3,* however, play different roles in the regulating skeletogenesis: Knockdown of *vegf3* leads to profound defects in PMC migration and skeletogenesis (Duloquin *et al*., 2007; Chapter 3), while a knockdown of *pax2/5/8* leads to a significant delay in skeletogenesis and the synthesis of shortened skeletal rods (Cavalieri *et al*., 2011). The expression pattern of *Lv-otp* is distinct both temporally and spatially from the expression patterns of the other three genes. *Lv-otp* is expressed later in development and in a chain of cells in the oral ectoderm that does not directly overlie the VLCs (Figs. 4.3, 4.4, 4.5). Cells expressing *Lv-otp* therefore only significantly overlap with *Lv-pax2/5/8* expression domains (Fig. 4.5), as *Lv-pax2/5/8* is expressed in a wider region of ectoderm than either *Lv-fgfa* or *Lv-vegf3* at these later stages.

We have shown in Chapter 3 that VEGF signaling regulates *Lv-fgfa* expression in the PMCs, but not *Lv-pax2/5/8* expression. FGF signaling, on the other hand, strongly regulates *Lv-pax2/5/*8 expression and slightly regulates *Lv-vegf3* expression. As the ligands for the FGF and VEGF pathways are expressed in the ectoderm and their receptors are expressed in the PMCs, any regulation of gene expression in the ectoderm by these pathways would have to be through reciprocal signals from the PMCs. Our results showed that the expression patterns of *Lv-fgfa*, *Lv-vegf3, Lv-pax2/5/8*, and *Lv-otp* were altered in the absence of PMCs (Fig. 4.6). We observed that the expression patterns of these genes were not equally affected. *Lv-vegf3, Lv-pax2/5/8* and *Lv-otp* were downregulated while *Lv-fgfa* was upregulated in the absence of PMCs, an interesting

finding due to the fact that *Lv-fgfa* is the only gene tested which is expressed in the PMCs as well as the ectoderm. These findings indicate that under normal conditions, *Lv-fgfa* expression is restricted in the ectoderm by signals from the PMCs, whereas the expression of *Lv-vegf3*, *Lv-pax2/5/8* and *Lv-otp* are maintained by signals from the PMCs. It is unclear whether these distinct effects are caused by different signals from PMCs or represent different responses to the same signal.

The sea urchin embryonic ectoderm is specified very early during development by complex interactions between maternal determinants and genes transcribed by the early zygote prior to the specification of PMCs (reviewed in Ettensohn and Sweet, 2000; Angerer and Angerer, 2000). Signals from the PMCs are therefore unlikely to be affecting ectodermal patterning at an early step, and it is more probable that PMC signals regulate the expression of a specific subset of genes in the ectoderm. Further work is necessary to identify the full complement of genes expressed in the ectoderm that are sensitive to the presence of PMCs, and whether or not all genes under the influence of PMC signals in turn play a role in the regulation of PMC behavior during skeletogenesis.

The expression of *Lv-fgfa*, *Lv-vegf3*, *Lv-pax2/5/8*, and *Lv-otp* in the ectoderm responds to the removal of PMCs and the respecification of these cells after surgical manipulation (Fig. 4.7). About 3 hr after PMCs are surgically removed from the blastocoel of a mesenchyme blastula stage embryo, non-skeletogenic mesenchyme (NSM) cells at the tip of the elongating archenteron begin to express transcription factors essential for PMC specification (Ettensohn *et al*., 2007; Ettensohn, 2009), an event followed by the recapitulation of the PMC gene regulatory network in these transfating NSM cells (Sharma and Ettensohn, 2011). 10-12 hr after PMC depletion, the respecified PMCs, which are able to respond to ectodermal cues, are arranged into a ring at the vegetal pole of the embryo, and the two VLCs are visible (Ettensohn, 1990). Triradiate spicule rudiments are formed at the VLCs, and these elongate and branch to form an endoskeleton comparable to control embryos, though on a delayed schedule (Ettensohn and McClay, 1988). Our results show changes in gene expression as early as 3 hr post-PMC depletion (Fig. 4.7), and this quick response suggests that the PMCs are in constant communication with the ectoderm under normal conditions. Interestingly, we observed a recapitulation of earlier expression patterns of the four genes tested during PMC respecification,

as the expression patterns of all four genes 12 hours post-PMC depletion appeared to correlate with control embryos at earlier stages of development. PMC signaling therefore affects not only the expression levels of genes in the ectoderm, but their intricate expression patterns as well.

Reciprocal signaling between epithelial and mesenchymal cells has not been clearly identified during early embryogenesis and gastrulation, though the phenomenon is prevalent later in embryonic development. There are a number of examples of mesenchyme cells influencing the expression growth factors in adjacent epithelia. In the developing chick limb bud, *brachyury* expression in the lateral plate mesoderm regulates development and gene expression in the apical ectodermal ridge, particularly the expression of *fgf8, fgf10*, and *wnt5*. *fgf10*, a known mediator of reciprocal epithelial-mesenchymal signaling in this system, in turn regulates *brachyury* expression (Liu *et al*., 2003). During mouse development, *fgf10* in the palatal mesenchyme signals to the palatal epithelium to regulate *sonic hedgehog* expression, which in turn regulates *bmp2*, *bmp4*, and *fgf10* expression in the palatal mesenchyme. These signals work in concert to increase cell proliferation in both the epithelial and mesenchymal tissues (Lan and Jiang, 2009). Additionally, *bmp4* expression in the dental mesenchyme mediates *sonic hedgehog* and *bmp2* expression in the dental epithelium in the mouse (Zhang *et al*., 2000). The expression patterns and knockdown phenotype of *brachyury* in the sea urchin embryo as described by Gross and McClay (2001) do not correlate with it playing a role in mediating PMC-to-ectoderm signaling, and *bmp2/4* is essential for the early specification of the ectoderm in functions unrelated to this phenomenon (Duboc *et al*., 2004). The *fgfa* ligand, which is expressed in the PMCs as well as the ectoderm (Rottinger *et al*., 2008; Fig. 4.1; Appendix Fig. 2), is the most likely candidate for the mediation of PMC-to-ectoderm signaling. The knockdown of *Lv-fgfa* leads to the upregulation of *Lv-fgfa* expression and the downregulation of *Lv-pax2/5/8* expression, results consistent with the changes in gene expression we observe in the absence of PMCs. However, *Lv-vegf3* is only slightly upregulated by *Lv-fgfa* knockdown, and *Lv-otp* expression is unaltered in *Lv-fgfa* morphants, results inconsistent with their expression patterns in the absence of PMCs. Thus, FGF signaling is most likely not the sole regulator of PMC-to-ectoderm signaling. Nevertheless, the role of *fgfa* in regulating PMC-to-ectoderm signaling can be analyzed by transplanting PMCs from *Lv-fgfa* morphants into control embryos to create embryos lacking *fgfa* in the PMCs only, and observing the expression of *Lv-otp, Lv-pax2/5/8, Lv-fgfa,* and *Lv-vegf3* in these embryos. With the recent identification of numerous uncharacterized genes in the sea

urchin embryo (Rafiq *et al*., 2012; Rafiq and Ettensohn, unpublished observations), it is likely that the regulators of PMC-ectoderm signaling will soon be identified.

We conclude that though the ectoderm of the sea urchin embryo is specified early in development, there exists a level of plasticity in the regulation of gene expression in the ectoderm which is at least partly dependent on signals from the PMCs. However, our work does not identify the nature of this signal or signals from the PMCs or the mechanisms by which this signal regulates gene expression. Additionally, our research has not identified the specific functions of signals from the PMCs to the ectoderm. Our results suggest that the PMC-ectoderm signaling loop most likely serves to fine-tune gene expression levels and domains in both the ectoderm and the PMCs to achieve ideal levels of gene expression optimal for the regulation of directional PMC migration and later differentiation to form the endoskeleton.

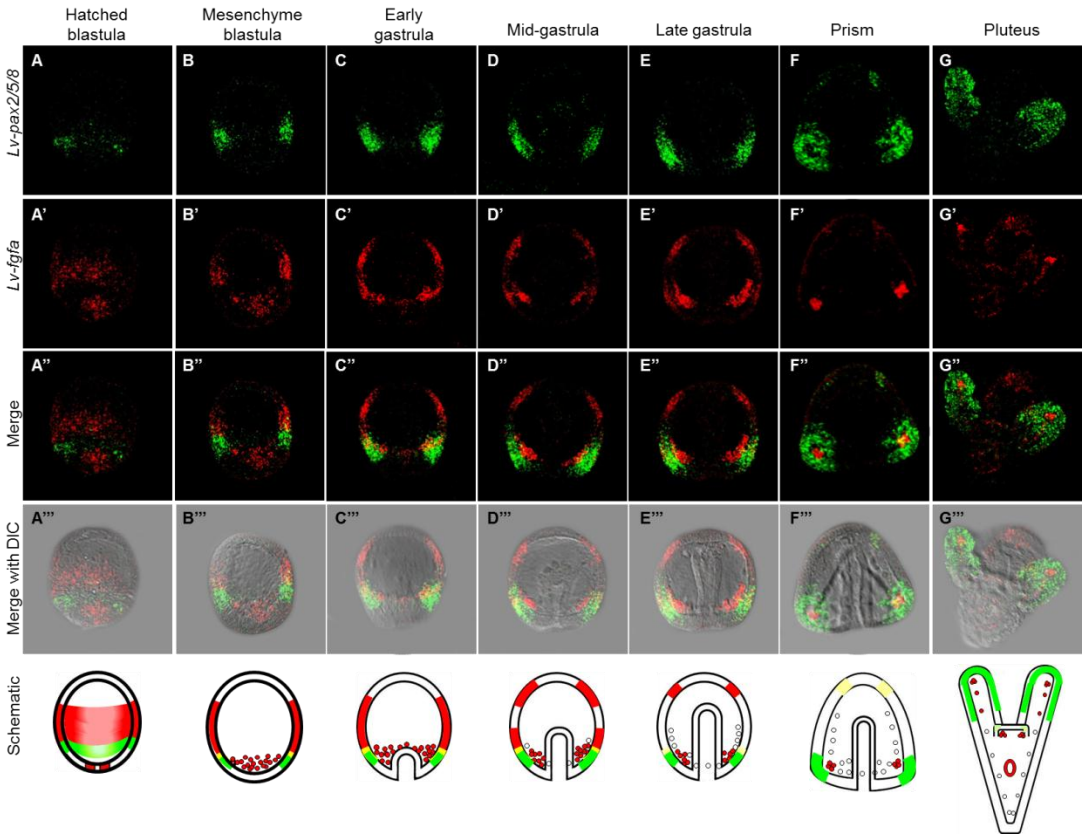

Figure 4.1: *Lv-pax2/5/8* and *Lv-fgfa* are expressed in mostly independent domains in the ectoderm. Double fluorescent in situ hybridization analyses of *Lv-pax2/5/8* (A-G) and *Lv-fgfa* (A'-G') expression show that their expression domains are separate at hatched blastula (A-A''') and slightly overlapping at mesenchyme blastula (B-B'''), early gastrula (C-C''') mid-gastrula (D-D''') and late gastrula (E-E''') stages. At the prism (F-F''') and pluteus (G-G''') stages, *Lv-fgfa* and *Lv-pax2/5/8* are once again expressed in independent domains, with the exception of two domains close to the animal pole of the prism embryo where *Lv-pax2/5/8* and *Lv-fgfa* are coexpressed (F-F'''). Schematic diagrams illustrate expression patterns.

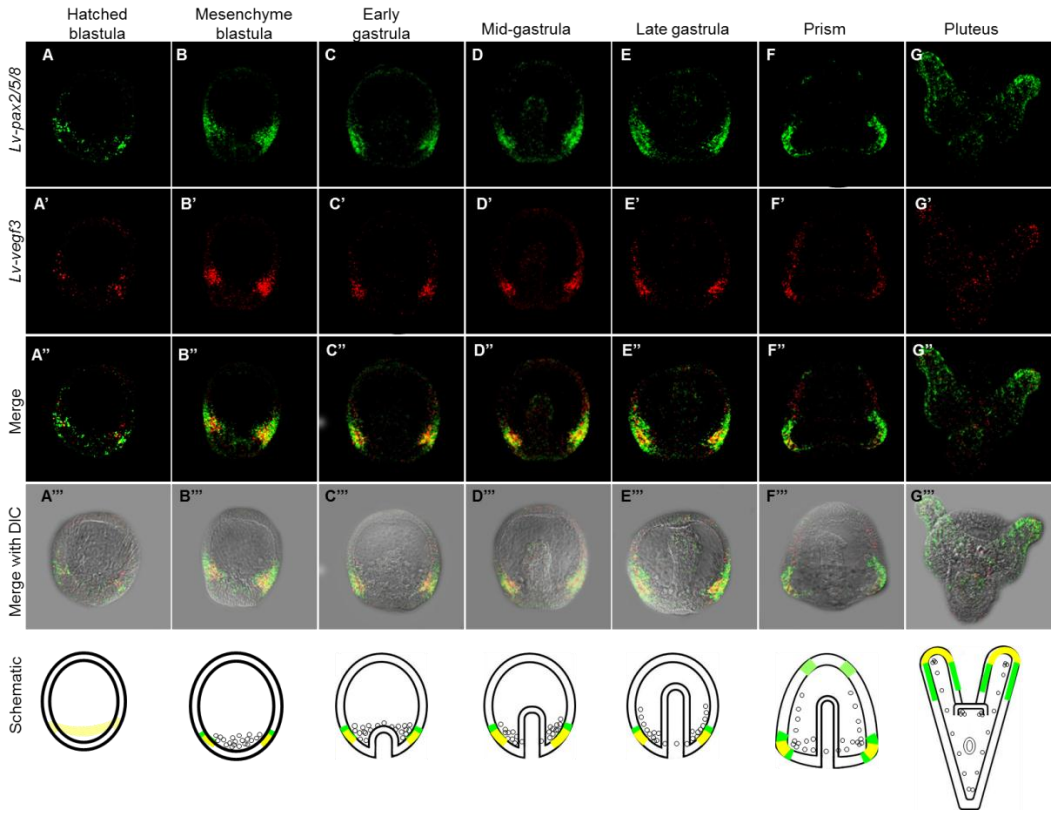

Figure 4.2: *Lv-pax2/5/8* and *Lv-vegf3* are expressed in overlapping domains in the ectoderm. Double fluorescent in situ hybridization analyses of *Lv-pax2/5/8* (A-G) and *Lv-vegf3* (A'-G') expression show that their expression domains are overlapping at hatched blastula (A-A'''), mesenchyme blastula (B-B'''), early gastrula (C-C'''), mid-gastrula (D-D'''), late gastrula (E-E'''), prism (F-F''') and pluteus (G-G''') stages. At the prism stage, however, *Lv-pax2/5/8*, but not *Lv-vegf3* is expressed in two domains of ectoderm close to the animal pole of the prism embryo (F-F'''). At all stages, *Lv-pax2/5/8* is expressed in a wider domain than *Lv-vegf3*. Schematic diagrams illustrate expression patterns.

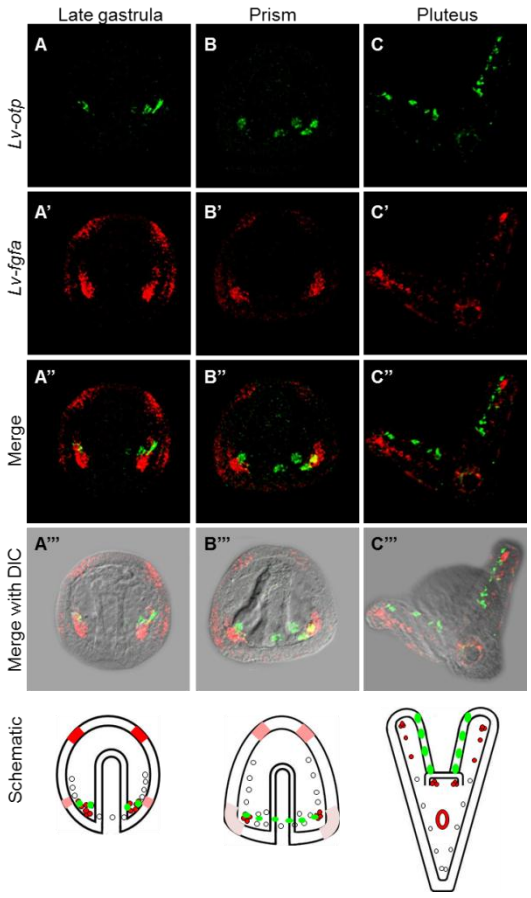

Figure 4.3: *Lv-otp* and *Lv-fgfa* are expressed in independent domains in the ectoderm. Double fluorescent in situ hybridization analyses of *Lv-otp* (A-C) and *Lv-fgfa* (A'-C') expression show that their expression domains are separate at late gastrula (A-A'''), prism (B-B''') and pluteus (C-C''') stages. *Lv-otp* is expressed in a small number of cells in the oral ectoderm, while *Lv-fgfa* is expressed mostly in the PMCs at these stages and in the ectoderm at the animal pole of the prism embryo. Schematic diagrams illustrate expression patterns.

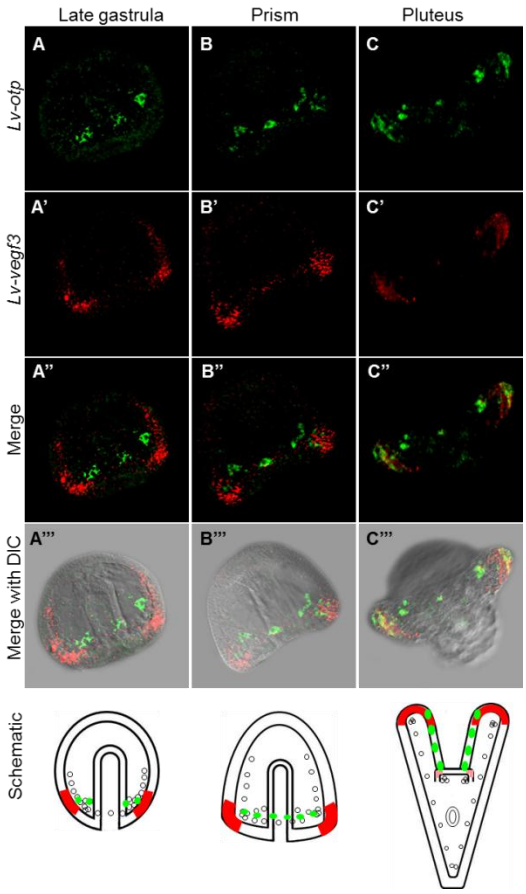

Figure 4.4: *Lv-otp* and *Lv-vegf3* are expressed in mostly independent domains in the ectoderm. Double fluorescent in situ hybridization analyses of *Lv-otp* (A-C) and *Lv-vegf3* (A'-C') expression show that their expression domains are separate at late gastrula (A-A''') and prism (B-B''') stages. At the pluteus stage (C-C''') *Lv-otp* and *Lv-vegf3* expressions overlap in a small number of cells in ectoderm overlying the growing postoral rods (C'', C'''). Schematic diagrams illustrate expression patterns.

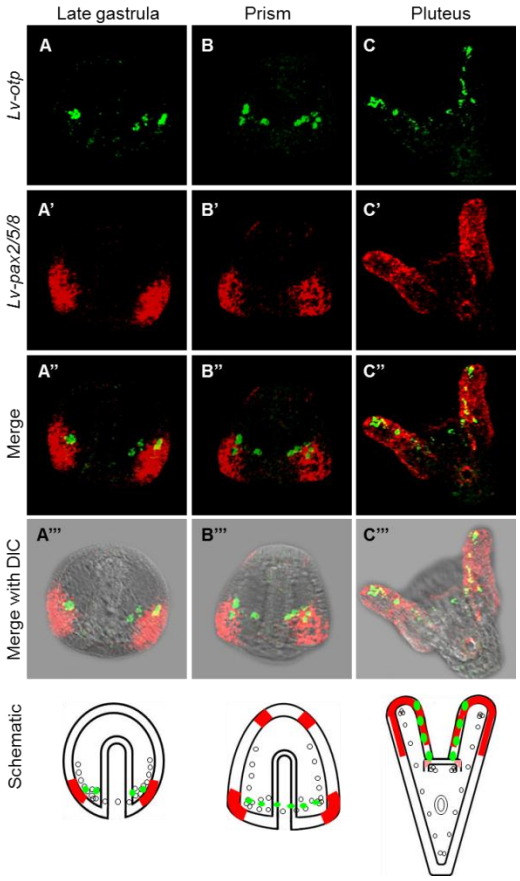

Figure 4.5: *Lv-otp* and *Lv-pax2/5/8* are expressed in moderately overlapping domains in the ectoderm. Double fluorescent in situ hybridization analyses of *Lv-otp* (A-C) and *Lv-pax2/5/8* (A'-C') expression show that their expression domains slightly overlap at late gastrula (A-A''') and prism (B-B''') stages, and significantly overlap at the pluteus stage (C-C'''). Schematic diagrams illustrate expression patterns.

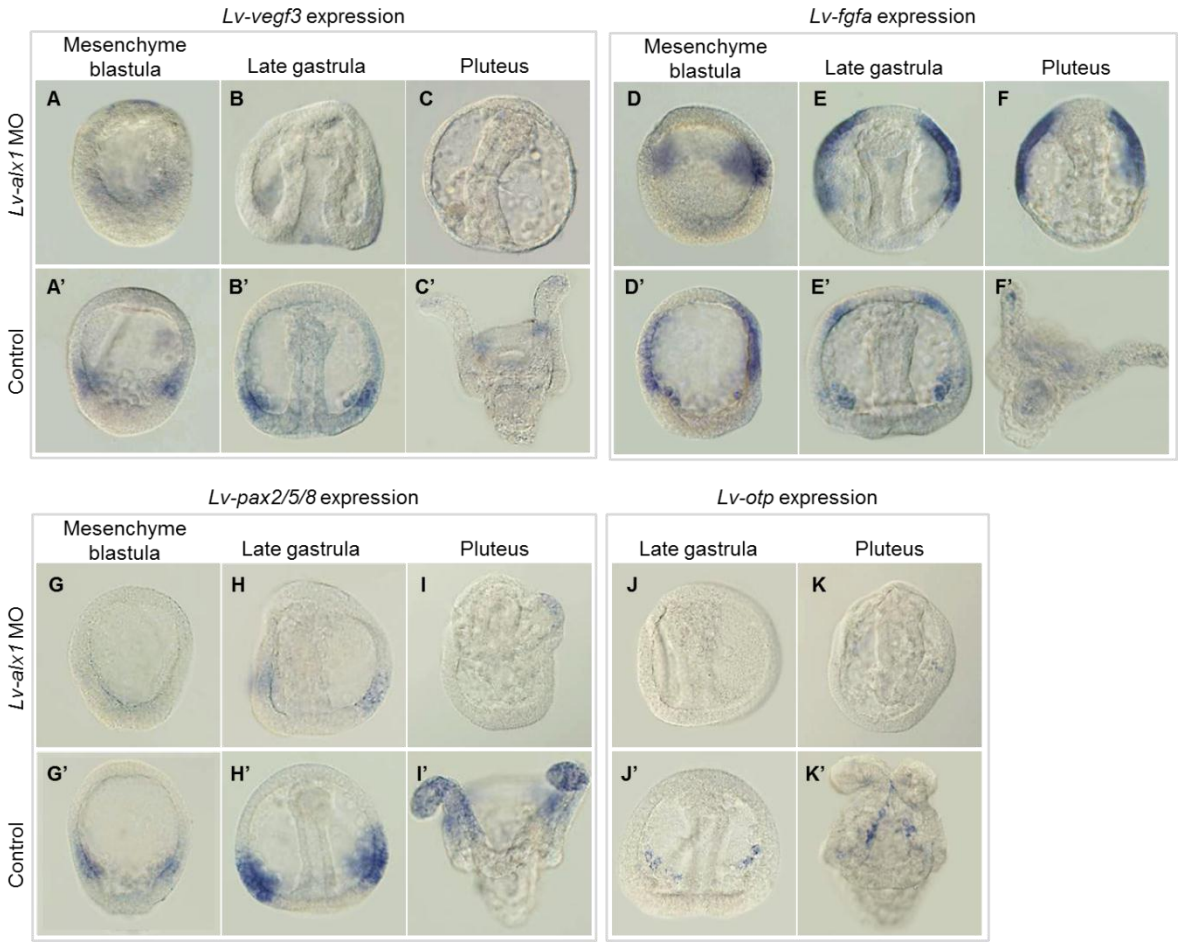

Figure 4.6: Expression patterns of *Lv-vegf3, Lv-fgfa, Lv-pax2/5/8* and *Lv-otp* are altered in the absence of PMCs. WMISH analyses of changes in expression patterns of *Lv-vegf3* (A-C, A'-C'), *Lv-fgfa* (D-F, D'-F'), *Lv-pax2/5/8* (G-I, G'-I') and *Lv-otp* (J, K, J', K') between *Lv-alx1* morphants, which lack PMCs (A-K), and control embryos (A'-K'). *Lv-vegf3, Lv-pax2/5/8* and *Lv-otp* are downregulated in the absence of PMCs, while *Lv-fgfa* is upregulated in the ectoderm in these embryos.

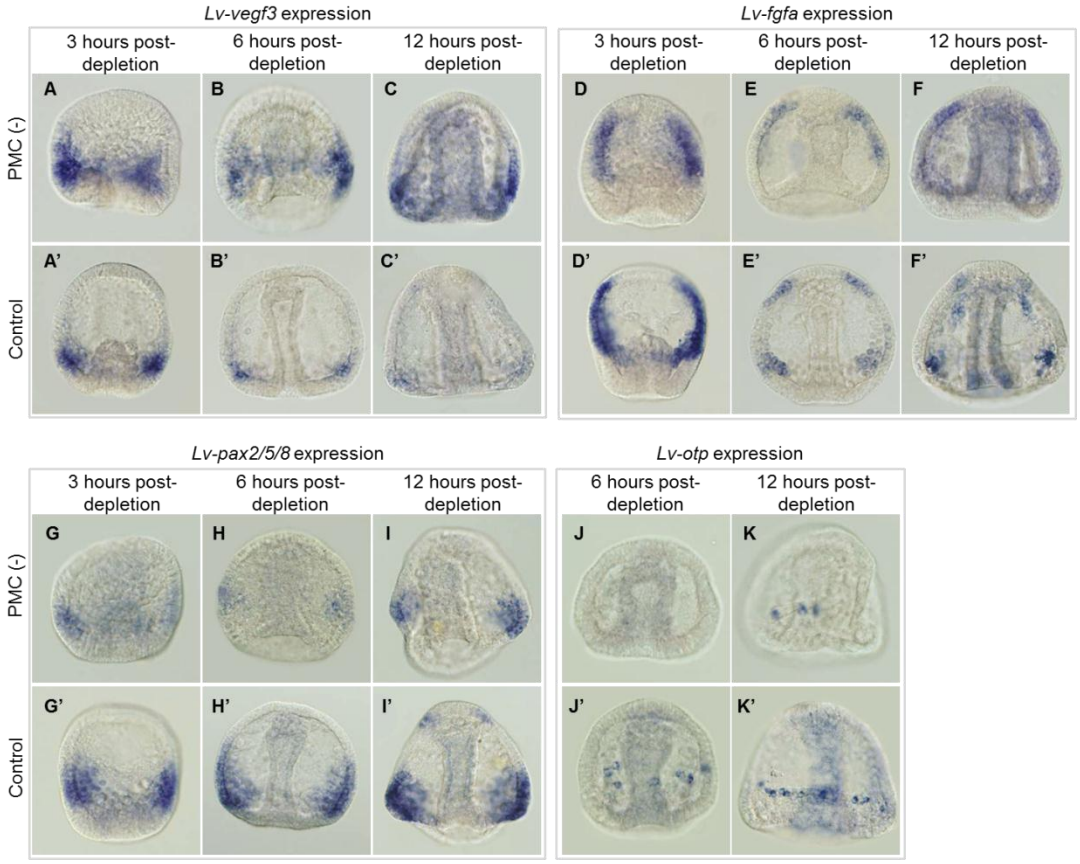

Figure 4.7: Changes in expression patterns of *Lv-vegf3*, *Lv-fgfa*, *Lv-pax2/5/8* and *Lv-otp* correlate with PMC depletion and respecification in surgically manipulated embryos. WMISH analyses of changes in expression patterns of *Lv-vegf3* (A-C, A'-C'), *Lv-fgfa* (D-F, D'-F'), *Lv-pax2/5/8* (G-I, G'-I') and *Lv-otp* (J, K, J', K') between PMC (-) embryos, in which PMCs have been surgically removed (A-K), and control, unmanipulated embryos (A'-K'). *Lv-fgfa*, *Lv-pax2/5/8* and *Lv-otp* are downregulated in response to PMC removal, while *Lv-vegf3* is upregulated. All four genes attempt a return to normal expression patterns with time as PMCs are respecified.

Chapter 5

Conclusions and Future Directions

5.1 Conclusions and Future Directions

Morphogenesis of the developing embryo is an intricate process involving complex interactions between genes with a wide diversity of functions. The work we have described uses skeletogenesis in the sea urchin embryo as a model to investigate the genetic basis of morphology. In line with this aim, we have identified two novel genes, *p58-a* and *p58-b*, which encode similar transmembrane proteins expressed exclusively in the PMCs during embryonic development. Our analyses showed that *p58-a* and *p58-b* do not perform redundant functions as both are independently necessary for skeletogenesis. Nonetheless, a double knockdown of both genes exacerbated defects in skeletogenesis. The contributions of *p58-a* and *p58-b* during skeletogenesis are restricted to biomineralization, as neither gene regulates PMCs specification, migration or fusion. This study has expanded on the presently limited knowledge of the roles of downstream morphoeffector genes during skeletogenesis. Numerous novel genes have recently been identified utilizing high throughput techniques (Zhu *et al.*, 2001; Illies *et al.*, 202; Livingston *et al.*, 2006; Mann *et al*., 2010; Rafiq *et al*., 2012, Rafiq and Ettensohn, unpublished observations), and their functions are overwhelmingly unknown. The strategies we have used to study *p58-a* and *p58-b* can easily be applied to the study of these newly-identified genes. The genes *p58-a* and *p58-b* lie in tandem on the chromosome, suggesting the occurrence of a gene duplication event. Other potentially duplicated genes have been identified in the sea urchin genome: the *sm30, msp130* and *p16* families are all composed of similar genes clustered in the genome (Livingston *et al.*, 2006). Likewise, *tsp, lasp1* and *alx1* are found as pairs of related genes (Rafiq *et al*., 2012). Additional comparative studies of the functions of members of these and other gene families will result in a better understanding not only of the mechanisms regulating skeletogenesis, but of the roles duplicated genes and gene families play during development as well.

Though biomineralization is regulated by different mechanisms in the echinoderm embryo and in vertebrates, duplicated genes are a prominent factor in this process in both systems. As gene duplication has been shown to be crucial to the evolution of vertebrate biomineralization (Kawasaki *et al*., 2007; Kawasaki *et al*., 2009), it will be informative to analyze the role of duplicated genes in the evolution of the echinoderm embryonic endoskeleton. Presently, efforts are underway to sequence the genome of the sea star *Patiria miniata*, an echinoderm which does

not form an embryonic endoskeleton. The identification of homologs of *p58-a* and *p58-b* as well as other duplicated genes, and a comparative study of the sequences, gene structures, locations in the genome and functions of these genes in the sea star will yield great insight into the importance of gene duplication in the evolution of biomineralization in the echinoderm embryo.

As in previous studies analyzing other morphoeffector genes involved in biomineralization (Peled-Kamar *et al*., 2002; Cheers and Ettensohn, 2005; Wilt *et al.*, 2008) the specific functions of *p58-a* and *p58-b* during biomineralization have not been identified. To fully understand the roles of morphoeffector genes during skeletogenesis, it is essential to expand our studies from gene expression patterns and phenotypes resulting from knockdown experiments to the biochemical functions of the proteins encoded by these genes. One potential function of P58-A and P58-B is the stabilization of amorphous calcium carbonate into calcite, which occurs as the spicules elongate and branch (Politi *et al.*, 2008). The P58 proteins, on the other hand, may play a role in calcium uptake from seawater, a process essential for skeletogenesis (Wilt, 1999). A more detailed analysis of the knockdown phenotypes of these genes and an in-depth study of the nature of the spicule deposits present in *p58* morphants may help identify their specific functions.

Identifying the location of the P58 proteins during development is also important in the study of their functions. Kitajima *et al*. (2000) and Wilt *et al*. (2008) conducted studies examining the secretion and trafficking of two spicule matrix proteins: SM30 and SM50. These groups observed that while SM30 was concentrated in the cell bodies of the PMCs found along the skeletal rods and later occluded within the spicule, SM50 was found on the surface of the spicule. It would be interesting to investigate the localization of P58 along these lines using GFP-fusion constructs and immunostaining. Additionally, the identification of the cis regulatory modules regulating *p58-a* and *p58-b* would provide invaluable information on the upstream regulation of these two genes during development.

In Chapter 3, we presented results from a detailed analysis of the functions of growth factor signaling during skeletogenesis. Previous studies (Duloqin *et al*., 2007; Rottinger *et al*., 2008) showed that the VEGF and FGF pathways are important regulators of skeletal morphogenesis, though the intricate details of their respective functions were not described. We have shown that in the sea urchin species *L. variegatus,* the VEGF pathway plays a more prominent role than the

FGF pathway in the regulation of PMC migration and differentiation. Blocking VEGF signaling leads to the complete elimination of directional PMC migration and biomineralization, while blocking FGF signaling results in the formation of truncated but well-patterned skeletal elements. We have studied in detail the requirements for VEGF signaling during skeletogenesis and identified multiple roles for this pathway during PMC migration and differentiation. VEGF signaling regulates both the initial migration of PMCs to form the sub-equatorial ring and the later phase of migration where two chains of cells move from the VLCs to target two domains of ectoderm at the animal pole of the embryo. These defects in PMC migration are at least partly due to the fact that the extension of filopodia is compromised upon blocking the VEGF pathway. Additionally, VEGF signaling regulates the synthesis of the calcium carbonate biomineral that constitutes the endoskeleton, independent of its effects on PMC migration. We noticed that various skeletal rods were differentially affected by the absence of VEGF signaling, and the postoral and anterolateral rods, which exhibit the most rapid growth at later stages, were the most reliant on the VEGF pathway. Finally, our analysis of the expression of genes in the PMC GRN has shown that VEGF signaling regulates the expression of several, but not all genes with predicted or proven roles in biomineralization.

Our analyses have provided significant insights into the functions of VEGF signaling during skeletogenesis. However, we have not identified the downstream pathway in the PMCs responsible for mediating VEGF signals from the ectoderm. The two most likely candidates are the MAPK and P13K pathways, as they are known to play this role in other developmental systems (Schlessinger, 2000). Both the MAPK and PI3K pathways have been shown to regulate skeletogenesis, albeit in different ways (Rottinger *et al*., 2004; Fernandez-Serra *et al*., 2004; Bradham *et al*., 2004). Though the perturbation of either pathway by small molecule inhibitors does not phenocopy a loss of VEGF signaling (Rottinger *et al*. 2004; Fernandez-Serra *et al*., 2004; Bradham *et al*., 2004; Fig. 3.10), it is possible that VEGF signaling may feed into both the MAPK and PI3K pathways in regulating various aspects of skeletogenesis. Alternatively, several other pathways in addition to VEGF signaling may feed into the MAPK or PI3K pathways, and hence blocking either pathway may have more global effects on embryonic development than simply perturbing VEGF signaling. Either way, progress can be made towards answering this question by the use of small molecule inhibitors such as U0126 and Wortmannin to inhibit MAPK and PI3K signaling respectively, later during development to circumvent defects in PMC

specification. Detailed analyses of the changes in gene expression patterns and phenotypes observed under such conditions and a comparison of these phenotypes with results observed upon blocking the VEGF pathway by axitinib treatments will help identify which of these pathways mediates VEGF signaling.

Our preliminary results (Appendix Figs. 16-19) show that VEGF signaling regulates PMC specification during NSM transfating, as we have observed that blocking VEGF signaling after the surgical removal of PMCs from the blastocoel inhibits the respecification of PMCs by the blastocoelar cells. This observation is surprising in light of the fact that VEGF signaling does not regulate PMC specification under normal conditions. Previous studies have suggested that the PMC GRN is recapitulated during NSM transfating (Ettensohn *et al.*, 2007; Sharma and Ettensohn, 2011). However, our results show that the transcription factors Alx1 and Ets1, which are upstream regulators of *vegfr-10-Ig* under normal conditions, may be regulated by VEGF signaling during transfating. Additionally, WMISH analyses have shown that *vegfr-10-Ig* is expressed at earlier time-points than the aforementioned transcription factors after PMC removal. These preliminary data strongly suggest that VEGF signaling serves a critical role in activating the transfating response in NSM cells, though the exact function of the VEGF pathway in this process is unclear. Elucidating the function of VEGF signaling during transfating is essential to a more complete understanding of its intricate roles during embryogenesis. Additionally, it is important to detail the differences in the GRN which runs in the PMCs during NSM transfating and the downstream targets of VEGF signaling during this process. In line with this aim, it would be informative to conduct a detailed analysis of the spatial and temporal expression patterns of genes in the PMC GRN during transfating. This can be achieved by performing WMISH on transfating embryos at various time-points using probes complementary to numerous genes in the PMC GRN and by measuring gene expression levels using the Nanostring nCounter analysis system.

VEGF signaling is obviously necessary for PMC respecification during transfating. Whether or not this pathway is sufficient to induce NSM transfating in the presence of PMCs is unclear. It has previously been shown that the overexpression of *vegf3* causes an increase in the number of PMCs specified (Duloquin *et al.*, 2007). The hypothesis that these extra PMCs arise as a result of transfating NSM cells can be tested by assaying the ectopic expression of genes specific to the

PMC GRN, such as *alx1, ets1, tbr, p58-a* and *p58-b* in the NSM cells at the tip of the archenteron in embryos overexpressing *vegf3*. Another essential facet of this research would be the identification of the downstream pathways that mediate VEGF signaling during transfating. The MAPK pathway is essential for the transfating response (Ettensohn *et al.*, 2007; Sharma and Ettensohn, 2011), though whether or not this pathway regulates NSM transfating through an effect of VEGF signaling is unknown. A detailed comparison between phenotypes and changes in gene expression observed upon blocking MAPK and VEGF signaling during transfating will shed light on this question.

In addition to further studies into the mechanisms of function of VEGF signaling, it would be valuable to further analyze the role of FGF signaling during skeletogenesis. Though we have determined that in *L. variegatus*, FGF signaling does not regulate PMC migration, this pathway still contributes to the process of biomineralization (Fig. 3.2). It will therefore be interesting to identify the exact role that FGF signaling plays during biomineralization by the identification of the downstream targets of this pathway. The Nanostring nCounter system can be applied for a comprehensive analysis of the targets of FGF signaling during skeletogenesis.

Lastly, our analysis of PMC-to-ectoderm signaling shows that skeletogenesis in the sea urchin embryo is a valuable model for the study of intercellular communications and reciprocal cell signaling during embryonic development. We have shown that the expression patterns of *Lv-vegf3, Lv-pax2/5/8, Lv-otp* and *Lv-fgfa* are dependent on the presence of PMCs, presumably regulated by specific signals transmitted from the PMCs to the ectoderm. To expand on this study, it will be important to identify the full complement of genes expressed in the ectoderm which are regulated by PMC signals. This analysis would require the assessment of expression patterns of several previously identified and novel genes by WMISH in the absence of PMCs. In addition to the four genes we have analyzed, Cavalieri *et al*. (2011) have described the expression of *strim1*, which encodes a tripartite domain-containing protein essential for skeletogenesis. It would be informative to assay any overlap between the expression domains of *Lv-strim1* and *Lv-vegf3, Lv-pax2/5/8, Lv-otp* and *Lv-fgfa*, and to analyze the expression of *strim1* in the absence of PMCs. As the sea urchin embryo develops into a larva, several new skeletal rods are synthesized independent of the embryonic endoskeleton (Yajima and Kiyomoto 2006; Rahman *et al*., 2012). It would be valuable to analyze the expression patterns of *Lv-vegf3, Lv-*

pax2/5/8, *Lv-otp* and *Lv-fgfa*, as well as any additional genes identified, in the ectoderm overlying these newly-forming larval rods. Most importantly, it will be necessary to identify the exact nature of the signal or signals transmitted by the PMCs and to analyze whether these signals are unidirectional or constitute a feedback loop with signals from the ectoderm to the PMCs. So far, the most likely candidate for this PMC-to-ectoderm signal is *fgfa*, which is expressed in the PMCs as well as the ectoderm (Rottinger *et al*., 2008; Fig. 4.1) and the role of *fgfa* in this process can be tested by transplanting PMCs from *fgfa* morphants into control embryos and assaying the expression of genes in the ectoderm in these embryos.

Our research has provided significant insights into the molecular regulation of mesenchyme cell migration and differentiation during embryogenesis and expanded our understanding of the genetic basis of morphology. The future experiments we have proposed, coupled with a more comprehensive understanding of the architecture of the gene regulatory network that is progressively deployed in the PMC lineage, will further enhance our knowledge regarding this fundamental aspect of embryonic development.

Appendix

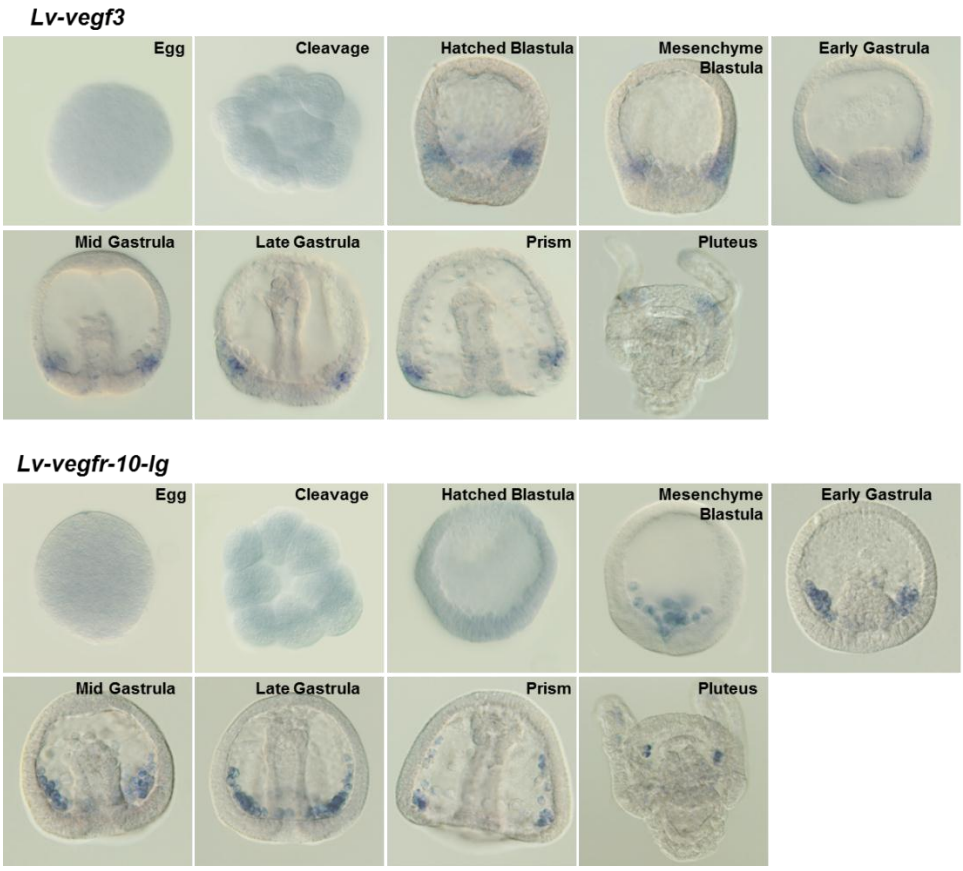

Appendix Figure 1: WMISH analysis of the expression patterns of *vegf3* and *vegfr-10-Ig* during embryogenesis in *L. variegatus*. *Lv-vegf3* is expressed in the ectoderm overlying the VLCs from the hatched blastula stage to the prism stage, and in the ectoderm overlying the postoral rods and in the oral hood at pluteus stage. *Lv-vegfr-10-Ig* is expressed in the PMCs from the mesenchyme blastula stage to the pluteus stage.

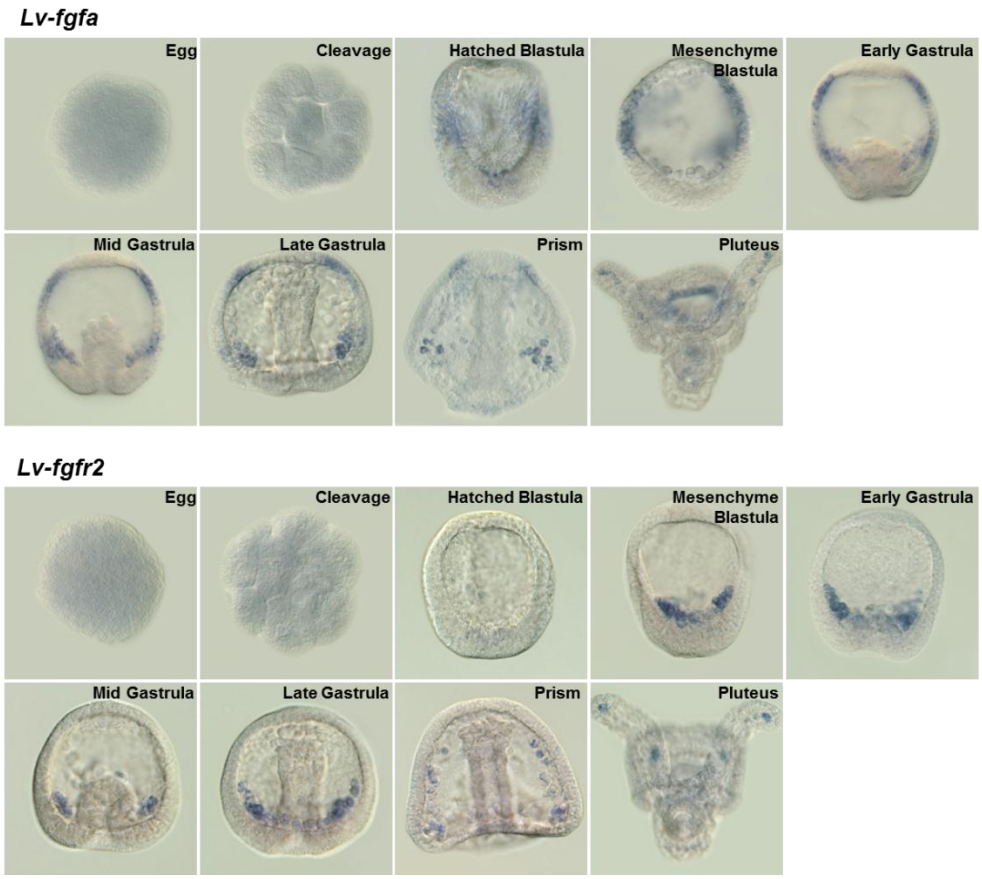

Appendix Figure 2: WMISH analysis of the expression patterns of *fgfa* and *fgfr2* during embryogenesis in *L. variegatus*. *Lv-fgfa* is expressed in the ectoderm and presumptive PMCs at the hatched blastula stage, in the PMCs and in the ectoderm from the mesenchyme blastula to the prism stage, and in the PMCs and endoderm at the pluteus stage. *Lv-fgfr2* is expressed in the PMCs from the mesenchyme blastula stage to the pluteus stage.

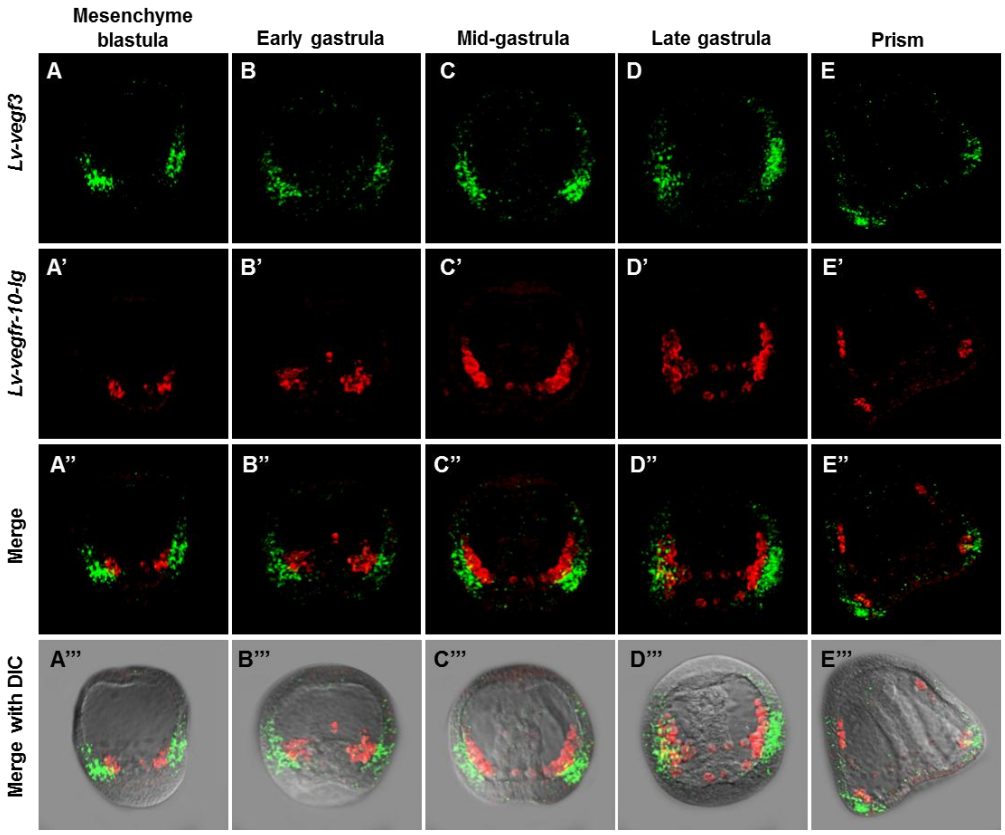

Appendix Figure 3: *Lv-vegf3* expression domains in the ectoderm are tightly correlated with PMC position during development. Double fluorescent in situ hybridization analyses of *Lv-vegf3* (A-E) and *Lv-vegfr-10-Ig* (A'-E') expression show that the expression domains of *Lv-vegf3* are strongly linked to the presence of PMCs at the mesenchyme blastula (A-A'''), early gastrula (B-B'''), mid-gastrula (C-C'''), late gastrula (D-D''') and prism (E-E''') stages.

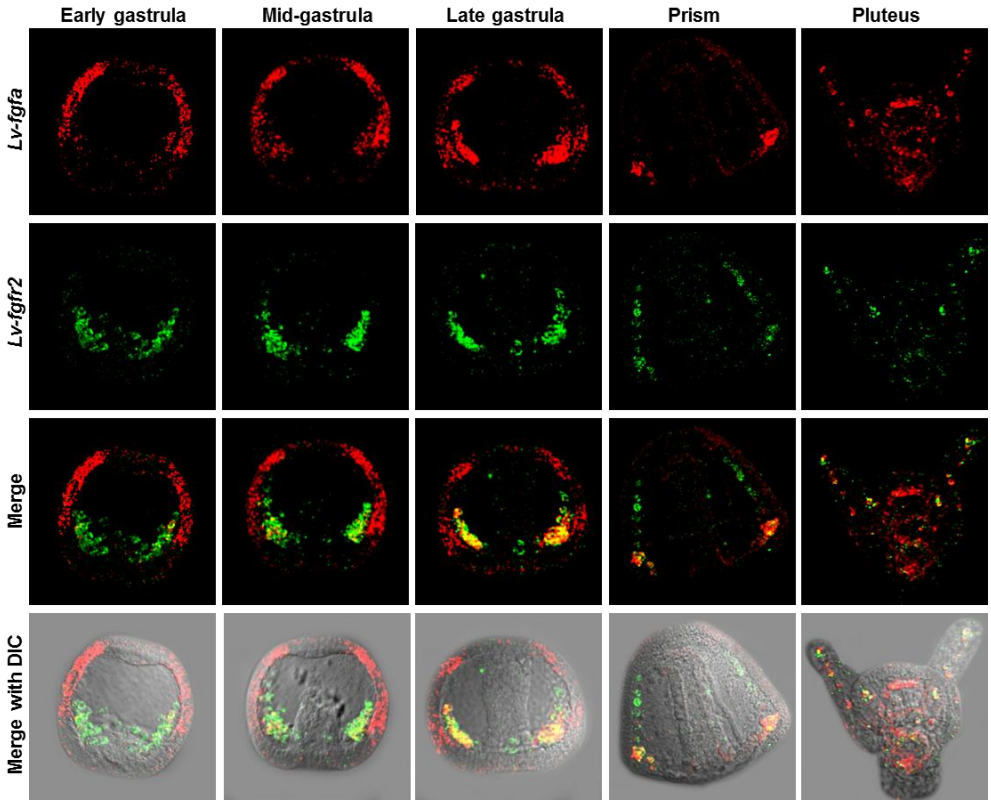

Appendix Figure 4: *Lv-fgfa* and *Lv-fgfr2* are coexpressed in the PMCs during embryonic development. Double fluorescent in situ hybridization analyses of *Lv-fgfa* (A-E) and *Lv-fgfr2* (A'-E') expression show that both genes are expressed in the PMCs at the early gastrula (A-A'''), mid-gastrula (B-B'''), late gastrula (C-C'''), prism (D-D''') and pluteus (E-E''') stages.

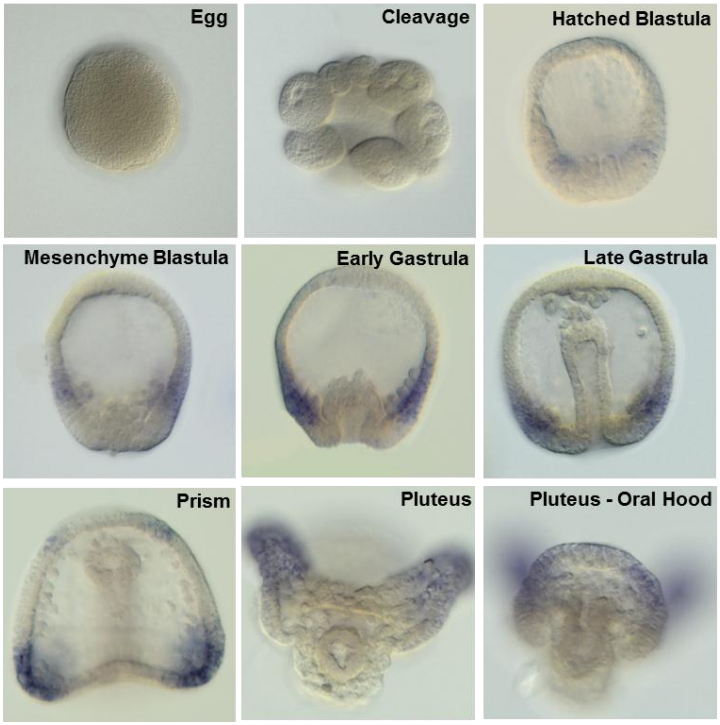

Appendix Figure 5: WMISH analysis of the expression patterns of *pax2/5/8* during embryogenesis in *L. variegatus*. *Lv-pax2/5/8* is expressed in the ectoderm overlying the PMCs from the hatched blastula stage to the prism stage, at which it is also expressed in two domains of ectoderm near the animal pole. *Lv-pax2/5/8* is expressed in the ectoderm overlying the growing postoral rods and in the oral hood at the pluteus stage.

Appendix Figure 6: WMISH analysis of the expression patterns of *otp* during embryogenesis in *L. variegatus*. *Lv-otp* is expressed in two groups of cells in the oral ectoderm at the late gastrula stage, and in a chain of cells in the oral ectoderm at the prism and pluteus stages.

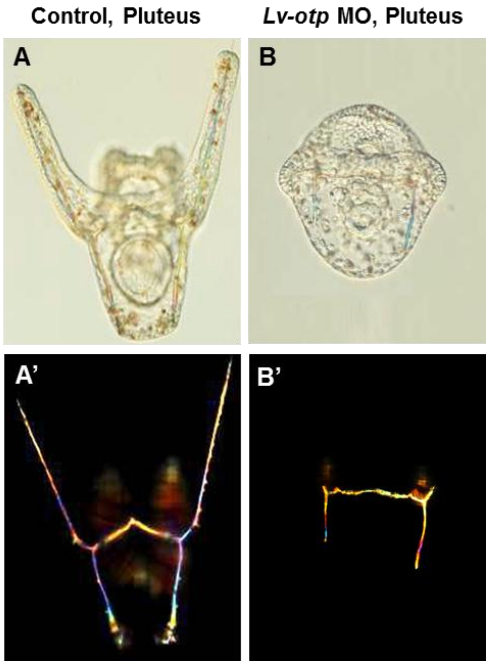

Appendix Figure 7: Knockdown of *Lv-otp* inhibits the elongation of skeletal rods. DIC (A, B) and polarized light (A', B') images of control (A, A') and *Lv-otp* morphant (B, B') embryos show that well-patterned but truncated skeletal elements are formed upon the knockdown of *otp* in *L. variegatus*.

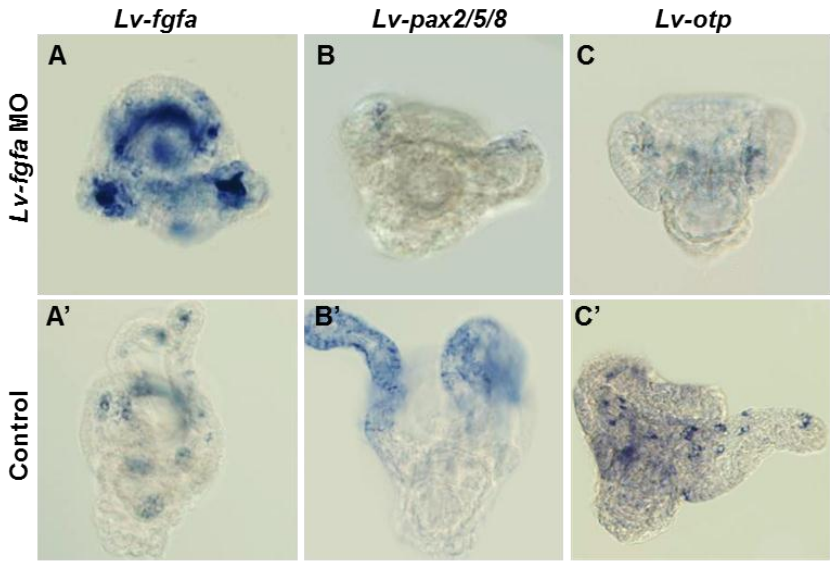

Appendix Figure 8: FGF signaling regulates the expression of *Lv-fgfa* and *Lv-pax2/5/8*, but not *Lv-otp*, at the pluteus stage. WMISH analysis of *Lv-fgfa* (A, A'), *Lv-pax2/5/8* (B, B') and *Lv-otp* (C, C') expression in *Lv-fgfa* morphants (A-C) and control embryos (A'-C') at the pluteus stage shows that upon the knockdown of *Lv-fgfa*, *Lv-fgfa* expression is upregulated, while *Lv-pax2/5/8* is downregulated. There is no significant change in *Lv-otp* expression.

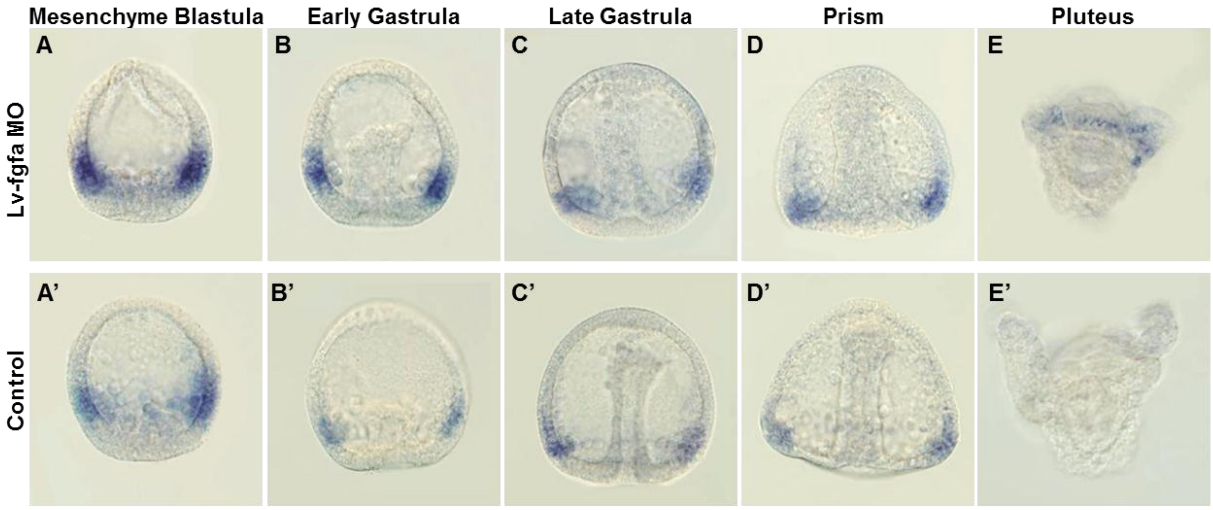

Appendix Figure 9: FGF signaling does not significantly regulate the expression of *Lv-vegf3*. WMISH analysis of *Lv-vegf3* expression in *Lv-fgfa* morphants (A-E) and control embryos (A'-E') shows that *Lv-vegf3* expression is slightly upregulated upon the knockdown of *Lv-fgfa.*

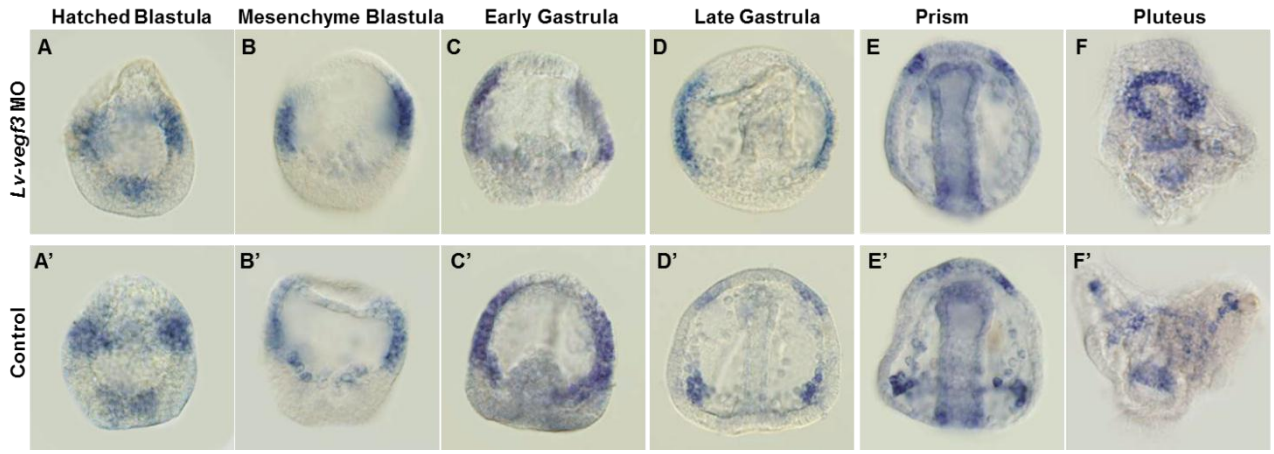

Appendix Figure 10: VEGF signaling regulates *Lv-fgfa* expression in the PMCs. WMISH analysis of *Lv-fgfa* expression in *Lv-vegf3* morphants (A-F) and control embryos (A'-F') at the hatched blastula (A, A'), mesenchyme blastula (B, B'), early gastrula (C, C'), late gastrula (D, D'), prism (E, E') and pluteus (E, F') stages. *Lv-fgfa* expression in *Lv-vegf3* morphants is comparable to control embryos at the hatched blastula stage, though *Lv-fgfa* is subsequently downregulated in the PMCs and upregulated in the ectoderm from the mesenchyme blastula to late gastrula stages. At the prism stage, the domain of expression of *Lv-fgfa* in the ectoderm is comparable to control embryos, and at the pluteus stage, *Lv-fgfa* is expressed in the endoderm as seen in control embryos, even though at these later stages *Lv-fgfa* expression is not recovered in the PMCs.

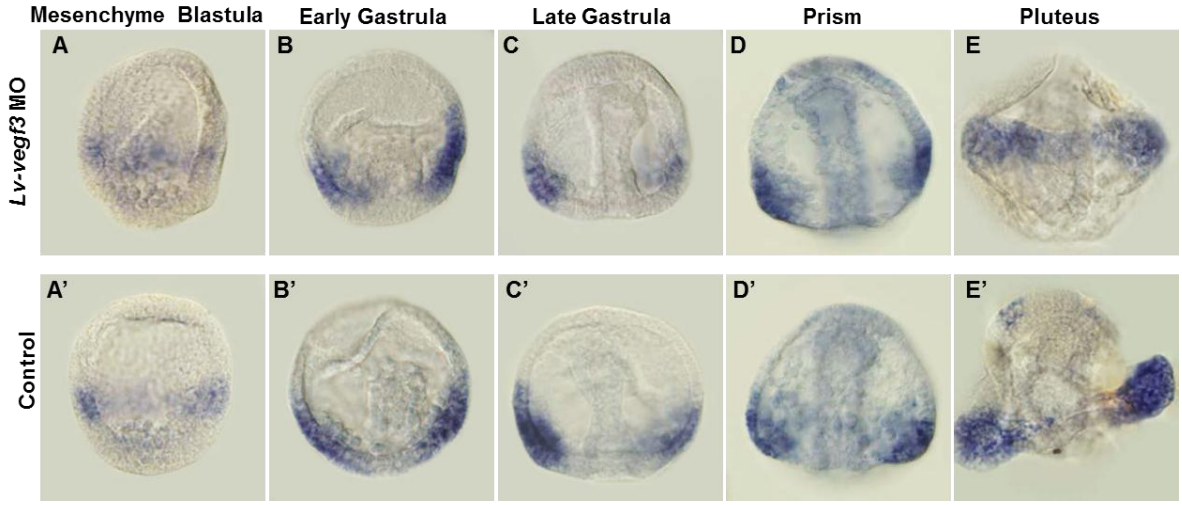

Appendix Figure 11: VEGF signaling does not significantly regulate *Lv-pax2/5/8* expression. WMISH analysis of *Lv-pax2/5/8* expression in *Lv-vegf3* morphants (A-E) and control embryos (A'-E') at the mesenchyme blastula (A, A'), early gastrula (B, B'), late gastrula (C, C'), prism (D, D') and pluteus (E, E') stages shows that there is little change in *Lv-pax2/5/8* expression upon the knockdown of *Lv-vegf3*.

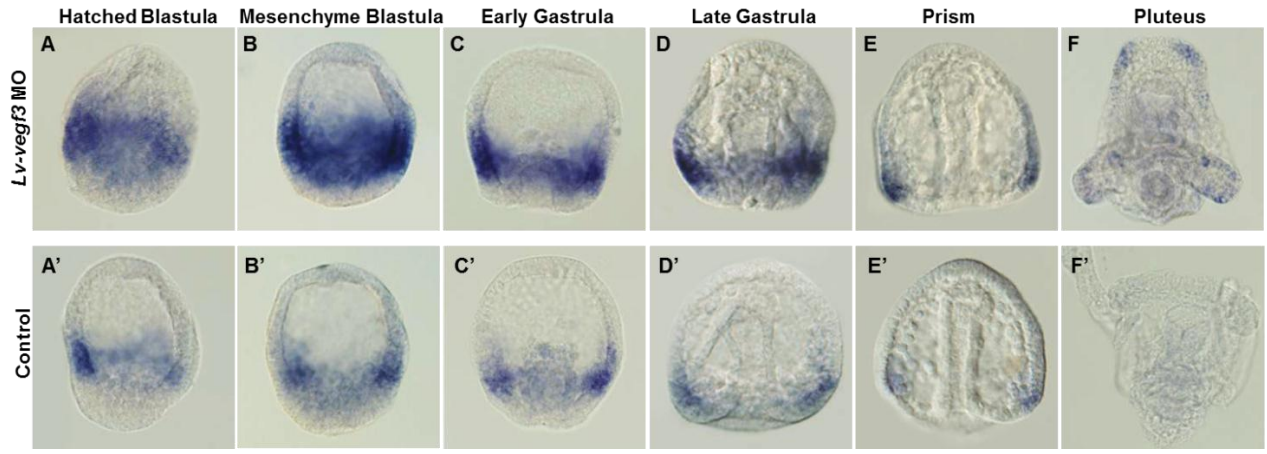

Appendix Figure 12: VEGF signaling regulates *Lv-vegf3* expression. WMISH analysis of *Lv-vegf3* expression in *Lv-vegf3* morphants (A-F) and control embryos (A'-F') at the hatched blastula (A, A'), mesenchyme blastula (B, B'), early gastrula (C, C'), late gastrula (D, D'), prism (E, E') and pluteus (E, F') stages shows that *Lv-vegf3* expression is upregulated upon *Lv-vegf3* knockdown.

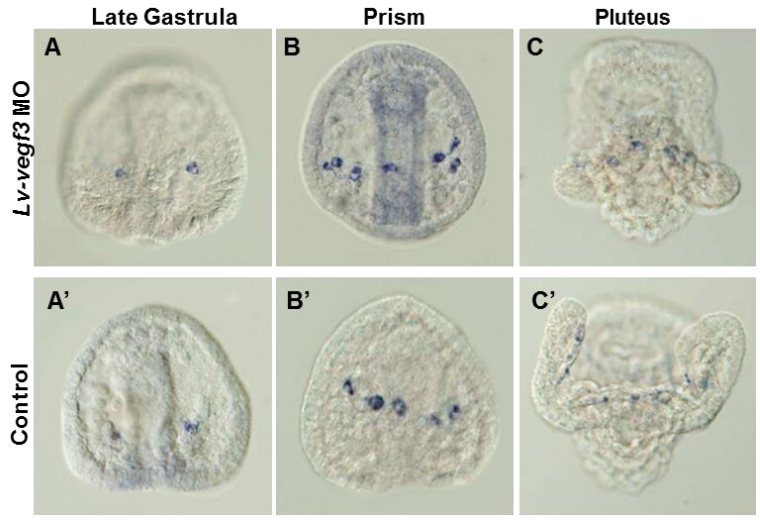

Appendix Figure 13: VEGF signaling does not regulate *Lv-otp* expression. WMISH analysis of *Lv-otp* expression in *Lv-vegf3* morphants (A-C) and control embryos (A'-C') at the late gastrula (A, A'), prism (B, B') and pluteus (C, C') stages shows that there is no significant change in *Lv-otp* expression upon the knockdown of *Lv-vegf3*.

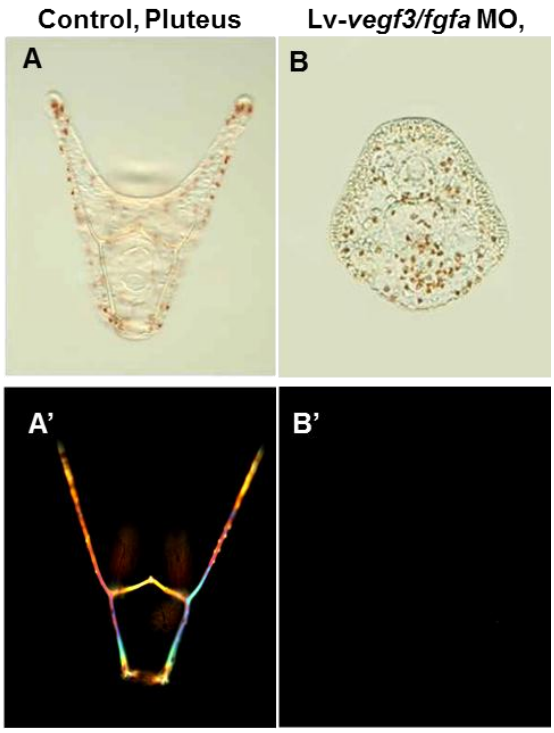

Appendix Figure 14: *Lv-vegf3/ Lv-fgfa* double knockdown phenocopies *Lv-vegf3* knockdown. DIC (A, B) and polarized light (A', B') images of control (A, A') and *Lv-vegf3/Lv-fgfa* double morphant (B, B') embryos show that skeletogenesis is eliminated in these double morphant embryos.

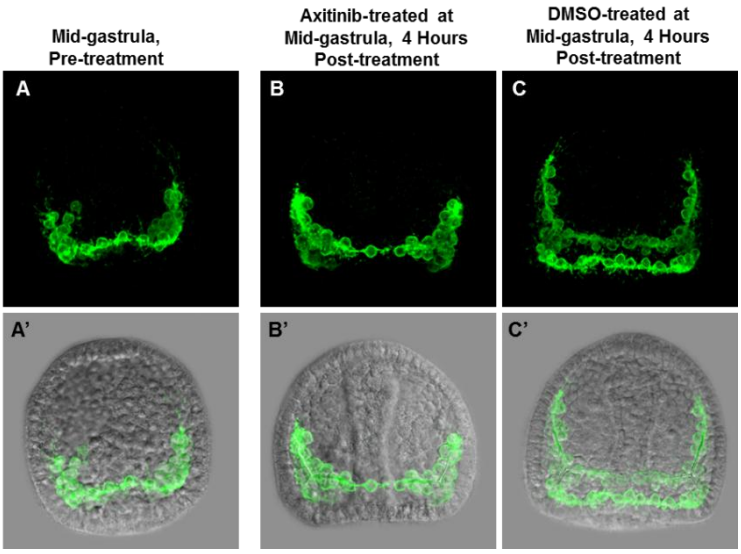

Appendix Figure 15: VEGF signaling regulates later phases of PMC migration. Fluorescence (A-C) and merged images with DIC (A'-C') of mid-gastrula embryo immediately prior to axitinib treatment (A, A'), late gastrula embryos treated with axitinib from the mid-gastrula stage (B, B') and control late gastrula embryos treated with DMSO from the mid-gastrula stage (C, C'). 6a9 immunostaining shows that PMC migration toward the animal pole is inhibited by axitinib treatment, even after the ventro-lateral clusters have formed.

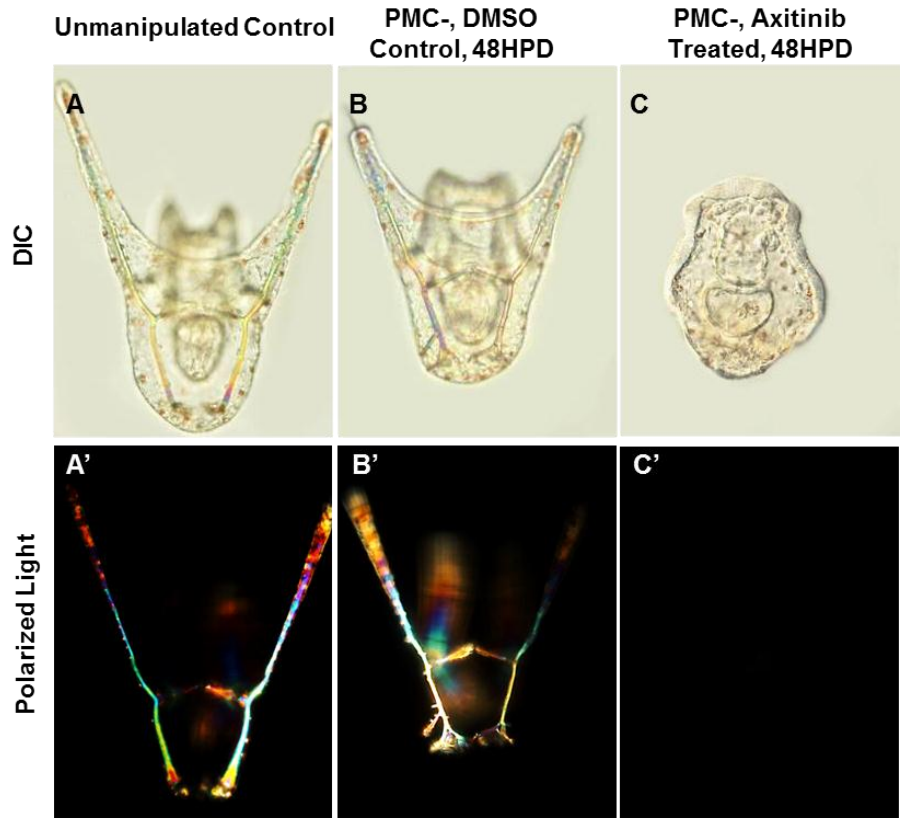

Appendix Figure 16: Perturbation of VEGF signaling inhibits NSM transfating. DIC (A-C) and polarized light (A'-C') images of unmanipulated control (A, A'), PMC depleted DMSO-treated control (B, B'), and PMC depleted axitinib-treated (C, C') embryos 48 hours post depletion (hpd) show that upon PMC depletion, skeletogenesis is recovered in DMSO-treated embryos, but axitinib-treated embryos do not form skeletal elements.

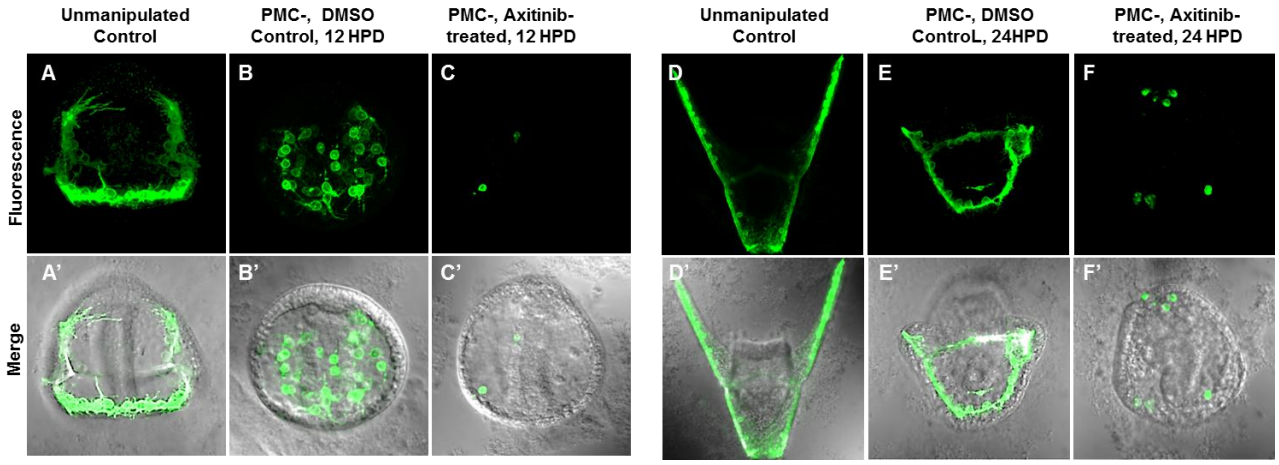

Appendix Figure 17: Perturbation of VEGF signaling inhibits PMC specification during transfating. Fluorescence (A-F) and merged images with DIC (A'-F') of unmanipulated control (A, A', D, D'), PMC depleted DMSO-treated control (B, B', E, E'), and PMC depleted axitinib-treated (C, C',F, F') embryos 12 (A-C, A'-C') and 24 (D-F, D'-F') hours post depletion (hpd). 6a9 immunostaining shows that PMCs are not respecified upon blocking VEGF signaling by axitinib treatment.

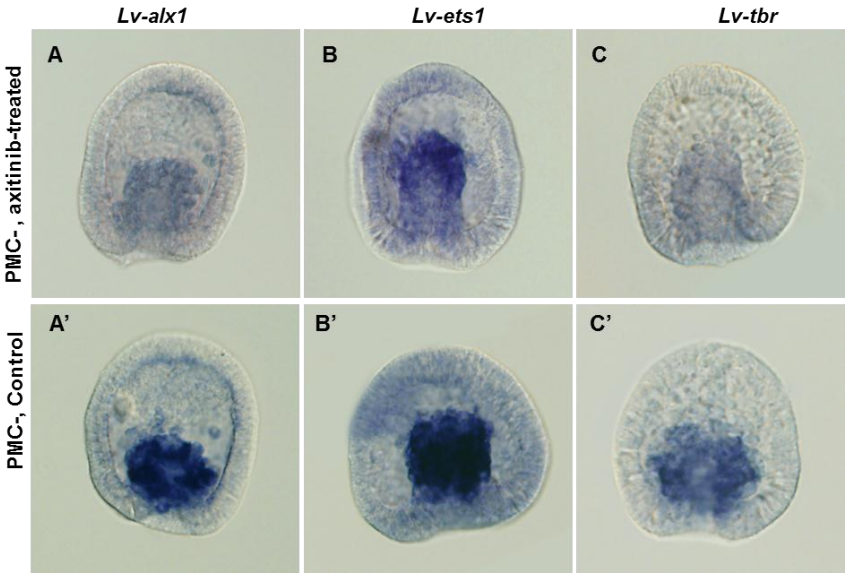

Appendix Figure 18: VEGF signaling regulates the expression of *Lv-alx1*, *Lv-ets1* and *Lv-tbr* during transfating. WMISH analysis of *Lv-alx1* (A, A'), *Lv-ets1* (B, B') and *Lv-tbr* (C, C') expression in PMC depleted embryos treated with axitinib (A-C), and depleted control embryos (A'-C') 3 hours post depletion. *Lv-alx1* and *Lv-tbr* are significantly downregulated upon blocking VEGF signaling during transfating, while *Lv-ets1* is moderately downregulated under these conditions.

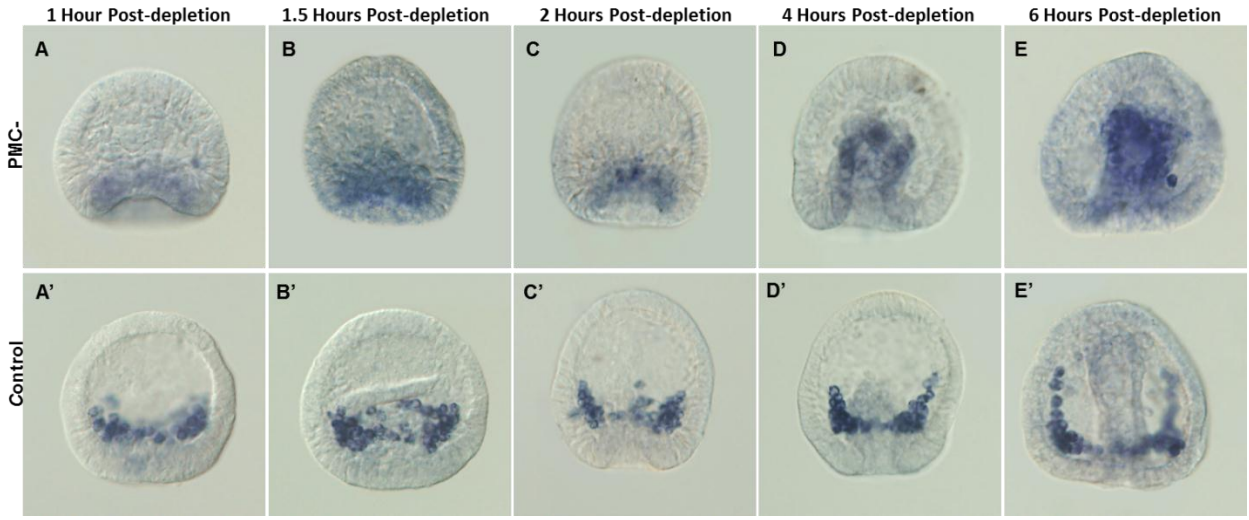

Appendix Figure 19: *Lv-vegfr-10-Ig* is expressed early during transfating. WMISH analysis of the expression patterns of *Lv-vegfr-10-Ig* in PMC depleted embryos (A-E) and control embryos (A'-E'), 1 (A, A'), 1.5 (B, B'), 2 (C, C'), 4 (D, D') and 6 (E, E') hours post-depletion shows that *Lv-vegfr-10-Ig* is expressed as early as 1 hour after PMCs are surgically removed from the blastocoel.

References

Adomako-Ankomah, A., Ettensohn, C. A. (2011). P58-A and P58-B: Novel proteins that mediate skeletogenesis in the sea urchin embryo. *Developmental Biology* **353**, 81-93.

Amaya, E., Stein, P.A., Musci, T.J., Kirschner, M.W. (1993). FGF signalling in the early specification of mesoderm in Xenopus. *Development* **118**, 477-487.

Amore, G., Yavrouian, R.G., Peterson, K.J., Ransick, A., McClay, D.R., Davidson, E.H., (2003). Spdeadringer, a sea urchin embryo gene required separately in skeletogenic and oral ectoderm gene regulatory networks. *Developmental Biology* **261**, 55-81.

Angerer, L. M., Angerer, R. C. (2000). Animal–Vegetal Axis Patterning Mechanisms in the Early Sea Urchin Embryo. *Developmental Biology* **218**, 1–12.

Angerer, L. M., Oleksyn, D. W., Logan, C. Y., McClay, D. R., Dale, L., Angerer, R. C. (2000). A BMP pathway regulates cell fate allocation along the sea urchin animal-vegetal embryonic axis. *Development* **127**, 1105-1114.

Angerer, L. M., Oleksyn, D. W., Levine, A. M., Li, X., Klein, W. H., Angerer, R. C. (2001). Sea urchin goosecoid function links fate specification along the animal-vegetal and oral-aboral embryonic axes. *Development* **128**, 4393-4404.

Anstrom, J.A., Chin, J.E., Leaf, D.S., Parks, A.L., Raff, R.A. (1987). Localization and expression of msp130, a primary mesenchyme lineage-specific cell surface protein in the sea urchin embryo. *Development* **101**, 255-265.

Armstrong, N., Hardin, J., McClay, D.R. (1993). Cell-cell interactions regulate skeleton formation in the sea urchin embryo. *Development* **119**, 833-840.

Armstrong, N., McClay, D.R. (1994). Skeletal pattern is specified autonomously by the primary mesenchyme cells in sea urchin embryos. *Developmental Biology* **162**, 329-338.

Ataliotis, P., Symes, K., Chou, M.M., Ho, L., Mercola, M. (1995). PDGF signalling is required for gastrulation of Xenopus laevis. *Development* **121**, 3099-3110.

Bhargava, P., Robinson, M.O. (2011). Development of second-generation VEGFR tyrosine kinase inhibitors: current status. *Current Oncology Reports* **13**, 103-111.

Benson, S., Sucov, H., Stephens, L., Davidson, E., Wilt, F. (1987). A lineage-specific gene encoding a major matrix protein of the sea urchin embryo spicule. I. Authentication of the cloned gene and its developmental expression. *Developmental Biology* **120**, 499-506.

Böttcher, R. T., Niehrs, C. (2004). Fibroblast Growth Factor Signaling during early vertebrate development. *Endocrine Reviews* **10**, 2003-0040.

Boulet, A.M., Capecchi, M.R. (2012). Signaling by FGF4 and FGF8 is required for axial elongation of the mouse embryo. *Developmental Biology* **371**, 235-245.

Bradham, C.A., Miranda, E.L., McClay, D.R. (2004). PI3K inhibitors block skeletogenesis but not patterning in sea urchin embryos. *Developmental dynamics : an official publication of the American Association of Anatomists* **229**, 713-721.

Bradham, C. A., McClay, D. R. (2005). p38 MAPK is essential for secondary axis specification and patterning in sea urchin embryos. *Development* **133**, 21-32.

Cavalieri, V., Spinelli, G., Di Bernardo, M. (2003). Impairing Otp homeodomain function in oral ectoderm cells affects skeletogenesis in sea urchin embryos. *Developmental Biology* **262**, 107–118.

Cavalieri, V., Guarcello, R., Spinelli, G. (2011). Specific expression of a TRIM-containing factor in ectoderm cells affects the skeletal morphogenetic program of the sea urchin embryo. *Development* **138**, 4279-4290.

Cheers, M. S., Ettensohn, C. A. (2004). Rapid microinjection of fertilized eggs. In: Ettensohn, C.A., Wessel, G.M., Wray, G.A. (Eds.), Development of sea urchins, ascidians, and other invertebrate deuterostomes: experimental approaches. *Methods in Cell Biology*, **74**, 287-310.

Cheers, M. S., Ettensohn, C. A. (2005). P16 is an essential regulator of skeletogenesis in the sea urchin embryo. *Developmental Biology* **283**, 384 – 396.

Ciruna, B., Rossant, J. (2001). FGF signaling regulates mesoderm cell fate specification and morphogenetic movement at the primitive streak. *Developmental Cell* **1**, 37-49.

Coffman, J. A., McCarthy, J. J., Dickey-Sims, C., Robertson, A. J. (2004). Oral–aboral axis specification in the sea urchin embryo II. Mitochondrial distribution and redox state contribute to establishing polarity in Strongylocentrotus purpuratus. *Developmental Biology* **273**, 160–171.

Damm, E.W., Winklbauer, R. (2011). PDGF-A controls mesoderm cell orientation and radial intercalation during Xenopus gastrulation. *Development* **138**, 565-575.

Chuai, M., Weijer, C.J. (2009). Regulation of cell migration during chick gastrulation. *Current Opinion in Genetics & Development* **19**, 343-349.

Croce, J., Lhomond, G., Lozano, J.C., Gache, C. (2001). Ske-T, a T-box gene expressed in the skeletogenic mesenchyme lineage of the sea urchin embryo. *Mechanisms of Development* **107**, 159-162.

Cserzö, M., Wallin, E., Simon, I., von Heijne, G., Elofsson, A. (1997). Prediction of transmembrane alpha-helices in prokaryotic membrane proteins: the dense alignment surface method. *Protein Engineering* **10**, 673-676.

Di Bernardo, M., Castagnetti, S., Bellomonte, D., Oliveri, P., Melfi, R., Palla, F., Spinelli, G. (1999). Spatially restricted expression of PlOtp, a *Paracentrotus lividus* Orthopedia related homeobox gene, is correlated with oral ectodermal patterning and skeletal morphogenesis in late-cleavage sea urchin embryos. *Development* **126**, 2171-2179.

Dorey, K., Amaya, E. (2010). FGF signalling: diverse roles during early vertebrate embryogenesis. *Development* **137**, 3731-3742.

Duboc, V., Röttinger, E., Besnardeau, L., Lepage, T. (2004). Nodal and BMP2/4 Signaling Organizes the Oral-Aboral Axis of the Sea Urchin Embryo. *Developmental Cell*, **6**, 397–410.

Duboc, V., Röttinger, E., Lapraz, F., Besnardeau, L., Lepage, T. (2005). Left-Right Asymmetry in the Sea Urchin Embryo Is Regulated by Nodal Signaling on the Right Side. *Developmental Cell*, **9**, 147–158.

Duboc, V., Lapraz, F., Besnardeau, L., Lepage, T. (2008). Lefty acts as an essential modulator of Nodal activity during sea urchin oral–aboral axis formation. *Developmental Biology* **320**, 49-59.

Duloquin, L., Lhomond, G., Gache, C. (2007). Localized VEGF signaling from ectoderm to mesenchyme cells controls morphogenesis of the sea urchin embryo skeleton *Development* **134**, 2293-2302.

Emanuelsson, O., Brunak, S., von Heijne, G., Nielsen, H. (2007). Locating proteins in the cell using TargetP, SignalP, and related tools. *Nature Protocols* **2**, 953-971.

Emily-Fenouil, F., Ghiglione, C., Lhomond, G., Lepage, T., Gache, C. (1998). GSK3beta/shaggy mediates patterning along the animal-vegetal axis of the sea urchin embryo. *Development* **125**, 2489-2498.

Ettensohn, C. A., McClay, D. R. (1986). The regulation of primary mesenchyme cell migration in the sea urchin embryo: Transplantations of cells and latex beads. *Developmental Biology* **117**, 380-39.

Ettensohn, C. A., McClay, D. R. (1988). Cell lineage conversion in the sea urchin embryo. *Developmental Biology* **125**, 396-409.

Ettensohn, C. A. (1990). The Regulation of Primary Mesenchyme Cell Patterning. *Developmental Biology* **140**, 261-271

Ettensohn, C. A., Malinda, K. M. (1993). Size regulation and morphogenesis: a cellular analysis of skeletogenesis in the sea urchin embryo. *Development* **119**, 155-167.

Ettensohn, C. A., Guss, K. A., Hodor, P. G., Malinda, K. M. (1997) The morphogenesis of the skeletal system of the sea urchin embryo. *Progress in Developmental Biology **8** (Reproductive Biology of Invertebrates), John Wiley and Sons, New York*, 225-265.

Ettensohn, C.A. (1999). Cell movements in the sea urchin embryo. *Current Opinion in Genetics & Development* **9**, 461-465.

Ettensohn, C.A., Sweet, H.C. (2000). Patterning the early sea urchin embryo. *Current Topics in Developmental Biology* **50**, 1-44.

Ettensohn, C. A., Illies, M. R., Oliveri, P., De Jong, D. L. (2003). Alx1, a member of the Cart1/Alx3/Alx4 subfamily of Paired-class homeodomain proteins, is an essential component of the gene network controlling skeletogenic fate specification in the sea urchin embryo. *Development* **130**, 2917-2928.

Ettensohn, C.A., Kitazawa, C., Cheers, M.S., Leonard, J.D., Sharma, T. (2007). Gene regulatory networks and developmental plasticity in the early sea urchin embryo: alternative deployment of the skeletogenic gene regulatory network. *Development* **134**, 3077-3087.

Ettensohn, C. A. (2009). Lessons from a gene regulatory network: echinoderm skeletogenesis provides insights into evolution, plasticity and morphogenesis. *Development* **136**, 11-21.

Ettensohn, C. A. (2013). Encoding Anatomy: Developmental Gene Regulatory Networks and Morphogenesis. *Genesis* (in press).

Fernandez-Serra, M., Consales, C., Livigni, A., Arnone, M.I. (2004). Role of the ERK-mediated signaling pathway in mesenchyme formation and differentiation in the sea urchin embryo. *Developmental Biology* **268**, 384-402.

Flowers, V. L., Courteau, G. R., Poustka, A. J., Weng, W., Venuti, J. M. (2004). Nodal/Activin Signaling Establishes Oral–Aboral Polarity in the Early Sea Urchin Embryo. *Developmental Dynamics* **231**, 727–740.

Fuchikami, T., Mitsunaga-Nakatsubo, K., Amemiya, S., Hosomi, T., Watanabe, T., Kurokawa, D., Kataoka, M., Harada, Y., Satoh, N., Kusunoki, S., Takata, K., Shimotori, T., Yamamoto, T., Sakamoto, N., Shimada, H., Akasaka K. (2002). T-brain homologue (HpTb) is involved in the archenteron induction signals of micromere descendant cells in the sea urchin embryo. *Development* **129**, 5205-5216.

Galileo, D. S., Morrill, J. B. (1985). Patterns of cells and extracellular material of the sea urchin Lytechinus variegatus (Echinodermata, Echinoidea) embryo, from hatched blastula to late gastrula. *Journal of Morphology* **185**, 387-402.

Geiss, G.K., Bumgarner, R.E., Birditt, B., Dahl, T., Dowidar, N., Dunaway, D.L., Fell, H.P., Ferree, S., George, R.D., Grogan, T., James, J.J., Maysuria, M., Mitton, J.D., Oliveri, P., Osborn, J.L., Peng, T., Ratcliffe, A.L., Webster, P.J., Davidson, E.H., Hood, L., Dimitrov, K. (2008). Direct multiplexed measurement of gene expression with color-coded probe pairs. *Nature Biotechnology* **26**, 317-325.

George, N.C., Killian, C.E., Wilt, F.H. (1991). Characterization and expression of a gene encoding a 30.6-kDa Strongylocentrotus purpuratus spicule matrix protein. *Developmental Biology*. **147**, 334-342.

Gerhardt, H. (2008). VEGF and endothelial guidance in angiogenic sprouting. *Organogenesis* **4**, 241-246.

Gong, Y.U., Killian, C.E., Olson, I.C., Appathurai, N.P., Amasino, A.L., Martin, M.C., Holt, L.J., Wilt, F.H., Gilbert, P.U. (2012). Phase transitions in biogenic amorphous calcium carbonate. *Proceedings of the National Academy of Sciences of the United States of America* **109**, 6088-6093.

Gross, J.M., McClay, D.R. (2001). The role of Brachyury (T) during gastrulation movements in the sea urchin Lytechinus variegatus. *Developmental Biology* **239**, 132-147.

Guss, K. A., Ettensohn, C. A. (1997). Skeletal morphogenesis in the sea urchin embryo: regulation of primary mesenchyme gene expression and skeletal rod growth by ectoderm-derived cues. *Development* **124**, 1899-1908.

Gustafson, T., Wolpert, L. (1961). Studies on the cellular basis of morphogenesis in the sea urchin embryo. Directed movements of primary mesenchyme cells in normal and vegetalized larvae. *Experimental Cell Research*. **24**, 64-79.

Gustafson, T., Wolpert, L., (1999). Studies on the cellular basis of morphogenesis in the sea urchin embryo. Directed movements of primary mesenchyme cells in normal and vegetalized larvae. *Experimental Cell Research* **253**, 288-295.

Hahn, M.W. (2009). Distinguishing among evolutionary models for the maintenance of gene duplicates. *Journal of Heredity* **100**, 605–617.

Hardin, J., Coffman, J. A., Black, S. D., McClay, D. R. (1992). Commitment along the dorsoventral axis of the sea urchin embryo is altered in response to NiCl2. *Development* **116,** 671-685.

Harkey, M. A., Whiteley, H. R., Whiteley, A. H. (1992). Differential expression of the *msp130* gene among skeletal lineage cells in the sea urchin embryo: a three dimensional in situ hybridization analysis. *Mechanisms of Development.* **37**, 173-184.

Harkey, M.A., Klueg, K., Sheppard, P., Raff, R.A. (1995). Structure, expression, and extracellular targeting of PM27, a skeletal protein associated specifically with growth of the sea urchin larval spicule. *Developmental Biology* **168**, 549-566.

Hellstrom, M., Phng, L.K., Gerhardt, H. (2007). VEGF and Notch signaling: the yin and yang of angiogenic sprouting. *Cell Adhesion & Migration* **1**, 133-136.

Hodor, P.G., Ettensohn, C.A. (1998). The dynamics and regulation of mesenchymal cell fusion in the sea urchin embryo. *Developmental Biology* **199**, 111 –124.

Hodor, P.G., Illies, M.R., Broadley, S., Ettensohn, C.A. (2000). Cell-substrate interactions during sea urchin gastrulation: migrating primary mesenchyme cells interact with and align extracellular matrix fibers that contain ECM3, a molecule with NG2-like and multiple calcium-binding domains. *Developmental Biology* **222**, 181-194.

Hodor, P.G., Ettensohn, C.A. (2008). Mesenchymal cell fusion in the sea urchin embryo. *Methods in Molecular Biology* **475**, 315-334.

Hogan, B.L. (1999). Morphogenesis. *Cell* **96**, 225-233.

Hubbard, S. R., Till, J. H. (2000). Protein tyrosine kinase structure and function. *Annual Review of Biochemistry* **69**, 373–98.

Hu-Lowe, D.D., Zou, H.Y., Grazzini, M.L., Hallin, M.E., Wickman, G.R., Amundson, K., Chen, J.H., Rewolinski, D.A., Yamazaki, S., Wu, E.Y., McTigue, M.A., Murray, B.W., Kania, R.S., O'Connor, P., Shalinsky, D.R., Bender, S.L. (2008). Nonclinical antiangiogenesis and antitumor activities of axitinib (AG-013736), an oral, potent, and selective inhibitor of vascular endothelial growth factor receptor tyrosine kinases 1, 2, 3. *Clinical Cancer Research* **14**, 7272-7283.

Illies, M. R., Peeler, M. T., Dechtiaruk, A. M., Ettensohn, C. A. (2002). Identification and developmental expression of new biomineralization proteins in the sea urchin Strongylocentrotus purpuratus. *Development Genes and Evolution* **212**, 419–431.

Ingersoll, E. P. (1993). Identification of an extracellular matrix determinant that plays a key role in sea urchin gastrulation. Carnegie Mellon University, Pittsburgh. [Ph.D. thesis].

Innan, H., Kondrashov, F. (2010). The evolution of gene duplications: classifying and distinguishing between models. *Nature Reviews Genetics* **11**, 97-108.

Isaacs, H.V., Pownall, M.E., Slack, J.M. (1994). eFGF regulates Xbra expression during Xenopus gastrulation. *The EMBO journal* **13**, 4469-4481.

Kadam, S., McMahon, A., Tzou, P., Stathopoulos, A. (2009). FGF ligands in Drosophila have distinct activities required to support cell migration and differentiation. *Development* **136**, 739-747.

Karp, G.C., Solursh, M. (1985). Dynamic activity of the filopodia of sea urchin embryonic cells and their role in directed migration of the primary mesenchyme in vitro. *Developmental Biology* **112**, 276-283.

Katow, H., Yazawa, S., Sofuku, S. (1990). A fibronectin-related synthetic peptide, Pro-Ala-Ser-Ser, inhibits fibronectin binding to the cell surface, fibronectin-promoted cell migration in vitro, and cell migration in vivo. *Experimental Cell Research* **190**, 17-24.

Kawasaki, K., Buchanan, A.V., Weiss, K.M. (2007). Gene duplication and the evolution of vertebrate skeletal mineralization. *Cells, Tissues, Organs* **186**, 7-24.

Kawasaki, K., Buchanan, A.V., Weiss, K.M. (2009). Biomineralization in humans: making the hard choices in life. *Annual Reviews Genetics* **43**, 119-142.

Killian, C.E., Croker, L., Wilt, F.H. (2010). SpSM30 gene family expression patterns in embryonic and adult biomineralized tissues of the sea urchin, Strongylocentrotus purpuratus. *Gene Expression Patterns : GEP* **10**, 135-139.

Killian, C.E., Wilt, F.H. (2008). Molecular aspects of biomineralization of the echinoderm endoskeleton. *Chemical Reviews* **108**, 4463-4474.

Kitajima, T., Urakami, H. (2000). Differential distribution of spicule matrix proteins in the sea urchin embryo skeleton. *Development, Growth & Differentiation* **42**, 295-306.

Knapp, R.T., Wu, C.H., Mobilia, K.C., Joester, D. (2012). Recombinant sea urchin vascular endothelial growth factor directs single-crystal growth and branching in vitro. *Journal of the American Chemical Society* **134**, 17908-17911.

Kurokawa D., Kitajima T., Mitsunaga-Nakatsubo K., Amemiya S., Shimada H., Akasaka K. (1999). HpEts, an ets-related transcription factor implicated in primary mesenchyme cell differentiation in the sea urchin embryo. *Mechanisms of Development* **80**, 41-52.

Kurosaka, S., Kashina, A. (2008). Cell biology of embryonic migration. *Birth Defects Research. Part C, Embryo Today* : Reviews **84**, 102-122.

Lamalice, L., Le Boeuf, F., Huot, J. (2007). Endothelial cell migration during angiogenesis. *Circulation Research* **100**, 782-794.

Lan, Y., Jiang, R. (2009). Sonic hedgehog signaling regulates reciprocal epithelial-mesenchymal interactions controlling palatal outgrowth. *Development* **136**, 1387-1396.

Lapraz, F, Röttinger, E., Duboc, V., Range, R., Duloquin, L., Walton, K., Wu, S.-Y., Bradham, C., Loza, M. A., Hibino, T., Wilson, K., Poustka A., McClay, D., Angerer, L., Gache, C., Lepage, T. (2006). RTK and TGF-β signaling pathways genes in the sea urchin genome. *Developmental Biology* **300**, 132–152.

Lauffenburger, D.A., Chu, L., French, A., Oehrtman, G., Reddy, C., Wells, A., Niyogi, S., Wiley, H.S. (1996). Engineering dynamics of growth factors and other therapeutic ligands. *Biotechnology and Bioengineering* **52**, 61-80.

Le Clainche, C., Carlier, M.F. (2008). Regulation of actin assembly associated with protrusion and adhesion in cell migration. *Physiological Reviews* **88**, 489-513.

Lee, Y., Britten, R. J., Davidson, E. H. (1999). SM37, a skeletogenic gene of the sea urchin embryo linked to the SM50 gene. *Development, Growth and Differentiation* **41**, 303-312.

Lepage, T., Sardet, C., Gache, C. (1992). Spatial expression of the hatching enzyme gene in the sea urchin embryo. *Developmental Biology* **150**, 23-32.

Li, E., Materna, S.C., Davidson, E.H. (2012). Direct and indirect control of oral ectoderm regulatory gene expression by Nodal signaling in the sea urchin embryo. *Developmental Biology* **369**, 377-385.

Liu, C., Nakamura, E., Knezevic, V., Hunter, S., Thompson, K.., Mackem. S. (2003) A role for the mesenchymal T-box gene Brachyury in AER formation during limb development. *Development* **130**, 1327-1337.

Livingston, B.T., Killian, C.E., Wilt, F., Cameron, A., Landrum, M.J., Ermolaeva, O., Sapojnikov, V., Maglott, D.R., Buchanan, A.M., Ettensohn, C.A. (2006). A genome-wide analysis of biomineralization-related proteins in the sea urchin *Strongylocentrotus purpuratus*. *Developmental Biology* **300**, 335–348.

Logan, C.Y., Miller, J.R., Ferkowicz, M.J., McClay, D.R. (1999). Nuclear beta-catenin is required to specify vegetal cell fates in the sea urchin embryo. *Development* **126**, 345-357.

Lunn, J.S., Fishwick, K.J., Halley, P.A., Storey, K.G. (2007). A spatial and temporal map of FGF/Erk1/2 activity and response repertoires in the early chick embryo. *Developmental Biology* **302**, 536-552.

Lyons, D.C., Kaltenbach, S.L., McClay, D.R. (2012). Morphogenesis in sea urchin embryos: linking cellular events to gene regulatory states. *Wires Developmental Biology* **1**, 231-252.

Mackenzie, F., Ruhrberg, C. (2012). Diverse roles for VEGF-A in the nervous system. *Development* **139**, 1371-1380.

Malinda, K.M., Ettensohn, C.A. (1994). Primary mesenchyme cell migration in the sea urchin embryo: distribution of directional cues. *Developmental Biology* **164**, 562-578.

Malinda, K. M., Fisher, G. W., Ettensohn, C. A. (1995). Four-Dimensional Microscopic Analysis of the Filopodial Behavior of Primary Mesenchyme Cells during Gastrulation in the Sea Urchin Embryo. *Developmental Biology* **172,** 552–566.

Mattila, P.K., Lappalainen, P. (2008). Filopodia: molecular architecture and cellular functions. *Nature Reviews. Molecular Cell Biology* **9**, 446-454.

Matsumoto, T., Claesson-Welsh, L. (2001). VEGF receptor signal transduction. *Sci. STKE* **21**.

Mann, K., Poustka, A.J., Mann, M. (2008). In-depth, high-accuracy proteomics of sea urchin tooth organic matrix. *Proteome Science*. **6**, 33.

Mann, K., Poustka, A.J., Mann, M. (2010). Phosphoproteomes of Strongylocentrotus purpuratus shell and tooth matrix: identification of a major acidic sea urchin tooth phosphoprotein, phosphodontin. *Proteome Science* **8**, 6.

Mann, K., Wilt, F.H., Poustka, A.J. (2010). Proteomic analysis of sea urchin (Strongylocentrotus purpuratus) spicule matrix. *Proteome Science* **8**, 33.

McCarthy, R.A., Spiegel, M. (1983). Serum effects on the in vitro differentiation of sea urchin micromeres. *Experimental Cell Research* **149**, 433-441.

McLennan, R., Teddy, J.M., Kasemeier-Kulesa, J.C., Romine, M.H., Kulesa, P.M. (2010). Vascular endothelial growth factor (VEGF) regulates cranial neural crest migration in vivo. *Developmental Biology* **339**, 114-125.

McMahon, A., Reeves, G.T., Supatto, W., Stathopoulos, A. (2010). Mesoderm migration in Drosophila is a multi-step process requiring FGF signaling and integrin activity. *Development* **137**, 2167-2175.

Miller, J., Fraser S. E., McClay, D. (1995). Dynamics of thin filopodia during sea urchin gastrulation. *Development* **121**, 2501-2511.

Miller, J.R., McClay, D.R. (1997). Characterization of the role of cadherin in regulating cell adhesion during sea urchin development. *Developmental Biology* **192**, 323-339.

Montell, D.J. (1999). The genetics of cell migration in Drosophila melanogaster and Caenorhabditis elegans development. *Development* **126**, 3035-3046.

Montero, J.A., Kilian, B., Chan, J., Bayliss, P.E., Heisenberg, C.P. (2003). Phosphoinositide 3-kinase is required for process outgrowth and cell polarization of gastrulating mesendodermal cells. *Current Biology* **13**, 1279-1289.

Morino, Y., Koga, H., Tachibana, K., Shoguchi, E., Kiyomoto, M., Wada, H. (2012). Heterochronic activation of VEGF signaling and the evolution of the skeleton in echinoderm pluteus larvae. *Evolution & Development* **14**, 428-436.

Nagel, M., Tahinci, E., Symes, K., Winklbauer, R. (2004). Guidance of mesoderm cell migration in the Xenopus gastrula requires PDGF signaling. *Development* **131**, 2727-2736.

Page, L., Benson, S. (1992). Analysis of competence in cultured sea urchin micromeres. *Experimental Cell Research* **203**, 305-311.

Okazaki, K. (1965). Skeleton formation of sea urchin larvae. V. Continuous observation of the process of matrix formation. *Experimental Cell Research* **40**, 585-596.

Okazaki, K. (1975). Normal development to metamorphosis. *In: "The Sea Urchin Embryo" (G. Czihak, Ed.), Springer-Verlag, New York*. 177-232.

Oliveri, P., Carrick, D. M., Davidson, E. H. (2002). A regulatory gene network that directs micromere specification in the sea urchin embryo. *Developmental Biology* **246**, 209-228.

Oliveri, P., Davidson, E.H., McClay, D.R. (2003). Activation of pmar1 controls specification of micromeres in the sea urchin embryo. *Developmental Biology* **258**, 32-43.

Oliveri, P., Tu, Q., Davidson, E. H. (2008). Global regulatory logic for specification of an embryonic cell lineage. *Proc. Natl. Acad. Sci. USA* **105**, 5955-5962.

Ornitz, D., Itoh, N. (2001). Fibroblast growth factors. *Genome Biology* **2**, 3005.1–3005.12.

Peled-Kamar, M., Hamilton, P., Wilt, F.H. (2002). Spicule matrix protein LSM34 is essential for biomineralization of the sea urchin spicule. *Experimental Cell Research*. **272**, 56-61.

Politi, Y., Metzle, R.A., Abrecht, M., Gilbert, B., Wilt, F.H., Sagi, I., Addadi, L., Weiner, S., Gilbert, P.U. (2008). Transformation mechanism of amorphous calcium carbonate into calcite in the sea urchin larval spicule. *Proc Natl Acad Sci U S A* **105**, 17362-17366.

Rafiq, K., Cheers, M.S., Ettensohn, C.A. (2012). The genomic regulatory control of skeletal morphogenesis in the sea urchin. *Development* **139**, 579-590.

Rahman, M.A., Yusoff, F.M., Arshad, A., Shamsudin, M.N., Amin, S.M. (2012). Embryonic, larval, and early juvenile development of the tropical sea urchin, Salmacis sphaeroides (Echinodermata: Echinoidea). *The Scientific World Journal* **2012**, 938482.

Range, R., Lapraz, F., Quirin, M., Marro, S., Besnardeau, L., Lepage, T. (2007). Cis-regulatory analysis of *nodal* and maternal control of dorsal-ventral axis formation by Univin, a TGF-related to Vg1. *Development* **134**, 3649-3664.

Reim, I., Hollfelder, D., Ismat, A., Frasch, M. (2012). The FGF8-related signals Pyramus and Thisbe promote pathfinding, substrate adhesion, and survival of migrating longitudinal gut muscle founder cells. *Developmental Biology* **368**, 28-43.

Revilla-i-Domingo, R., Oliveri, P., Davidson, E.H. (2007). A missing link in the sea urchin embryo gene regulatory network: hesC and the double-negative specification of micromeres. *Proceedings of the National Academy of Sciences of the United States of America* **104**, 12383-12388.

Rho, H.K., McClay, D.R. (2011). The control of foxN2/3 expression in sea urchin embryos and its function in the skeletogenic gene regulatory network. *Development* **138**, 937-945.

Rottinger, E., Besnardeau, L., Lepage, T. (2004). A Raf/MEK/ERK signaling pathway is required for development of the sea urchin embryo micromere lineage through phosphorylation of the transcription factor Ets. *Development* **131**, 1075-1087.

Röttinger, E., Saudemont, A., Duboc, V., Besnardeau, L., McClay, D., Lepage, T. (2008). FGF signals guide migration of mesenchymal cells, control skeletal morphogenesis and regulate gastrulation during sea urchin development. *Development* **135**, 353-365.

Schlessinger, J. (2000). Cell signaling by receptor tyrosine kinases. *Cell* **103**, 211-225.

Sharma, T., Ettensohn, C. A. (2010). Activation of the skeletogenic gene regulatory network in the early sea urchin embryo. *Development* **137**, 1149-57.

Sharma, T., Ettensohn, C.A. (2011). Regulative deployment of the skeletogenic gene regulatory network during sea urchin development. *Development* **138**, 2581-2590.

Smith, A.B., Pisani, D., Mackenzie-Dodds, J.A., Stockley, B., Webster, B.L., Littlewood, D.T. (2006). Testing the molecular clock: molecular and paleontological estimates of divergence times in the Echinoidea (Echinodermata). *Molecular Biolology and Evolution*. **10**, 1832-1851.

Smith, E.M., Mitsi, M., Nugent, M.A., Symes, K. (2009). PDGF-A interactions with fibronectin reveal a critical role for heparan sulfate in directed cell migration during Xenopus gastrulation. *Proceedings of the National Academy of Sciences of the United States of America* **106**, 21683-21688.

Sun, X., Meyers, E.N., Lewandoski, M., Martin, G.R. (1999). Targeted disruption of Fgf8 causes failure of cell migration in the gastrulating mouse embryo. *Genes & Development* **13**, 1834-1846.

Tammela, T., Zarkada, G., Wallgard, E., Murtomaki, A., Suchting, S., Wirzenius, M., Waltari, M., Hellstrom, M., Schomber, T., Peltonen, R., Freitas, C., Duarte, A., Isoniemi, H., Laakkonen, P., Christofori, G., Yla-Herttuala, S., Shibuya, M., Pytowski, B., Eichmann, A., Betsholtz, C., Alitalo, K. (2008). Blocking VEGFR-3 suppresses angiogenic sprouting and vascular network formation. *Nature* **454**, 656-660.

Tekaia, F., Yeramian, E. (2006). Evolution of proteomes: fundamental signatures and global trends in amino acid compositions. *BMC Genomics* **7**, 307.

Thompson, J.D., Higgins, D.G., Gibson, T.J. (1994). CLUSTAL W: improving the sensitivity of progressive multiple sequence alignment through sequence weighting, position-specific gap penalties and weight matrix choice. *Nucleic Acids Research* **22**, 4673-4680.

Tomanek, R.J., Christensen, L.P., Simons, M., Murakami, M., Zheng, W., Schatteman, G.C. (2010). Embryonic coronary vasculogenesis and angiogenesis are regulated by interactions between multiple FGFs and VEGF and are influenced by mesenchymal stem cells. *Developmental Dynamics* **239**, 3182-3191.

Voronina, E., Wessel, G.M. (2001). Apoptosis in sea urchin oocytes, eggs, and early embryos. *Molecular Reproduction and Development* **60**, 553-561.

Weitzel, H.E., Illies, M.R., Byrum, C.A., Xu, R., Wikramanayake, A.H., Ettensohn, C.A. (2004). Differential stability of beta-catenin along the animal-vegetal axis of the sea urchin embryo mediated by dishevelled. *Development* **131**, 2947-2956.

Wilson, R., Leptin, M. (2000). Fibroblast growth factor receptor-dependent morphogenesis of the Drosophila mesoderm. *Philosophical transactions of the Royal Society of London. Series B, Biological Sciences* **355**, 891-895.

Wilt, F.H., Ettensohn, C. A. (2007). Morphogeneisis and biomineralizatiion of the sea urchin larval endoskeleton. *Handbook of Biomineralization.* Edited by E. Bauerlein. Wiley-VCH, Weinheim, 183-210.

Wilt, F.H. (1999). Matrix and mineral in the sea urchin larval skeleton. *Journal of Structural Biology* **126**, 216-226.

Wilt, F.H., Killian, C.E., Hamilton, P., Croker, L. (2008). The dynamics of secretion during sea urchin embryonic skeleton formation. *Experimental Cell Research* **314**, 1744-1752.

Wilt, F., Croker, L., Killian, C. E., McDonald, K. (2008). Role of LSM34/SpSM50 proteins in endoskeletal spicule formation in sea urchin embryos. *Invertebrate Biology* **127**, 452–459.

Winklbauer, R., Muller, H.A. (2011). Mesoderm layer formation in Xenopus and Drosophila gastrulation. *Physical Biology* **8**, 045001.

Wu, S.Y., Ferkowicz M., McClay, D.R. (2007). Ingression of primary mesenchyme cells of the sea urchin embryo: a precisely timed epithelial mesenchymal transition. *Birth Defects Research* **81**, 241-252.

Wu, M.Y., Hill, C.S. (2009). Tgf-beta superfamily signaling in embryonic development and homeostasis. *Developmental Cell* **16**, 329-343.

Wu, S.Y., McClay, D.R. (2007). The Snail repressor is required for PMC ingression in the sea urchin embryo. *Development* **134**, 1061-1070.

Wu, S.Y., Yang, Y.P., McClay, D.R. (2008). Twist is an essential regulator of the skeletogenic gene regulatory network in the sea urchin embryo. *Developmental Biology* **319**, 406-415.

Yajima, M., Kiyomoto, M. (2006). Study of larval and adult skeletogenic cells in developing sea urchin larvae. *The Biological Bulletin* **211**, 183-192.

Yang, C., Svitkina, T. (2011). Filopodia initiation: focus on the Arp2/3 complex and formins. *Cell Adhesion & Migration* **5**, 402-408.

Yang, X., Chrisman, H., Weijer, C.J. (2008). PDGF signalling controls the migration of mesoderm cells during chick gastrulation by regulating N-cadherin expression. *Development* **135**, 3521-3530.

Yang, X., Dormann, D., Munsterberg, A.E., Weijer, C.J. (2002). Cell movement patterns during gastrulation in the chick are controlled by positive and negative chemotaxis mediated by FGF4 and FGF8. *Developmental Cell* **3**, 425-437.

Zhang, Y., Zhang, Z., Zhao, X., Yu, X., Hu, Y., Geronimo B., Fromm, S.H., Chen, Y. (2000). A new function of BMP4: dual role for BMP4 in regulation of Sonic hedgehog expression in the mouse tooth germ. *Development* **127**, 1431-1443.

Zhu, X., Mahairas, G., Illies, M., Cameron, R.A., Davidson, E.H., Ettensohn, C.A. (2001). A large-scale analysis of mRNAs expressed by primary mesenchyme cells of the sea urchin embryo. *Development* **128**, 2615-2627.